

2008

Investigation of roller-integrated compaction monitoring and in-situ testing technologies for characterization of pavement foundation layers

Pavana Kumar Reddy Vennapusa
Iowa State University

Follow this and additional works at: <https://lib.dr.iastate.edu/etd>

 Part of the [Civil and Environmental Engineering Commons](#)

Recommended Citation

Vennapusa, Pavana Kumar Reddy, "Investigation of roller-integrated compaction monitoring and in-situ testing technologies for characterization of pavement foundation layers" (2008). *Graduate Theses and Dissertations*. 11190.
<https://lib.dr.iastate.edu/etd/11190>

This Dissertation is brought to you for free and open access by the Iowa State University Capstones, Theses and Dissertations at Iowa State University Digital Repository. It has been accepted for inclusion in Graduate Theses and Dissertations by an authorized administrator of Iowa State University Digital Repository. For more information, please contact digirep@iastate.edu.

Investigation of roller-integrated compaction monitoring and in-situ testing technologies for characterization of pavement foundation layers

by

Pavana Kumar Reddy Vennapusa

A dissertation submitted to the graduate faculty
in partial fulfillment of the requirements for the degree of
DOCTOR OF PHILOSOPHY

Major: Civil Engineering (Geotechnical Engineering)

Program of Study Committee:
David J. White, Major Professor
Vernon R. Schaefer
Max Morris
Charles T. Jahren
Halil Ceylan

Iowa State University

Ames, Iowa

2008

Copyright © Pavana Kumar Reddy Vennapusa, 2008. All rights reserved.

DEDICATION

This thesis would be incomplete without a mention of the support given to me by my mother, father, fiancé, sister, and brother-in-law for whom this thesis is dedicated. I doubt it should ever have been completed without their unconditional love and inspiration throughout this work. They knowingly or unknowingly led me to an understanding of some of the more subtle challenges and my ability to succeed.

TABLE OF CONTENTS

LIST OF FIGURES	VI
LIST OF TABLES	IX
CHAPTER 1. INTRODUCTION	1
1.1 Overview	1
1.2 Research Objectives and Anticipated Benefits	3
1.3 Thesis Organization	4
1.4 References	6
CHAPTER 2. COMPARISON OF LIGHT WEIGHT DEFLECTOMETER MEASUREMENTS FOR PAVEMENT FOUNDATION MATERIALS	10
2.1 Abstract	10
2.2 Introduction	10
2.3 Theoretical Determination of Elastic Modulus	11
2.4 Comparison of In-Situ LWD Test Devices	12
2.5 Factors Influencing E_{LWD} Measurements	12
2.5.1 Size of Loading Plate	13
2.5.2 Plate Contact Stress	14
2.5.3 Type and Location of Deflection Sensor	15
2.5.4 Plate Rigidity	15
2.5.5 Load Transducer	17
2.5.6 Loading Rate and Stiffness of Buffer	17
2.6. Experimental Comparison of LWD Devices from the Authors' Study	18
2.6.1 Light Drop Weight Tester – ZFG 2000	18
2.6.2 Keros and Dynatest 3031 Portable Falling Weight Deflectometers	19
2.6.3 Static Plate Load Test	19
2.6.4 Field Studies	20
2.6.5 E_{LWD} comparison between different LWDs and static plate load E_{V1} and E_{V2}	20
2.6.6 Variability of E_{LWD} measurements	22

2.6.7 Influence of Plate Diameter on E_{LWD}	22
2.6.8 Influence of Applied Contact Stress on E_{LWD}	23
2.6.9 Influence of Buffer Stiffness on E_{LWD}	24
2.7 Conclusions.....	25
2.8 Acknowledgements.....	27
2.9 Notations.....	27
2.10 References.....	29
CHAPTER 3. GEOSTATISTICAL ANALYSIS FOR SPATIALLY REFERENCED ROLLER-INTEGRATED COMPACTION MEASUREMENTS	52
3.1 Abstract.....	52
3.2 Introduction.....	52
3.2 Background.....	54
3.2.1 Roller-Integrated Compaction Measurement Values.....	54
3.3 Geostatistical Analysis.....	56
3.3.1 Fitting a Theoretical Model	57
3.4 Case Studies.....	58
3.4.1 Case Study I.....	58
3.4.2 Case Study II.....	61
3.5 Concluding Remarks.....	64
3.6 Acknowledgments.....	65
3.7 Notations.....	65
3.8 References.....	66
CHAPTER 4. ALTERNATIVES TO HEAVY TEST ROLLING FOR COHESIVE SUBGRADE ASSESSMENT	84
4.1 Abstract.....	84
4.2 Introduction.....	84
4.3 Background.....	87
4.3.1 Roller-Integrated compaction measurements	87
4.3.2 Test rolling.....	88
4.3.3 In-situ point measurements.....	88
4.4 Experimental Testing.....	89

4.4.1 Correlations between different QA test measurements	90
4.4.2 Bearing capacity analysis on layered cohesive soil stratum	91
4.5 Implementation Aspects.....	94
4.6 Concluding Remarks.....	94
4.7 Acknowledgements.....	95
4.8 References.....	95
CHAPTER 5. IN-SITU MECHANISTIC CHARACTERIZATION OF GRANULAR PAVEMENT FOUNDATION LAYERS	106
5.1 Abstract.....	106
5.2 Introduction.....	106
5.3 Background.....	108
5.3.1 Roller-Integrated Compaction Measurements	109
5.3.2 Resonant Meter Value (RMV).....	109
5.3.2 In-Situ Point Measurements.....	110
5.3.3 Earth Pressure Cells	112
5.4 Experimental Testing.....	112
5.5 Stresses in Pavement Foundation Layers.....	113
5.6 Comparison of Roller-Integrated and In-Situ Point Measurements	115
5.7 Summary and Conclusions	118
5.8 Acknowledgements.....	119
5.9 References.....	119
CHAPTER 6. CONCLUSIONS AND RECOMMENDATIONS FOR FUTURE WORK	137
6.1 Summary.....	137
6.2 Conclusions.....	137
6.2.1 Review and investigation of LWD devices	137
6.2.2 Geostatistical Analysis on RICM measurements.....	138
6.2.3 Mechanistic Characterizations of Pavement Foundation Layers.....	139
6.3 Recommendations for Future Research	141
ACKNOWLEDGMENTS	142

LIST OF FIGURES

FIG. 2.1—Relationship between material stiffness and diameter of bearing plate	42
FIG. 2.2—Relationship between plate rigidity, modulus of soil, and contact stress distribution under a plate for elastic subgrade material (using Borowicka (1936) procedure)	43
FIG. 2.3—Schematic with example output of LWD devices used in this study (a) Zorn ZFG 2000 (b) Keros (c) Dynatest 3031	44
FIG. 2.4—Relationships between ELWD values from different devices: (a) 200-mm Keros and Zorn, (b) 300-mm Keros and Zorn, (c) 200-mm Dynatest and Zorn, (d) 200-mm Dynatest and Keros, (e) 200-mm Zorn and 300-mm static plate load test initial modulus, and (f) 200-mm Zorn and 300-mm static plate load test reload modulus	45
FIG. 2.5— Results from field study 1a and 1b: (a) Comparison between deflection measurements by Zorn and Keros devices, (b) Frequency distribution of impact force by Keros LWD device and comparison to Zorn assumed impact force	46
FIG. 2.6—Frequency distribution of impact force at drop height 50 cm by Keros and Dynatest LWD devices and comparison to Zorn assumed impact force (field study 4) ...	47
FIG. 2.7— Relationship between 200-mm and 300-mm plate Zorn E_{LWD}	48
FIG. 2.8— Influence of plate diameter and applied stress on Zorn E_{LWD} from field studies 3 and 4.....	49
FIG. 2.9— Influence of applied stress and effect of buffer stiffness on ELWD with different plate diameters from field study 5	50
FIG. 2.10— Effect of buffer type and stiffness on applied force for different LWD devices.....	51
FIG. 3.1—Typical sample semivariogram. Comparatively, a semivariogram with a lower sill and longer range represents improved uniformity and spatial continuity.....	75
FIG. 3.2— (color) Figures for case study I showing (a) in-situ subsurface conditions and spot test locations, (b) picture of compaction process using the Caterpillar’s CS 533E	

roller	76
FIG. 3.3— (color) CMV (left) and MDP (right) data for case study I represented as points.....	77
FIG. 3.4—Histogram (on left) and omni-directional semivariogram plots (on right) of CMV (a) actual data and (b) residuals after quadratic detrending from case study I	78
FIG. 3.5—Histogram (on left) and omni-directional semivariogram plots (on right) of residuals of (a) MDP, (b) DCP values (blows/250mm), and (c) ELWD after quadratic deterending in case study I.....	79
FIG. 3.6—(color) Kriged contour maps of (a) CMV (b) MDP, (c) DCPI, and (d) ELWD in case study I.....	80
FIG. 3.7—Change in univariate (μ , σ) and spatial statistics (a, $C+C_0$) of CMV with roller passes for calibration strip 1 (on left) calibration strip 2 (on right) in case study II.....	81
FIG. 3.8— Comparison between calibration and proof areas with univariate and spatial statistics for acceptance criteria	82
FIG. 3.9— Kriged surface maps and semivariograms of a selected portion of the proof showing variations with modifications in the actual CMV data.....	83
FIG. 4.1— DCP- s_u profiles from compacted glacial till subgrade at US14 (White et al. 2007a)	100
FIG. 4.2— (a) CP-563 roller, (b) CS-563 roller, (c) Towed pneumatic dual-wheel test roller with 650 kPa contact tire pressure, (d) Shelby tube sampler, (e) DCP, (f) Zorn 200- mm diameter plate LWD, (g) 6.2 kN capacity static plate load test setup.	101
FIG. 4.3— Relationships between: (a) DPI and s_u , (b) DPI and E_{LWD} , (c) rut depth and E_{LWD} , (d) rut depth and CMV, (e) E_{LWD} and MDP*, and (f) E_{LWD} and CMV.....	102
FIG. 4.4— Comparison of DCP- s_u profiles with rut depth measurements.....	103
FIG. 4.5— (a) Relationship between calculated ultimate bearing capacity and measured rut depth, and (b) influence of undrained shear strength properties of top and bottom layers at different H (thickness of the top layer) to achieve a minimum $q_{ult} = 1050$	

kPa.....	104
FIG. 4.6— Comparison of estimating ultimate bearing capacity from layered bearing capacity analysis and 300 mm plate load test measurements.	105
FIG. 5.1— Illustration of differences in measurement influence depths of different testing devices.....	127
FIG. 5.2— Example CPT profile from a test location in the test strip area describing general foundation soil information.....	128
FIG. 5.3— Total vertical and lateral stresses induced by roller during vibratory loading at a = 0.85 and 1.70 mm nominal settings and drum jumping at a = 1.70 mm.....	129
FIG. 5.4— Peak vertical and lateral stress increase profiles (measured and theoretical Boussinesq) for roller induced vibratory loads, and FWD and LWD dynamic loads, and estimated residual stresses to calculate K_o from Duncan and Seed (1986).....	130
FIG. 5.5— Comparison of total stress paths under roller vibratory load (Positions 1 to 2 loading and Positions 2 to 3 unloading), FWD and LWD dynamic loads, and stresses applied during laboratory M_r tests on base/subbase materials.....	131
FIG. 5.6— Roller-integrated measurements from test strip with nominal $v = 3.2$ km/h and $f = 30$ Hz settings: (a) repeatability of CMV at two amplitude settings, (b) influence of RMV on CMV measurements.	132
FIG. 5.7— Comparison of roller-integrated compaction measurements with in-situ mechanistic point measurements – DCP index, CPT q_t , and E_{FWD} profiles at two select points.....	133
FIG. 5.8— Relationships between different measurements (E_{FWD-D3} at $F \sim 26.7$ kN).....	134
FIG. 5.9— Relationships between roller-integrated CMV and point measurements (E_{FWD-D3} at $F \sim 53.4$ kN).....	135
FIG. 5.10— Results of multiple regression analysis illustrating the effect of RMV.....	136

LIST OF TABLES

TABLE 2.1— Summary of shape factors in E_{LWD} estimation (Terzaghi and Peck 1967; Fang 1991).....	34
TABLE 2.2— Brief comparison between different LWD devices.....	35
TABLE 2.3—Correlations between different in-situ modulus test devices.	36
TABLE 2.4—Summary of Zorn and Keros/Dynatest 3031 LWD test conditions.	38
TABLE 2.5—Summary of field studies and index properties of materials.....	39
TABLE 2.6—Summary statistics of modulus measurements from different field studies.	41
TABLE 3.1—Commonly used theoretical semivariogram models	71
TABLE 3.2—Case studies summary	72
TABLE 3.3—Summary of soil index properties	73
TABLE 3.4—Comparison of spatial and univariate statistics of CMV with quality assurance criteria for calibration strips – case study II.....	74
TABLE 4.1— Summary of soil index properties.....	98
TABLE 4.2—Summary of QA target values as an alternative to heavy testing rolling rut depth of 50 mm.	99
TABLE 5.1—Summary of soil index properties	124
TABLE 5.2—Summary of regression relationships.....	125
TABLE 5.3—Summary statistics of roller and in-situ point measurements at surface.....	126

CHAPTER 1. INTRODUCTION

1.1 Overview

The performance and durability of pavement structures depend heavily on the pavement foundation layer support conditions. Construction of pavement foundation layers with adequate support capacities require use of proper construction methods and following proper quality control (QC) procedures. The QC procedures often used during earthwork construction involve proper material selection and identification, controlling the material lift thickness and moisture content, and using appropriate compaction equipment that is conducive to field conditions. Compliance of the compacted layers based on presumed “target” values (e.g., relative compaction) is commonly checked by performing in-situ quality assurance (QA) tests.

Since R.R. Proctor’s development of the laboratory Proctor test method to determine moisture-density relationship of soils (Proctor 1933), most QC/QA specifications in highway construction practice have been based on this laboratory test (see Handy and Spangler 2007, Walsh et al. 1997). The use of density criteria for QC/QA is primarily a consequence of historical tradition and convenience, and is based on a presumption that an increase in soil density increases soil strength (Selig 1982). While this is generally true, the relationship between soil strength and soil density is complex and is influenced by several factors such as soil structure, soil moisture content, and differences between laboratory and field compaction methods, pore pressure induced during compaction, etc. (see Seed and Chan 1959, Seed et al. 1961, Handy and Spangler 2007).

Strength and stiffness properties of the foundation layers are primary inputs in pavement design. Realizing the importance of measuring the “true” design properties of pavement foundation layers in-situ, there has been growing interest among highway agencies over the past decade in the United States in evaluating various strength or stiffness based measurement techniques for QC/QA testing (see Killingsworth and Quintas 1996, White et al. 1999, Mn/DOT 2000, White et al. 2002, Zambrano et al. 2006, Mn/DOT 2006, Peterson et al. 2007, White et al. 2007c).

Several in-situ testing methods have been developed over the past five decades to

evaluate the strength/stiffness properties of pavement foundation layers *in-situ* (see Newcomb and Birgisson 1999) (e.g., test rolling or proof rolling, static plate load test (PLT), falling weight deflectometer (FWD), light weight deflectometer (LWD), dynamic cone penetrometer (DCP), piezocone or static cone penetrometer (CPT), dirt seismic pavement analyzer (D-SPA), soil stiffness gauge (SSG)). FWD and DCP tests are recommended in the newly introduced pavement design guide (AASHTO 2008) to estimate the design input parameters (e.g., CBR, elastic or resilient modulus) from empirical relationships. Although there are guidelines in the design guide on how these different measurements are related, the relationships are not thoroughly understood in a mechanistic standpoint. LWD which is a portable version of FWD is being increasingly considered as a QC/QA tool by highway agencies across the globe. Recent research showed that LWD measurements are significantly influenced by the type of mechanical sensors used on the devices and operating conditions (see Fleming 2000, White et al. 2007a). To aid in effective implementation of these devices into construction QC/QA practice, a thorough study investigating the factors influencing the measurements and relationships with conventionally used modulus test measurements (PLT or FWD) is warranted.

A significant improvement over the above described conventional in-situ discrete point measurement methods is roller-integrated compaction monitoring (RICM) which offers 100% coverage with real-time data visualization (also referred to as intelligent compaction or continuous compaction control). Specifications have been proposed by many highway agencies for implementing RICM technologies into earthwork construction (*see* ZTVE-StB 1994, RVS 8S.02.6 1999, ATB Väg 2004, ISSMGE 2005, Mn/DOT 2006). RICM for vibratory soil compactors was initiated some 30 years ago in Europe for compaction of mostly granular materials (see Forssblad 1980, Thurner and Sandström 1980). There are different manufacturers of vibratory-based technologies and they all make use of accelerometers mounted to the roller drum to create a record of machine-ground interaction. The analysis approaches have been explained by others (e.g., Adam 1997, Brandl and Adam 1997, Sandström and Petterson, 2004). Recently, a new measurement technology termed as machine drive power (MDP) has been developed for use in granular or cohesive soils and is based on the principal of rolling resistance due to drum sinkage. The approach has the

advantage of working in both the vibratory and static modes. A significant amount of research was conducted on evaluating the MDP measurement technology at Iowa State University since 2004 (see White et al. 2005, White et al. 2007b, White and Thompson 2008, Thompson and White 2008) prompting its application on a full-scale pavement foundation layer construction project in Minnesota (see Chapter 4).

Many scholarly articles have been published over the past three decades presenting relationships between different RICM technologies and soil physical and mechanical properties (Turner and Sandström 1980, Forssblad 1980, Floss *et al.* 1983, Samaras et al. 1991, Brandl and Adam 1997, Kröber *et al.* 2001, Preisig *et al.* 2003, Thompson and White 2008, White and Thompson 2008, White *et al.* 2005, 2007a, 2007b, 2008a, 2008b). Considering the increasing demand in implementation of these technologies and significant knowledge gap between researchers and practicing engineers on how these measurements are correlated with conventionally used in-situ test measurements (see survey results in White 2008), there is still much need for detailed field investigations. This research investigated relationships between two RICM measurements (accelerometer-based compaction meter value (CMV) and MDP) and conventionally used strength/stiffness measurements (FWD, LWD, PLT, DCP, and test rolling rut depths).

Spatially referenced RICM measurements offer a unique opportunity to construct more “uniform” foundation layers. Non-uniform support conditions can contribute to distresses in pavement layers causing fatigue cracks at the surface (see White et al. 2004). To date, most RICM specifications provide QC/QA criteria are based on univariate statistics (mean, standard deviation, etc.) which do not address the issue of uniformity in a spatial standpoint. Using geostatistical methods in analyzing RICM measurements to characterize non-uniformity of constructed pavement foundation layers and its potential to help improve process control (or QC) during construction are explored as part of this research.

1.2 Research Objectives and Anticipated Benefits

The primary objectives of this research are to: (a) investigate factors influencing the LWD measurements and relationships with conventionally used modulus measurements to

aid in effective implementation of these devices into construction QC/QA practice (b) analyze spatially referenced RICM measurements using geostatistical methods to characterize non-uniformity and develop methods that can potentially improve process control during construction, (c) develop correlations between RICM measurements and different conventionally used in-situ test measurements, (d) develop an understanding on factors influencing these correlations in a mechanistic stand point.

The results from this research are expected to benefit geotechnical, pavement, and construction engineering researchers and practitioners working in the field of soil compaction. Achieving the objectives is anticipated to promote and aid in effective implementation of RICM and different in-situ testing technologies into earthwork construction practice and help build long-lasting pavement foundation layers.

1.3 Thesis Organization

This dissertation is comprised of four scholarly papers that have been submitted to geotechnical and pavement engineering related peer reviewed journals for publication. Each paper appears as a dissertation chapter and includes reference to pertinent literature, significant findings based on field and laboratory investigations, conclusions, and recommendations. Following these chapters, most significant research findings and recommendations for future work is provided.

The first paper (Chapter 2) presents a comprehensive review of literature related to LWD devices, experimental test results comparing three different LWD devices (Dynatest, Keros, and Zorn), demonstrating the influence of plate diameter, plate contact stress, buffer stiffness, and measurement techniques on different soil types. Although the three LWD devices used exhibit similarities in operation and methodology, there are differences on how plate contact stresses and deflections are measured, leading to differences in calculated modulus values. Plate diameter, plate contact stress, are found to significantly influence the LWD modulus values. Relationships between LWD modulus and more commonly used static PLT modulus are presented.

The second paper (Chapter 3) presents geostatistical analysis of RICM with an

overview of the semivariogram modeling procedures, key aspects to consider during analysis, and results of analysis from two case studies. First case study demonstrates the importance of exploratory data analysis of RICM data to determine non-stationary field situations, and the second case study demonstrates the advantage of semivariogram modeling to gain better understanding of compaction process and a new approach to improve process control during construction. Use of geostatistical analysis and spatially referenced RICM represent a paradigm shift in how compaction analysis and specifications could be implemented in the future.

The third paper (paper 3) presents experimental results from a field study conducted on US 60 in Minnesota assessing the support conditions of cohesive subgrades using heavy test rolling, RICM, LWD, and DCP. The study explores the use of LWD, DCP, and RICM as possible alternatives to heavy test rolling rut depth measurement that is traditionally used for QA by Minnesota Department of Transportation (see Mn/DOT 2000). Results indicate that the alternative technologies can reliably indicate the support conditions of the cohesive subgrades and are empirically related to rut measurements. Support capacities under test roller tire are analyzed using layered bearing capacity solutions and compared to rut measurements. A simple chart solution is developed that can be used by field engineers to determine target undrained shear strength properties of compacted subgrades from DCP profiles.

The fourth paper (paper 4) presents experimental test results comparing FWD, LWD, DCP, CPT, and RICM on granular pavement foundation layers. In-ground vertical and horizontal stresses developed under roller, FWD, and LWD loading were measured as a means to better understand and interpret the relationships between different measurements. Significant differences are noticed in the stress states and stress paths in the foundation layers under roller, FWD, and LWD loading. In-sights into differences in measurement influence depths between different devices are presented. Some practical considerations and factors influencing the relationships are discussed.

1.4 References

- Adam, D. (1997). “Continuous compaction control (CCC) with vibratory rollers.” *Proc., 1st Australia-Newzealand Conf. on Environmental Geotechnics – GeoEnvironment* 97, Melbourne, Australia, 26-28 November.
- Brandl, H., and Adam, D. (1997). “Sophisticated continuous compaction control of soils and granular materials.” *Proc. 14th Intl. Conf. Soil Mech. and Found. Engrg.*, Hamburg, Germany, 1–6.
- ATB Väg. (2004). “Kapitel E - Obundna material VV Publikation 2004:111,” *General technical construction specification for roads*, Road and Traffic Division, Sweden.
- Fleming, P. R., 2000, “Small-scale dynamic devices for the measurement of elastic stiffness modulus on pavement foundations,” *Nondestructive Testing of Pavements and Backcalculation of Moduli, ASTM STP 1375*. Vol. 3, S. Tayabji and E. Lukanen, Eds., ASTM International, West Conshohocken, PA, pp. 41–58.
- Forssblad, L. (1980). “Compaction meter on vibrating rollers for improved compaction control”, *Proc. Intl. Conf. on Compaction*, Vol. II, 541-546, Paris.
- Floss, R., Gruber, N., Obermayer, J. (1983). “A dynamical test method for continuous compaction control.” *Proc. of the 8th Euro. Conf. on Soil Mech. and Found. Engg.* H.G. Rathmayer and K. Saari, Eds., May, Helsinki, 25-30.
- Handy, R.L., Spangler, M.G. (2007). *Geotechnical Engineering: Soil and Foundation Principles and Practice*. 5th Edition, McGraw Hill, New York.
- Killingsworth, B., and Quintas, H.V. (1996). *Backcalculation of Layer Moduli of SHRP-LTPP General Pavement Studies (GPS) sites*, Report No. FHWS-RD-97-086, Federal Highway Administration, Washington, D.C. July.
- ISSMGE. (2005). *Roller-Integrated continuous compaction control (CCC): Technical Contractual Provisions, Recommendations*, TC3: Geotechnics for Pavements in Transportation Infrastructure. International Society for Soil Mechanics and Geotechnical Engineering.

- Kröber, W., Floss, E., Wallrath, W. (2001). "Dynamic soil stiffness as quality criterion for soil compaction," *Geotechnics for Roads, Rail Tracks and Earth Structures*, A.A.Balkema Publishers, Lisse /Abingdon/ Exton (Pa) /Tokyo, 189-199.
- Mn/DOT. 2000. *Standard Specifications for Construction – Specification 2111 Test Rolling*. Minnesota Department of Transportation (Mn/DOT), St. Paul, MN.
- Mn/DOT. 2006. *Excavation and Embankment – Quality Compaction by IC, LWD, and Test Rolling (Pilot Specification for Embankment Grading Materials)*. S.P. 5305-55, Minnesota Department of Transportation (Mn/DOT), St. Paul, Minnesota.
- Newcomb, D.E., Birgisson, B. (1999). *Measuring In Situ Mechanical Properties of Pavement Subgrade Soils*. Synthesis of Highway Practice 278, National Cooperative Highway Research Program, National Academy Press, Washington, D.C.
- Peterson, J.S., Romanoschi, S.A., Hossain, M. (2007). *Development of stiffness-based specifications for in-situ embankment compaction quality control*. Report No. KSU-04-6, Kansas State University, Manhattan, Kansas.
- Preisig, M., Caprez, M., and Ammann, P. (2003). "Validation of continuous compaction control (CCC) methods." *Workshop on Soil Compaction*, September, Hamburg.
- Proctor, R. R. (1933). "Fundamental principles of soil compacton." *Engineering News Record*, Vol. III, August.
- RVS 8S.02.6. (1999). "Continuous compactor integrated compaction – Proof (proof of compaction)," *Technical Contract Stipulations RVS 8S.02.6 – Earthworks*, Federal Ministry for Economic Affairs, Vienna.
- Samaras, A., Lamm, R., and Treiterer, J. (1991). "Application of continuous dynamic compaction control for earthworks in railroad construction." *Transp. Res. Rec.*, No. 1309, Journal of the Transportation Research Board, 42-46.
- Sandström A. J., Pettersson, C. B., (2004). "Intelligent systems for QA/QC in soil compaction", *Proc. TRB 2004 Annual Meeting (CD-ROM)*, Transportation Research Board, Washington, D. C.

- Seed, H.B., and Chan, C.K. (1959). "Structure and strength characteristics of compacted clays," *J. of the Soil Mech. and Found. Div.*, ASCE, 85, No. SM5, 87-128.
- Seed, H.B., Mitchell, J.K., and Chan, C.K. (1961). "The strength of compacted cohesive soils," *Shear Strength of Cohesive Soils*, ASCE, Boulder, CO, 877-964.
- Selig, E.T. (1982). "Compaction procedures, specifications, and control considerations." *Transp. Res. Rec.*, No. 897, Journal of the Transportation Research Board, 1-8.
- Thompson, M., and White, D. (2008). "Estimating compaction of cohesive soils from machine drive power." *J. of Geotech. and Geoenviron. Engg.*, ASCE (in press).
- Turner, H. and Sandström, Å. (1980). "A new device for instant compaction control." *Proc. of the Intl. Conf. on Compaction*, Vol II: 611-614, Paris.
- Walsh, K. D., Houston, W.N., and Houston, S.L. (1997). "Field implications of current compaction specification design practices." *J. of Const. Engg. and Mgmt.*, 123 (4), ASCE, 363-370.
- White, D. J. (2008). *Report of the Workshop on Intelligent Compaction for Soils and HMA*, April 2-4, Des Moines, Iowa.
- White, D. J. Bergeson, K.L., Jahren, C.T., Wermager, M. (1999). *Embankment Quality: Phase II*. Final Report Iowa DOT Project TR-401, CTRE Project 97-8, Iowa State University, Ames, Iowa.
- White, D. J., Bergeson, K.L., Jahren, C.T. (2002). *Embankment Quality: Phase III*. Final Report Iowa DOT Project TR-401, CTRE Project 97-8, Iowa State University, Ames, Iowa.
- White, D. J., Rupnow, T., and Ceylan, H. (2004). "Influence of subgrade/subbase nonuniformity on pavement performance." *Proc., Geo-Trans 2004 – Geotechnical Engineering for Transportation Projects*, Geotechnical Special Publication No. 126, ASCE, Los Angeles, Ca., 1058–1065.
- White, D. J., Jaselskis, E., Schaefer, V., Cackler, T. (2005). "Real-time compaction monitoring in cohesive soils from machine response." *Transp. Res. Rec.*, No. 1936,

- Journal of the Transportation Research Board, Washington D.C., 173–180.
- White, D. J., Thompson, M., Vennapusa, P. (2007a). *Field study of compaction monitoring systems – Tamping foot 825 and vibratory smooth drum CS-533E rollers*. Final Report, Center of Transportation Research and Education, Iowa State University, Ames, Ia.
- White, D.J., Thompson, M. & Vennapusa, P. (2007b). *Field validation of intelligent compaction monitoring technology for unbound materials*. Final Report MN/RC-2007-10, Minnesota Department of Transportation, St. Paul, MN.
- White, D. J., Larsen, B.W., Jahren, C.T., Malama, J. (2007c). *Embankment Quality: Phase IV*. Final Report IHRB Project TR-492, CTRE Project 03-136, Iowa State University, Ames, Iowa.
- White, D., and Thompson, M. (2008). “Relationships between in-situ and roller-integrated compaction measurements for granular soils.” *J. of Geotech. and Geoenv. Engg.*, ASCE (in press).
- White, D., Thopmson, M., Vennapusa, P., and Siekmeier, J. (2008a). “Implementing intelligent compaction specifications on Minnesota TH 64: Synopsis of measurement values, data management, and geostatistical analysis.” *Transp. Res. Rec.*, No. 2045, Journal of the Transportation Research Board, 1-9.
- White, D., Vennapusa, P., Gieselman, H. (2008b). “Roller-integrated compaction monitoring technology: Field evaluation, spatial visualization, and specifications.” *Proc., 12th Intl. Conf. of Intl. Assoc. for Computer Methods and Advances in Geomechanics (IACMAG)*, 1-6 October, Goa, India (accepted).
- Zambrano, C., Drnevich, V., Bourdeau, P. (2006). *Advanced Compaction Quality Control*. Report No. FHWA/IN/JRTP-2006/10, Joint Transportation Research Program, Purdue University, West Lafayette, Indiana.
- ZTVE-StB. (1994). “Flächendeckende dynamische Prüfung der Verdichtung,” *Technische Prüfvorschriften für Boden und Fels im Straßenbau*, FGSV-Nr 599, FGSV Verlag GmbH, Köln (in German).

CHAPTER 2. COMPARISON OF LIGHT WEIGHT DEFLECTOMETER MEASUREMENTS FOR PAVEMENT FOUNDATION MATERIALS

Pavana K R. Vennapusa and David J. White

A paper submitted to the Geotechnical Testing Journal, ASTM

2.1 Abstract

Light weight deflectometers (LWDs) are increasingly being used in earthwork QC/QA testing to provide rapid determination of elastic modulus, which is an essential input for mechanistic pavement design. To successfully implement the use of these devices, it is important to understand how operating conditions affect the measurements and if differences exist between the various manufacturer devices. This paper provides a review of basic principles, different manufacturer LWD equipment, and correlations between LWD elastic modulus (E_{LWD}) and moduli determined from other in-situ testing devices. Comparison test measurements for three different LWD devices with different plate diameters, plate contact stresses, buffer stiffnesses, and measurement techniques, and correlations with static plate load test measurements are reported in this paper.

2.2 Introduction

Light weight deflectometers (LWDs) are increasingly being considered by state and federal agencies in the United States and several countries around the world for earthwork QC/QA testing. These in-situ testing devices can be used to rapidly determine elastic modulus, which provides an alternative to more time-consuming in-situ tests (e.g., static plate load test) and an input parameter for mechanistic pavement design. LWD elastic modulus (E_{LWD}) is calculated using elastic half-space theory, knowing plate contact stress and deflection, and making an assumption for stress distribution. Although most of the devices exhibit similarities in operation and methodology, there are differences in how plate contact stresses and deflections are determined. This leads to differences in the calculated E_{LWD} values. Currently, LWD devices are commercially available from at least four manufacturers

(Gerhard Zorn, Carl Bro Pavement Consultants, Dynatest International, and Al-Engineering). The LWD device components generally consist of a 100- to 300-mm diameter loading plate with a 10- to 20-kg drop weight, an accelerometer or geophone to determine deflection, and a load cell or calibrated drop height to determine plate contact stress. To successfully develop specifications and implement use of these devices, it is important to understand for what conditions they provide reliable measurements and also if differences exist between the various devices. This paper summarizes an extensive review of the literature and reports new comparison measurements between three different LWD devices, showing the influences of plate diameter, contact stress, and buffer stiffness, and correlations between static plate load test and LWD measurements.

2.3 Theoretical Determination of Elastic Modulus

Based on the well known Boussinesq elastic solution, the relationship between applied stresses and displacement in the soil for the case of a rigid or flexible base resting on an elastic half-space can be derived as follows:

$$E = \frac{(1-\nu^2)\sigma_0 a}{d_0} \times f \quad (2.1)$$

Where:

E = elastic modulus (MPa)

d_0 = measured settlement (mm)

ν = Poisson's Ratio

σ_0 = applied stress (MPa)

a = radius of the plate (mm)

f = shape factor depending on stress distribution (see Table 2.1)

All of the LWD devices use elastic half-space theory and the assumptions of stress distribution to calculate elastic modulus from a measured (or assumed) contact stress and peak deflection of the loading plate or the soil directly under the center of the plate. Some

LWD manufactures (e.g., Prima and Dynatest) give users the option of selecting the shape factor, while such an option is not available with other manufacturers (e.g., the Zorn and Loadman device assumes a fixed stress distribution factor of 2). It is well known that the stress distribution under a plate depends on both plate rigidity and soil type (Terzaghi and Peck 1967). Three different stress distributions are generally possible (inverse parabolic, parabolic, and uniform), as shown in Table 2.1. Results presented by Mooney and Miller (2008) further show that the stress distribution under a “rigid” LWD plate is dependent on soil type as well as soil profile (based on tests using CSM LWD device, see Table 2). Tests performed using a 300-mm diameter LWD with a contact force of 8.8 kN over a sand layer (250 mm thick) underlain by a clay layer showed a uniform stress distribution, while tests performed over two sand layers (240 mm thick each) underlain by a clay layer showed close to a parabolic stress distribution. From Eq. 1, the ELWD results can vary by 127% or 170% depending on the assumed stress distribution factor f (see Table 2.1).

2.4 Comparison of In-Situ LWD Test Devices

Seven LWD devices are commonly addressed in the literature; Table 2.2 summarizes some of their key features. Several researchers have reported correlations between LWD measurements and other in-situ test measurements, i.e., initial or reload modulus from static plate load test (E_{V1} or E_{V2}), modulus from falling weight deflectometer test (E_{FWD}) measurements, etc. (see Table 2.3). Variations in E_{LWD} for different devices have been documented (see Fleming et al. 2000, Hildebrand 2003). These differences are partly attributed to different load pulse shapes and to differences in deflection transducers (Fleming et al. 2000). There are several other factors, however, that could affect the E_{LWD} values; they are discussed in detail below.

2.5 Factors Influencing E_{LWD} Measurements

Factors that influence E_{LWD} values include size of loading plate, plate contact stress, type and location of deflection transducer, plate rigidity, loading rate, buffer stiffness, and measurement of load versus assumption of load based on laboratory calibration from a

standardized drop height. The ways in which these factors influence the modulus are treated separately and are discussed in the following sections.

2.5.1 Size of Loading Plate

Terzaghi (1955) proposed Eqs. 2.2 and 2.3 to estimate modulus of subgrade reaction (k_s) for different footing sizes from plate load tests. According to these equations, modulus of subgrade reaction determined from a 200-mm plate is approximately 1.45 times (for sand) to 1.50 times (for clay) greater than that from a 300-mm plate. Fig. 2.1 shows the influence of plate diameter with comparisons to experimental data presented by several researchers using static plate load tests and LWDs to Terzaghi's theoretical relationships (Eqs. 2.2 and 2.3). Results are shown by plotting the modulus of subgrade reaction (k_s) or elastic modulus (E or E_{LWD}) normalized to a 300-mm diameter plate.

$$k_s = k_1 \times \left[\frac{B_1}{B} \right] \quad \text{[for footings on clay]} \quad (2.2)$$

$$k_s = k_1 \times \left[\frac{B + B_1}{2B} \right]^2 \quad \text{[for footings on sand]} \quad (2.3)$$

Where:

B_1 = side dimension of a square plate used in load test (m)

B = width of footing (m)

k_s = modulus of subgrade reaction (kPa/m)

k_1 = stiffness estimated from a static plate load test (kPa/m)

Lin et al. (2006) conducted Prima LWD tests on a natural sandy soil deposit (AASHTO classification: A-1-b) and found that E_{LWD} for a 100-mm plate was approximately 1.5 to 1.6 times higher than for a 300-mm plate at similar applied loads. Chaddock and Brown (1995) reported test results by the TRL Foundation Tester (TFT) on crushed rock base and subbase materials underlain by compacted clay materials. For the same unit stress, E_{LWD-T2} (200-mm plate) was 1.2 to 1.4 times higher than E_{LWD-T3} (300-mm plate).

The manufacturer of Prima LWD suggests selecting plate sizes based on the material stiffness. For example, when the E_{LWD} is less than 125 MPa, the recommended plate size is 300 mm. For E_{LWD} between 125 and 170 MPa and $E_{LWD} > 170$ MPa, the 200-mm and 100-mm diameter plates, respectively, are recommended. By reducing the plate size with increasing modulus, it is possible to increase the plate contact stresses and therefore increase deflections to within a measurable range. Also, by using a larger plate for lower stiffness materials, the possibility of excessive deflection and bearing capacity failure can be avoided.

2.5.2 Plate Contact Stress

Fleming et al. (2000) investigated the influence of plate contact stress using the TFT and the Prima LWD by altering the drop height on gravelly silty clay subgrade and granular capping layers. Results showed that E_{LWD-P3} increased by approximately 1.15 times, while E_{LWD-T3} increased by approximately 1.3 times with increasing plate contact stress from 35 kPa to 120 kPa. In contrast, Lin et al. (2006) concluded that the effect of drop height on E_{LWD-P1} and E_{LWD-P3} is insignificant based on tests on a natural sandy soil deposit using Prima LWD. Camargo et al. (2006) showed that by increasing the drop height from 25 to 75 cm, the E_{LWD-K2} values increased, on average, approximately 1.1 times on a compacted granular material (AASHTO classification: A-1-b). Based on tests conducted on very stiff crushed aggregate and stabilized aggregate material ($E_{LWD-E3} = 59$ to 82 MPa), van Gurp et al. (2000) reported that E_{LWD-E3} values did not vary significantly ($< 3\%$ change) for a plate contact stress range of 140 to 200 kPa. Chaddock and Brown (1995) observed that the $E_{LWD-T2/3}$ decreased with increasing plate contact stresses at locations of thin granular capping (150 mm) over softer clay subgrade, and increased at locations of thicker granular layers.

Based on the discussion above, it appears that for dense and compacted granular materials, the E_{LWD} values tend to increase with increasing contact stresses, except where the values are influenced by underlying softer subgrade materials. Some materials with cementitious properties, however, may not be as sensitive to changes in contact stress (e.g., materials described in van Gurp et al. 2000). Some experimental test results from this study are presented later in this regard.

2.5.3 Type and Location of Deflection Sensor

Different deflection sensors and mounting positions are used by the various manufacturers. The Zorn device, for example, has an accelerometer built into the plate from which the readings are twice integrated to calculate deflection of the plate. Conversely, Keros, Prima, and TFT devices use a spring-loaded geophone in direct contact with the ground surface through a hole in the center of the plate. These differences apparently contribute to differences in the determined plate deflection. Fleming et al. (2002) indicated that the transducer mounted on the bearing plate will also record the initial acceleration of the plate, as opposed to one mounted on the soil. Therefore, devices with accelerometers that measure deflections on the plate are expected to measure larger deflections, which have been documented in several field studies (Weingart 1993; Shahid et al. 1997; ZTVA-StB 1997; Groenendijk et al. 2000; Livneh and Goldberg 2001; Hildebrand 2003), including this study described later.

2.5.4 Plate Rigidity

An assessment of LWD plate rigidity is important for predicting stress distribution under the plate and consequently for selecting the shape factor f used in Eq. 2.1. LWD manufacturers produce plates of different thicknesses and materials (see Table 2.2), and therefore rigidity. No discussion has been provided by the manufactures on the impact of the respective plate rigidities. As a point of reference, for pavement design or evaluation purposes, ASTM D1195-93 describes static plate load testing as using a 762 mm diameter plate with a 25.4 mm thick base plate and an additional four plates (152 to 762 mm in diameter) arranged in a pyramid fashion to “ensure rigidity”. But, no discussion is provided therein that quantifies rigidity or establishes a minimum requirement for rigidity. Further, a provision is allowed to conduct plate load tests using just a single 25.4 mm thick plate of any diameter for comparison purposes. A valid question is then to what extent are the various plate configurations considered rigid. To answer this question, the authors investigated an analytical solution developed by Borowicka (1936) wherein the relative rigidity of the plate is determined from Eq. 2.4. The relative rigidity constant K (Eq. 2.4) here is not only a function of the plate geometry and material properties but also as a function of the ratio of

the elastic modulus of the plate to the soil. Using Eq. 2.5, the relationships between soil elastic modulus, E_s , and K for Zorn and Keros/Dynatest device LWD plates with 300 and 200 mm plate diameters are presented in Fig. 2.2. For $K = 0$, the contact stress distribution under the footing is uniform and the plate is considered flexible. For $K > 0$, the contact stresses at the edge of the plate theoretically increase to infinity and stresses at the center of the plate vary with K . For $K = \infty$ (i.e., when the plate is perfectly rigid), the contact stresses at the center of the plate are 50% of the applied stress. By evaluating the relative rigidity as a function of soil modulus it can be seen that as the soil modulus decreases as the relative rigidity of the plate increases. Also, also as the plate diameter decreases for a given soil modulus, the relative rigidity increases. For the analysis presented in this paper, the various plates were assumed to behave as rigid to facilitate comparisons, but it is clear that a single assumption may not always be valid for a wide range of soil elastic modulus and plate diameters. To compensate for relative rigidity, change in contact stress distributions and the corresponding shape factor f (f changes from 2 to $\pi/2$ with change in K value from 0 to ∞) could be implemented. However, quantifying the rate of change in f with K is based on many assumptions and is beyond the scope of this paper.

$$K = \frac{1}{6} \frac{(1-\nu^2)}{(1-\nu_p^2)} \frac{E_p}{E_s} \left(\frac{h}{a}\right)^3 \quad (2.4)$$

where:

K = relative rigidity constant

E_p = modulus of elasticity of the plate material (MPa) (assumed as 193050 MPa for Zorn steel plate and 110310 MPa for Keros/Dynatest aluminum plates (Kent 1895))

E_s = modulus of elasticity of the soil (MPa)

ν_p = Poisson's ratio of the plate material (assumed as 0.3 for Zorn steel plate and 0.33 for Keros/Dynatest aluminum plates (Kent 1895))

ν = Poisson's ratio of the soil

h = thickness of the plate (m)

a = radius of the plate (m)

2.5.5 Load Transducer

Some devices (e.g., Zorn and Loadman) assume a constant applied force based on calibration tests performed on a stiff (e.g. concrete) surface, while other devices (e.g., Prima and Keros) measure the actual applied load using a load cell. Theoretically, the applied force on a surface cannot be constant, as it clearly depends on the stiffness of the material on which the load is applied (see Eq. 2.5). However, as the LWDs are commonly utilized for testing compacted layers that are relatively stiff, any error associated with the assumption of a constant applied force in calculations may not be practically significant. Davich (2005) reported laboratory test measurements to investigate error introduced from using an assumed applied load and concluded that the assumption of constant force can lead to an over-estimation of E_{LWD} in the range 4 to 8 %, based on testing soft to very stiff materials. Field and laboratory test results presented by Brandl et al. (2003), and Kopf and Adam (2004) using the Zorn LWD demonstrated that the assumption of constant applied force is reasonable. Results presented in this study also support this conclusion.

$$F = \sqrt{2 \times m \times g \times h \times C} \quad (2.5)$$

Where:

F = Applied force (kN)

m = mass of falling weight (kg)

g = acceleration due to gravity, 9.81 (m/s²)

h = drop height (m)

C = material stiffness constant (N/m)

2.5.6 Loading Rate and Stiffness of Buffer

With using elastic half-space theory in the E_{LWD} estimation procedure, the maximum transient deflection is assumed equivalent to the maximum deflection from a static plate of similar diameter and applied stress. Some studies, however, indicate that the rate of loading

affects E_{LWD} . The loading rate can be controlled by varying the stiffness of the buffer placed between the drop weight and contact plate. Fleming (2000) reports that a comparatively lower stiffness buffer provides more efficient load transfer and better simulates static plate loading conditions. Lenngren (1992) reports that with using a stiffer buffer, the load pulse time history is shortened, and the resulting E_{FWD} is increased by 10 to 20 % on some asphalt concrete pavements, while other locations showed little or no difference. Lukanen (1992) indicated that the shape of the load pulse and its rise and dwell time during an FWD test can affect the magnitude of the measured deflections to some extent but may not be considered “practically” significant. According to Adam and Kopf (2002), the applied load pulse can vary by about 30% with a change in rubber buffer temperature from 0 to 30°C, while remaining more constant for a steel spring buffer.

2.6. Experimental Comparison of LWD Devices from the Authors’ Study

2.6.1 Light Drop Weight Tester – ZFG 2000

The ZFG 2000 LWD device is manufactured by Gerhard Zorn, Germany, and is prescribed in German specifications for road construction (TP BF-StB Teil B 8.3, 1992). A schematic of this device is shown in Fig. 2. 3. The device is programmed for Poisson’s ratio of 0.5 and a uniform stress distribution shape factor $f = 2$. Based on the manufacturer’s calibration tests, the drop height was set at 72 cm to achieve an applied load of 7.07 kN. Deflections are measured via an accelerometer built in to the loading plate. Following three seating drops, deflection measurements are recorded during the execution of the last three load pulses and averaged (Zorn, 2003). Further technical details of the device are summarized in Table 2.2. If the user chooses a different drop height, the constant force value can be estimated using Eq. 2.5 with a spring stiff constant $C = 362396$ N/m (M. Weingart, personal communication, November 2006). Differences between the theoretical and experimental applied force will exist if the spring buffers behave non-linearly during loading.

The Zorn device was based on extensive model calculations and parametric studies performed by Weingart (1977). This device is recommended for use on stiff cohesive soils, mixed soils, and coarse-grained soils having maximum particle size of 63 mm (Zorn 2003).

Field tests are performed by placing the plate on flat ground in a way that full contact between the plate and the surface is achieved. The manufacturer suggests using a thin layer of sand at locations where a flat contact surface cannot be obtained.

2.6.2 Keros and Dynatest 3031 Portable Falling Weight Deflectometers

The Keros and Dynatest 3031 LWD devices are manufactured by Dynatest, Denmark. The Dynatest 3031 LWD model is a recently produced version by Dynatest. A schematic of these two devices are shown in Fig. 2.3. These devices are equipped with a load cell to measure the impact force from the falling weight and a geophone to measure induced deflections at the ground surface. Additional geophones can be added to obtain a deflection basin. The load and geophone sensors are connected to an electronic box to store and transmit the data either to a pocket PC or a laptop with Bluetooth[®] capability. Software provided with the device allows the user to enter Poisson's ratio and an appropriate stress distribution factor, depending on the soil conditions (Dynatest, 2004). Primary differences between the two models are the type and stiffness of rubber buffers. Conical-type rubber buffers are used in the Keros device, while two layered flat rubber buffers are used in the Dynatest 3031 device (Buffer A&B, see Fig. 2.3). The conical buffers used in the Keros device can be used in combinations of two or four. Laboratory tests were performed to determine the buffer stiffnesses. The rubber buffer stiffness is non-linear with increasing load. For a force range of 1 to 7kN, the stiffness for the Keros two buffer setup ranges between 170 N/mm to 440 N/mm, and the four buffer setup ranges between 290 N/mm and 700 N/mm. For the Dynatest 3031 device, if only Buffer A was used, the stiffness range was between 150 N/mm to 700 N/mm, and if both Buffers A and B were combined, the range was between 90 N/mm to 500 N/mm for a force range of 1 kN and 7 kN, respectively. Technical details of the two models are provided in Table 2.2.

2.6.3 Static Plate Load Test

Static plate load tests were conducted in field study 7 by applying a static load on a 300 mm diameter plate against a 6.2kN capacity reaction force. The applied load was measured using a 90-kN load cell and deformations were measured using three 50-mm linear voltage displacement transducers (LVDTs). The load and deformation readings were

continuously recorded during the test using a data logger. Initial and reload modulus (E_{V1} and E_{V2}) were determined using Eq. 2.1 for a stress range of 0.2 to 0.4 MPa.

2.6.4 Field Studies

Comparison tests using the Zorn, Keros, and Dynatest LWD devices, and static plate load device were performed at several pavement foundation construction project sites. Comparison tests at these project sites were performed within a spacing of approximately 0.7 m or less to minimize variation in soil properties between test locations. Tests were performed by preloading each testing area with three load pulses and measuring the average deflection for the succeeding three load pulses. To investigate the differences in E_{LWD} values, assumptions made in the calculations (e.g., Poisson's ratio and shape factors) and the test procedures were kept identical. Table 2.4 lists the field test procedures and the parameters used in the calculations. The devices were set up with 200- and 300-mm plate diameters, and the drop height was varied between 50 and 72 cm. Modulus values were estimated (using Eq. 2.1) for the last three drops by using the measured applied force and deflection values for the Keros and Dynatest devices, and an assumed constant force depending on the drop height (see Eq. 2.4) and measured deflection values for the Zorn device. The average estimated modulus of the last three drops was reported as the E_{LWD} value at a test point.

The primary objectives of the field investigations were to evaluate: (a) differences between LWD devices of similar plate diameters, (b) correlations between LWD and static plate load test modulus, (b) the influence of plate diameter (100, 150, 200 and 300 mm) and applied stress on modulus, and (c) the influence of buffer stiffness of modulus. A summary of soil index properties for each site is provided in Table 2.5.

2.6.5 E_{LWD} comparison between different LWDs and static plate load E_{V1} and E_{V2}

Comparison results between modulus measured by different devices are shown in Fig. 2.4. Linear regression relationships and associated R^2 values are also presented in Fig. 2.4. On average, E_{LWD-K2} and E_{LWD-D2} are approximately 1.75 and 1.56 times greater than E_{LWD-Z2} , respectively, with R^2 values around 0.8 to 0.9 (Fig. 2.4a, 2.4c); while E_{LWD-K3} is

approximately 2.16 times greater than E_{LWD-Z3} with a relatively poor R^2 value of 0.5 (Fig. 2.4b). A similar trend of lower modulus (by factor of about 2 times) from the Zorn device was observed in a study conducted by the Danish Road Directorate (Hildebrand 2003) when compared with the Keros. Others have also reported that the moduli from Zorn is generally in the range of about 0.5 to 0.6 times lower, compared to other LWD devices and FWD that employ load cell and geophone displacement sensors (e.g. Fleming et al. 2000 and 2002).

Comparison between deflection measurements from Zorn and Keros devices (Field Study 1) are presented in Fig. 2.5a, which shows that that the measurements from Zorn are on average 1.5 times higher than the Keros. The differences in E_{LWD} between Keros and Zorn are believed to be related to the following: a) the higher deflections from the Zorn (or lower from Keros), and (b) the assumption of constant applied force of 6.96 kN, in the case of the Zorn device versus measured loads for the Keros. However, the primary contributor to differences in E_{LWD} values is the difference in deflection values, as the constant assumed load of 6.69 kN by Zorn is comparable to the average load from the Keros (i.e., 6.56 kN, as shown in Fig.2.5b).

Fig. 2.4d presents comparison between E_{LWD} measurement values by Dynatest and Keros devices that were set up with 50-cm drop height. A best-fit linear regression with a slope of 1 and an R^2 value of about 0.93 is observed between the two measurements. Note that although the drop height is similar, due to differences in buffer stiffnesses, the applied impact force is not the same. A frequency distribution plot of measured impact force by the two devices for test measurements from Field Study 4 is shown in Fig. 2.6. On average, the Dynatest impact force was about 0.63 times lower than the Keros impact force. The estimated impact force for Zorn at 50-cm drop height is also shown on Fig. 2.6 for reference. Despite differences in the impact force between the two devices, no pronounced difference was observed between the calculated E_{LWD} values. The influence of applied stress and buffer stiffness is discussed later in this paper.

Fig. 2.4e, 3f shows correlations between E_{V1} , E_{V2} and E_{LWD-Z2} . Results showed relatively better correlations between E_{LWD-Z2} and E_{V1} with $R^2 = 0.7$ than between E_{LWD-Z2}

and E_{V2} where $R^2 = 0.4$. Similar relationship between E_{LWD-Z3} and E_{V2} was reported by Weingart (1993) (see Table 2.3).

2.6.6 Variability of E_{LWD} measurements

In earthwork acceptance testing, to achieve good reliability and confidence in test measurements, it is important to plan and calculate the number of tests depending on the variability of the measurements. The sources of this variability generally include inherent variability in soil properties, sensitivity of the device, operation errors, and repeatability of the measurements. Soil variability is the dominating factor, however, when it comes to measurement variability. The most commonly used statistical parameters in geotechnical engineering for description of variability are the standard deviation (σ) and coefficient of variation (COV). Table 2.6 provides a summary of statistics (μ , σ , and COV) for E_{LWD} measurements by the three devices from different field studies. Interestingly, the COV of Zorn E_{LWD} is generally lower, compared to Keros or Dynatest E_{LWD} values, with one exception at field study 3b. Some field studies showed considerable differences in the COV (e.g. field study 2 and 3a).

2.6.7 Influence of Plate Diameter on E_{LWD}

Zorn LWD was set up with 200- and 300-mm diameter plates at field study 2 for side-by-side comparison testing. A total of 46 tests was conducted on a well-graded granular capping layer, which is 50 mm in thickness underlain by sand. Fig. 2.7 shows the difference between E_{LWD-Z2} and E_{LWD-Z3} . A linear regression relationship between the two values is also shown with R^2 value of 0.63. On average, the Zorn device with 200-mm plate resulted in a modulus approximately 1.4 times greater than that with 300-mm plate. This difference in E_{LWD} between two plate diameters is in close agreement with the equation proposed by Terzaghi (1955) (shown in Eq. 2.3, for which a 200-mm plate modulus can be approximately 1.45 times greater than a 300-mm plate modulus) and experimental results presented by others (see Fig. 2.1).

To further investigate the influence of plate diameter, Zorn LWD was tested with four different plate sizes (100-, 150-, 200-, and 300-mm diameter) in field studies 3c and 4, while

Zorn, Keros, and Dynatest LWD devices were tested with 200- and 300-mm plate sizes in field study 5. Tests were conducted with each plate size, using drop heights varying from 10 to 80 cm at increments of 10 cm.

Results from field tests 3c and 4 are presented in Fig. 2.8. The trends indicate that at any level of applied contact stress, the calculated E_{LWD} values increase with decreasing plate size. On average, results from field study 3c show that the E_{LWD-Z2} , $E_{LWD-Z1.5}$, and E_{LWD-Z1} are about 1.3, 1.5, and 1.9 times greater than E_{LWD-Z3} . In field study 4 the average E_{LWD-Z2} , $E_{LWD-Z1.5}$, and E_{LWD-Z1} are about 1.2, 1.3, and 1.3 times greater than that of E_{LWD-Z3} .

LWD tests were conducted using Zorn, Dynatest, and Keros devices with 200- and 300-mm plate sizes at two locations in field study 5. Results from this study are presented in Fig. 2.9. Similar to findings from field study 4, Zorn E_{LWD} values increased with decreasing plate diameter from 300 to 200 mm. On average, the E_{LWD-Z2} is about 1.2 and 1.4 times greater than E_{LWD-Z3} for locations 1 and 2, respectively. On the other hand, E_{LWD} measured by Keros and Dynatest devices increased with decreasing plate diameter at location 1, while an opposite trend was observed at location 2. The E_{LWD-K2} and E_{LWD-D2} are about 1.3 and 1.2 times E_{LWD-K3} and E_{LWD-D3} , respectively, for location 1, while for location 2 the E_{LWD-K2} and E_{LWD-D2} are about 0.8 times E_{LWD-K3} and E_{LWD-D3} .

Based on the above field studies, a general conclusion can be made that the E_{LWD} values are increasing with decreasing plate diameters, which is consistent with observations by others (see Fig. 2.1). For most cases, the ratio of E_{LWD} from a 200- to 300-mm plate is about 1.2 to 1.4. As an exception, in field study 5, the Keros and Dynatest device showed a ratio of <1.0 . On the other hand, the ratio of E_{LWD} from 150-mm and 100-mm plates to E_{LWD} from the 300-mm plate showed considerable differences between field studies 3c and 4 (see Fig. 2.8). These differences can be attributed to the difference in material stiffness; i.e., the ratio generally tends to increase with increasing material stiffness.

2.6.8 Influence of Applied Contact Stress on E_{LWD}

Figs. 2.8 and 2.9 show relationships between applied contact stress and E_{LWD} . Fig. 2.8 shows a strong stress dependency with a consistent increase in E_{LWD-Z} with increasing contact stress for all plate diameters. For field study 3c, an increase in drop height from 10 to

80 cm increased E_{LWD} by 45%, 75%, 93%, and 77%, for 300-, 200-, 150-, and 100-mm diameter plates, respectively. At field study 4, an increase in E_{LWD} by 97%, 79%, 61%, and 54% was observed for 300-, 200-, 150-, and 100-mm diameter plates, respectively.

Fig. 2.9 shows comparison test results from field study 5 with E_{LWD} from Zorn, Keros, and Dynatest LWD devices. Similar to findings from field study 4, the E_{LWD-Z} increased with increase in applied contact stress for both 300- and 200-mm diameter plates. In contrast, both Keros and Dynatest devices showed a decrease in E_{LWD} with increasing contact stress. From the two test locations, on average the E_{LWD-K} decreased by about 32% and 17% with increasing contact stress from 30 to 139 kPa and 67 to 300 kPa for 300-mm and 200-mm plates, respectively. Similarly, on average from two test points, the E_{LWD-D} decreased by about 93% and 91% with increasing contact stresses from 22 to 75 kPa and 48 to 162 kPa for 300 mm and 200 mm plates, respectively.

The results presented above indicate that for the granular materials tested, the Zorn E_{LWD} increases with increasing plate contact stresses. The rate of increase in E_{LWD} , however, is dependent on the stiffness of the material; i.e., stiffer materials yielded a greater increase in modulus with increasing contact stress. Conversely, the Keros and Dynatest device measurements produced the opposite trend. However, the effect of applied stress on Keros and Dynatest E_{LWD} appears to have a comparatively reduced influence (less than about 10%) with increasing contact stresses above 100 kPa (for most QC/QA testing, applied stresses >100 kPa are typically used).

2.6.9 Influence of Buffer Stiffness on E_{LWD}

Steel spring buffers are used in the Zorn LWD device and conical/flat rubber buffers are used in Keros/Dynatest LWD devices (see Table 2.1). These different buffers vary significantly in their stiffness. The Keros device is set up to use two or four rubber conical buffers, and the Dynatest device uses a two-piece, flat rubber buffer (Buffer A and B, see Fig. 2.3). The effect of buffer stiffness on applied load at different drop heights is illustrated in Fig. 2.10. On average, the applied force on Dynatest LWD increased by about 25% by increasing the buffer stiffness (i.e., by removing Buffer B), while the applied force on the

Keros LWD increased by about 20% by increasing the buffer stiffness (i.e., adding two additional buffers (total four buffers)) under the impact load.

The effect of change in buffer stiffness on E_{LWD} measurements is presented in Fig. 2.9. Tests with Keros LWD were conducted by adding two additional buffers to the existing two, and tests with Dynatest LWD were conducted by removing Buffer B to alter the buffer stiffnesses. If the measurement values at same drop height are compared, the E_{LWD-D} and E_{LWD-K} measurement values varied on average by about 8% and 2%, respectively, with change in buffer stiffnesses. However, if the results are compared for similar applied contact stresses, the change in E_{LWD} values are insignificant (<1%).

2.7 Conclusions

An extensive review of literature and experimental test results presented in this paper demonstrate that several issues need to be considered when interpreting an E_{LWD} value to successfully implement the use of the LWD devices in earthwork QC/QA testing. The following are some of the key findings in this paper:

- Major factors that influence E_{LWD} values include: size of loading plate, plate contact stress, type and location of deflection transducer, plate rigidity, loading rate, buffer stiffness, and to some extent the measurement of load versus assumption of a constant load based on laboratory calibration.
- LWD devices that use accelerometers that measure deflection of the plate (e.g. Zorn) are expected to measure larger deflections compared to devices that measure deflections on the ground with a geophone (e.g. Keros/Dynatest and Prima).
- The Keros E_{LWD} is on average 1.75 and 2.16 times greater than Zorn E_{LWD} with 200-mm and 300-mm plate diameters, respectively. The Dynatest E_{LWD} is on average 1.7 times greater than Zorn E_{LWD} with 200-mm plate diameter. The constant applied force of 6.69 kN in the 200-mm Zorn device is comparable with average loads by 200-mm Keros device (6.56 kN) for a drop height of 63 mm. The primary contributor to differences in calculated E_{LWD} is the difference in measured deflections (on average, Zorn deflections are 1.5 times greater than Keros).

- Comparison between Zorn E_{LWD} and plate load test initial modulus (E_{V1}) showed relatively better correlations ($R^2 = 0.7$) compared to correlation between Zorn E_{LWD} and plate load test reload modulus (E_{V2}) ($R^2 = 0.4$). The Zorn E_{LWD} is on average 1.58 times E_{V1} and 0.47 times E_{V2} .
- The COV of Zorn E_{LWD} is observed to be generally lower compared to Keros or Dynatest E_{LWD} values with one exception at field study 3b. Some field studies showed considerable differences in the COV (e.g. field study 2 and 3a). To achieve good reliability and confidence in the test measurements, it is important to plan and calculate the number of tests depending on the variability of the measurements.
- Due to variations in buffer stiffnesses, differences in applied contact stresses should be expected between Keros and Dynatest 3031 devices set up with similar drop heights. Despite the differences in applied stresses, the $E_{LWD-D2(50)}$ and $E_{LWD-K2(50)}$ showed comparable results with a slope of linear regression equation close to 1 and R^2 value of 0.94.
- In general, the E_{LWD} values increase with decreasing plate diameters, which is consistent with observations by other researchers (e.g., Chaddock and Brown 1995; Lin et al. 2006). The ratio of E_{LWD} from 150-mm and 100-mm plates to E_{LWD} from 300-mm plate showed some considerable differences with difference in material stiffness; i.e., the ratio generally tends to increase with increase in material stiffness.
- For the granular materials tested, the Zorn E_{LWD} increases with increasing plate contact stresses with stiffer material presenting a greater increase in E_{LWD} . The Keros and Dynatest devices showed an opposite trend. However, the effect of applied stress on Keros and Dynatest E_{LWD} appear to have less influence (by about 10%) for increase in contact stresses above 100 kPa.
- Variations observed in E_{LWD-D} and E_{LWD-K} by modifying the buffer stiffnesses are insignificant when the results are compared at similar applied contact stresses, for the granular materials tested in field study 5.

2.8 Acknowledgements

The authors would like to acknowledge the support of the Minnesota Department of Transportation (Mn/DOT) and the Federal Highway Administration for sponsoring these field studies. The authors would like to thank John Siekmeier with Mn/DOT for providing helpful insight into LWD testing, and Heath Gieselman, Mark Thompson, Daniel Enz, John Puls, Brad Fleming, and several undergraduate research assistants at Iowa State University for providing assistance with field and lab testing.

2.9 Notations

a	=	Radius of the plate
B	=	Width of footing
B	=	Diameter of plate used in plate load test
C	=	Spring constant
D	=	Flexural rigidity of plate
COV	=	Coefficient of variation
d_0	=	Measured settlement
$d_{LWD-K2(y)}$	=	Deformation measured under a 200-mm diameter plate Keros LWD device with drop height of “y” cm
$d_{LWD-Z2(y)}$	=	Deformation measured under a 200-mm diameter plate Zorn LWD device with drop height of “y” cm
E	=	Elastic modulus
E_s	=	Soil elastic modulus
E_{FWD}	=	Elastic modulus determined using 300-mm diameter plate falling weight deflectometer (FWD) device
E_{LWD}	=	Elastic modulus determined using light weight deflectometer (LWD) device

E_{LWD-E3}	=	Elastic modulus determined using 300-mm diameter plate ELE LWD device
$E_{LWD-K2(y)}$	=	Elastic modulus determined using 200-mm diameter plate Keros LWD device with drop height of “y” cm
$E_{LWD-K3(y)}$	=	Elastic modulus determined using 300-mm diameter plate Keros LWD device with drop height of “y” cm
E_{LWD-LM}	=	Elastic modulus determined using Loadman LWD device
E_{LWD-P3}	=	Elastic modulus determined using 300-mm diameter plate Prima 100 LWD device
E_{LWD-T3}	=	Elastic modulus determined using 300-mm diameter plate TFT LWD device
$E_{LWD-Z2(y)}$	=	Elastic modulus determined using 200-mm diameter plate Zorn LWD device with drop height of “y” cm
$E_{LWD-Z2(y)}$	=	Elastic modulus determined using 300-mm diameter plate Zorn LWD device with drop height of “y” cm
E_p	=	Modulus of elasticity of plate
E_{V1}, E_{V2}	=	Initial or reload modulus, respectively, from 300-mm static plate load test
F	=	Applied force
f	=	Shape factor
g	=	Acceleration due to gravity
h	=	Drop height
k_s, k_{300}	=	Modulus of subgrade reaction from a static plate load test (300 – plate diameter in mm)
k_l	=	Stiffness estimated from a static plate load test
m	=	Mass of falling weight
n	=	Number of tests
μ	=	Statistical mean

ν	=	Poisson's Ratio
ν_p	=	Poisson's ratio of the plate
σ	=	Standard deviation
σ_0	=	Applied stress
σ_0	=	Applied stress

2.10 References

- Adam, D., and Kopf, F., 2002, *Meßtechnische und theoretische Untersuchungen als Grundlage für die Weiterentwicklung und normative Anwendung der dynamischen Lastplatte*. Report No. 68, Lecture: Fairs in the Geotechnik 2002, Braunschweig, Technical University of Braunschweig, Germany, 21–22 February (in German).
- Adam, D., Kopf, F., 2004, "Operational devices for compaction optimization and quality control (Continuous Compaction Control (CCC) and Light Falling Weight Device (LFWD))," *Proc., Intl. Sem. on Geotechnics in Pavement and Railway Design and Construction*, Athens, Greece, pp. 97–106.
- Alshibli, K. A., Abu-Farsakh, M., and Seyman, E., 2005, "Laboratory evaluation of the geogauge and light falling weight deflectometer as construction control tools," *J. Mat. in Civ. Engrg., ASCE*, Vol. 17, No. 5, pp. 560–569.
- ASTM D1195-93, 2004, *Standard Test Method for Repetitive Static Plate Load Tests for Soils and Flexible Pavement Components for Use in Evaluation and Design of Airport and Highway Pavements*, ASTM International, West Conshohocken, PA.
- Brandl, H., Adam, D., Kopf, F., and Niederbrucker, R., 2003, *The Dynamic Plate Loading Test with the Light Drop Weight Equipment*, Research Report, Federal Ministry for Traffic, Innovation, and Technology, Vienna.
- Borowicka, H., 1936, "Influence of rigidity of a circular foundation slab on the distribution of pressures over a contact surface," *Proc., Intl. Conf. on Soil Mech. and Found. Engrg.*, Vol. 2, Harvard University, Cambridge, MA.

- Camargo, F., Larsen, B., Chadbourn, B., Roberson, R., and Siekmeier, J., 2006, "Intelligent compaction: A Minnesota case history," *Proc., 54th Annual University of Minnesota Geotechnical Conf.*, St. Paul, MN.
- Chaddock, B. C. J., and Brown. A., 1995, "In-situ tests for road foundation assessment," *Proc., Unbound Aggregates in Roads – UNBAR 4*. A. Dawson and B. Jones, Eds., Nottingham, U.K.
- Davich, P., 2005, *Analysis of LWD load estimation from measurements of deflection*, Final Report, Minnesota Department of Transportation, St. Paul, MN.
- Dynatest, 2004, *Keros portable FWD – Instruction manual for use and maintenance*, Issue No. 010704, Denmark.
- Fang, H., 1991, *Foundation engineering handbook*, 2nd Ed., Van Nostrand Reinhold, NY, pp. 170–171.
- Fleming, P. R., Rogers, C., Frost, M., 1998, "Performance parameters and target values for construction of UK road foundations," *Fifth Intl. Conf. on the Bearing Capacity of Roads and Airfields*, Trondheim, pp. 1491–1502.
- Fleming, P. R., 2000, "Small-scale dynamic devices for the measurement of elastic stiffness modulus on pavement foundations," *Nondestructive Testing of Pavements and Backcalculation of Moduli, ASTM STP 1375*. Vol. 3, S. Tayabji and E. Lukanen, Eds., ASTM International, West Conshohocken, PA, pp. 41–58.
- Fleming, P. R., Frost, M.W., and Rogers, C., 2000, "A comparison of devices for measuring stiffness in-situ," *Proc., Unbound Aggregates in Road Construction – UNBAR 5*, A. Dawson, Ed., Balkema, Rotterdam, pp. 193–200.
- Fleming, P. R., Lambert J. P., Frost M. W., and Rogers, C., 2002, "In-situ assessment of stiffness modulus for highway foundations during construction," *Proc., 9th Intl. Conf. on Asphalt Pavements*. Copenhagen, Denmark (CD-ROM).

- Groenendijk, J., van Haasteren, C. R., and van Niekerk, A., 2000, "Comparison of stiffness moduli of secondary road base materials under laboratory and in-situ conditions," *Proc., Unbound Aggregates in Road Construction – UNBAR5*, A. Dawson, Ed., Balkema, Rotterdam, pp. 201–208.
- Hildebrand, G., 2003, "Comparison of various types of bearing capacity equipment," *Nordic Road and Transportation Research*, Vol. 15, No. 3, Linköping, Sweden, pp. 12–14.
- Kent, W., 1895, *The mechanical engineers pocket-book*, First Edition, John Wiley & Sons, New York.
- Kim, J., Kang, H., Kim, D., Park, D., and Kim, W., 2007, "Evaluation of in situ modulus of compacted subgrades using portable falling weight deflectometers and plate bearing load test," *J. Mat. in Civil Eng.*, Vol. 19, No. 6, pp. 492–499.
- Kopf, F., and Adam, D., 2004, "Load plate test with the light falling weight device," *Proc., 16th European Young Geotechnical Engineers Conference – EYGEC*, Vienna.
- Lenngren, C., 1992, "Discussion: Effects of buffers on falling weight deflectometer loadings and deflections, By Lukanen, E.O," *Transportation Research Record*, No. 1355, *Journal of Transportation Research Board*, Washington, DC, p. 51.
- Lin, D., Liau, C, and Lin, J., 2006, "Factors affecting portable falling weight deflectometer measurements," *J. Geotech. and Geoenviron. Engrg.*, ASCE, Vol. 132, No. 6, pp. 804–808.
- Livneh, M., Livneh, N. A., Elhadad, E., 1997, "Determining a pavement modulus from portable FWD testing," *Geotech. Test. J.*, ASTM International, Vol. 20, No. 4, pp. 373–382.
- Livneh, M., and Goldberg, Y., 2001, "Quality assessment during road formation and foundation construction: Use of falling-weight deflectometer and light drop weight," *Transportation Research Record*, No. 1755, *Journal of the Transportation Research Board*, Washington, D.C., pp. 69–77.

- Lukanen, E. O., 1992, "Effects of buffers on falling weight deflectometer loadings and deflections," *Transportation Research Record*, No. 1355, Journal of the Transportation Research Board, Washington, DC, pp. 37–51.
- Mooney, M. A., and Miller, P. K., 2008, "Analysis of falling weight deflectometer test based on in-situ stress and strain response," *J. Geotech. and Geoenviron. Engrg.*, 134(10). ASCE (to appear).
- Nazzal, M. D, Abu-Faraskh, M., Alshibli, K., and Mohammad, L., 2004, "Evaluating the potential use of a portable LFWD for characterizing pavement layers and subgrades," *Proc., Geo-Trans 2004 – Geotechnical Engineering for Transportation Projects*, Vol. 1, Geotechnical Special Publication No. 126, , Los Angeles, CA, pp. 915–924.
- Shahid, M. A., Thom, N. H., and Fleming, P., 1997, "In situ assessment of road foundations," *J. Institute of Highways and Transportation and IHIE*, Vol. 44, No. 11, pp. 15–17.
- Stratton, J. H., 1944, "Military airfields – Construction and design problems," *Proc., American Society of Civil Engineers*, Vol. 70, No. 1, pp. 28–54.
- Terzaghi, K., 1955, "Evaluation of coefficient of subgrade reaction," *Géotechnique*, Vol. 5, No. 4, pp. 297–326.
- Terzaghi, K., and Peck, R. B., 1967, *Soil Mechanics in Engineering Practice*, 2nd Ed., John Wiley & Sons, Inc., NY, pp. 281–283.
- TP BF-StB Teil B 8.3., 1992, *Technical Specification for Soil and Rock in Road Construction – Dynamic Plate Loading Test*, Road and Transportation Research Association, Köln (in German).
- Van Gorp, C., Groenendijk, J., and Beuving, E., 2000, "Experience with various types of foundation tests," *Proc., Unbound Aggregates in Road Construction – UNBAR5*, A. Dawson, Ed., Balkema, Rotterdam, pp. 239–246.
- Weingart, W., 1977, *Theoretische und experimentelle untersuchungen zur bestimmung der elastizität, viskosität und festigkeit von erdstabilisierungen mit hilfe einer registrierenden kleinschlagsonde*, Ph.D. Dissertation, Technical University Leipzig, Germany.

Weingart, W., 1993, "Control of road layers without binder using light drop-weight tester," *Transactions in Mineral Materials in Road Construction*, Vol. 6, Köln, pp. 50–53 (in German).

Zorn, G., 2003, *Operating manual: Light drop-weight tester ZFG2000*, Zorn Stendal, Germany.

ZTVA-StB., 1997, *Additional technical requirements and instructions for excavations in road constructions*, Road and Transportation Research Association, Köln, 1997 (in German).

TABLE 2.1— Summary of shape factors in E_{LWD} estimation (Terzaghi and Peck 1967; Fang 1991)

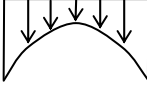
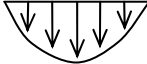
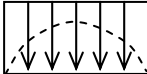
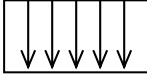
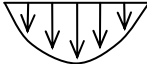
Plate type	Soil type	Stress distribution (shape)	Shape factor (f)
Rigid	Clay (elastic material)	Inverse Parabolic	 $\pi/2$
Rigid	Cohesionless sand	Parabolic	 $8/3$
Rigid	Material with intermediate characteristics	Inverse Parabolic to Uniform	 $\pi/2$ to 2
Flexible	Clay (elastic material)	Uniform	 2
Flexible	Cohesionless Sand	Parabolic	 $8/3$

TABLE 2.2— Brief comparison between different LWD devices.

Device [§]	Plate Diameter (mm)	Falling Weight (kg)	Maximum Applied Force (kN)	Load Cell	Total Load Pulse (ms)	Type of Buffers	Deflection Transducer		
							Type	Location	Range (mm)
Zorn	100, 150, 200, 300	10, 15	7.07	No	18 ± 2	Steel Spring	Accelerometer	Plate	0.2 to 30 (± 0.02)
Keros	150, 200, 300	10, 15, 20	15.0	Yes	15 – 30	Rubber (Conical shape)	Velocity	Ground	0 to 2.2 (± 0.002)
Dynatest 3031	100, 150, 200, 300	10, 15, 20	15.0	Yes	15 – 30	Rubber (Flat)	Velocity	Ground	0 to 2.2 (± 0.002)
Prima	100, 200, 300	10, 20	15.0	Yes	15 – 20	Rubber (Conical shape)	Velocity	Ground	0 to 2.2 (± 0.002)
Loadman	110, 132, 200, 300	10	17.6	No	25 – 30	Rubber	Accelerometer	Plate	— [†]
ELE	300	10	— [†]	No	— [†]	— [†]	Velocity	Plate	— [†]
TFT	200, 300	10	8.5	Yes	15 – 25	Rubber	Velocity	Ground	— [†]
CSM	200, 300	10	8.8	Yes	15 – 20	Urethane	Velocity	Plate	— [†]

Notes: [§]Light Drop Weight Tester ZFG2000 by Gerhard Zorn, Germany; Keros Portable FWD and Dynatest 3031 by Dynatest, Denmark; Prima 100 Light Weight Deflectometer by Carl Bro Pavement Consultants, Denmark; Loadman by AL-Engineering Oy, Finland; Light Drop Weight Tester by ELE; TRL Foundation Tester (TFT) – a working prototype at the Transport Research Laboratory, United Kingdom; Colorado School of Mines (CSM) LWD device. [†]Unknown.

TABLE 2.3—Correlations between different in-situ modulus test devices.

Correlation	Material description	Ref.
$E_{LWD-Z3} = 0.45 \text{ to } 0.56 E_{V2}$	Granular materials	Weingart (1993)
$E_{LWD-Z3} = 0.50 \text{ to } 0.60 E_{FWD-3}$	Unknown	Shahid et al. (1997)
$E_{LWD-Z3} = 0.50 \text{ to } 0.56 E_{V2}$	Unknown	ZTVA-StB (1997)
$E_{LWD-Z3} = 0.53 E_{FWD-3}$ $E_{LWD-T3} = 0.90 E_{FWD-3}$	Granular capping and clay subgrade materials	Fleming et al. (1998)
$E_{LWD-P3} = 0.97 E_{FWD-3}$ ($R^2 = 0.60$) $E_{LWD-Z3} = 0.63 E_{FWD-3}$ ($R^2 = 0.38$) $E_{LWD-T3} = 1.13 E_{FWD-3}$ ($R^2 = 0.53$) $E_{LWD-Z3} = 0.63 E_{LWD-P3}$ ($R^2 = 0.33$) $E_{LWD-T3} = 1.13 E_{LWD-P3}$ ($R^2 = 0.37$)	Granular capping materials	Fleming et al. (2000)
$E_{LWD-Z3} = 0.43 \text{ to } 1.43 E_{FWD-3}$ $E_{LWD-T3} = 0.81 \text{ to } 1.40 E_{FWD-3}$	Natural and stabilized clay, and granular capping materials	Fleming et al. (2000)
$E_{FWD} = 1.40 \text{ to } 2.50 E_{LWD-E3}$ (Avg. 2.0 E_{LWD-E3}) $E_{FWD} = 0.60 \text{ to } 1.60 E_{LWD-P3}$ (Avg. 1.0 E_{LWD-P3})	Hydraulic mix granulates (very stiff self-cementing materials)	Groenendijk et al. (2000)
$E_{LWD-Z3} = 0.30 \text{ to } 0.40 E_{FWD-3}$ $E_{V2} = 600 - \frac{300}{300 - E_{LWD-Z3}}$	Unknown	Livneh and Goldberg (2001)
$E_{LWD-LM} = 0.65 E_{FWD-3}$ $E_{LWD-LM} = 0.67 E_{PLT}$ (see Note a) $E_{LWD-Z3} = 0.40 E_{FWD-3}$ $E_{LWD-Z3} = 0.41 E_{PLT}$ (see Note a) $E_{LWD-K3} = 0.79 E_{FWD-3}$ $E_{LWD-K3} = 0.81 E_{PLT}$ (see Note a) $E_{LWD-K3} = 1.22 E_{LWD-LM}$ and $1.97 E_{LWD-Z3}$	Very gravelly moraine sand materials	Hildebrand (2003)

TABLE 2.3—Correlations between different in-situ modulus test devices (continued).

Correlation	Material description	Ref.
$E_{V1} = 22 + 0.70 E_{LWD-P3} \quad (R^2 = 0.92)$ $E_{V2} = 20.9 + 0.69 E_{LWD-P3} \quad (R^2 = 0.94)$ $E_{FWD-3} = 0.97 E_{LWD-P3} \quad (R^2 = 0.94)$ $E_{V1} = 1.041 E_{LWD-P3} \quad (R^2 = 0.92)$ $E_{V2} = 0.875 E_{LWD-P3} \quad (R^2 = 0.97)$	Natural and stabilized clay, and crushed limestone and stabilized aggregate base/subbase material	Nazzal et al. (2004)
$E_{V1} = \frac{5}{6} E_{LWD-Z3}$	Cohesive soils with E_{LWD-Z3} ranging between 10 to 90 MPa	Adam and Kopf (2004)
$E_{V1} = 150 \ln \left(\frac{180}{180 - E_{LWD-Z3}} \right)$ or $E_{V1} = \frac{5}{4} E_{LWD-Z3} - 12.5$	Non-cohesive soils with E_{LWD-Z3} ranging between 10 to 90 MPa	Adam and Kopf (2004)
$E_{V1} = 0.91 E_{LWD-P3} - 1.81 \quad (R^2 = 0.84)$ $E_{V2} = 25.25 e^{0.006 E_{LWD-P3}} \quad (R^2 = 0.90)$	USCS ^b : GC, GC, GW, GP, SP, CL-ML, CL	Alshibli et al. (2005)
$E_{LWD-Z3(72)} = 2.0 k_{300} \quad (R^2 = 0.76)$	USCS ^b : SM	Kim et al. (2007)
$E_{LWD-K2(63)} = 1.75 E_{LWD-Z2(63)} \quad (R^2 = 0.88)$	USCS ^b : CL, SP-SM	this paper
$E_{LWD-K3(72)} = 2.16 E_{LWD-Z3(72)} \quad (R^2 = 0.50)$	USCS ^b : SP to SW-SM	this paper
$E_{LWD-D2(50)} = 1.70 E_{LWD-Z2(50)} \quad (R^2 = 0.94)$	USCS ^b : SP, SP-SM, SM, CL	this paper
$E_{LWD-K2(50)} = 0.96 E_{LWD-D2(50)} \quad (R^2 = 0.94)$	USCS ^b : SM, CL	this paper

a it is unknown whether E_{PLT} refers to initial or reload modulus

b materials classified according to Unified Soil Classification System (USCS)

TABLE 2.4—Summary of Zorn and Keros/Dynatest 3031 LWD test conditions.

Description	Keros/Dynatest 3031	Zorn ZFG 2000
Drop Weight	10 kg	10 kg
Diameter of Plate	200 and 300 mm	100, 150, 200 and 300 mm
Load Sensor	Load Cell Range: 0 – 19.6 kN	None (constant applied force using Eq. 5.4)
Deflection Sensor	Geophone (velocity transducer)	Accelerometer
Modulus Estimation	Eq. 2.1 for modulus estimation with assumptions*: $\nu = 0.4$ (for all soils) $f = \pi/2$ for field study 1a (clay subgrade) $f = 2$ for field study 1b (granular base underlain by clay subgrade) $f = 8/3$ for field studies 2, 3a, 3b, 3c, 4, and 5.	

*LWD plates and plate used for static PLT tests are assumed as truly rigid.

TABLE 2.5—Summary of field studies and index properties of materials.

Parameter	Field Study 1a	Field Study 1b	Field Study 2	Field Study 3a	Field Study 3b	Field Study 3c
Device	Zorn and Keros		Zorn and Keros	Dynatest 3031 and Zorn		Zorn
Testing Layer	Subgrade	Class 5 Base	Granular subgrade and capping	Select granular subbase	Granular base	Gravel road
c_u^*	—	22.07	2.67 to 7.67	4.54	4.82	3.05
c_c^*	—	0.90	0.12 to 0.71	1.42	1.23	1.23
LL (%)	31	Non-plastic	Non-plastic	Non-plastic	Non-plastic	Non-plastic
PI	13	Non-plastic	Non-plastic	Non-plastic	Non-plastic	Non-plastic
AASHTO Classification	A-6 (5)	A-1-b	A-3	A-1-b	A-1-b	A-1-a
USCS Classification and Material Description (ASTM D2487-00)	CL Sandy lean clay	SP-SM Poorly graded sand with silt and gravel	SP to SW-SM Poorly graded sand to well-graded sand with silt	SP Poorly graded sand	SP-SM Poorly graded sand with silt	GP Poorly graded gravel

* c_u – coefficient of uniformity, c_c = coefficient of curvature

TABLE 2.5—Summary of field studies and index properties of materials (continued).

Parameter	Field Study 4	Field Study 5	Field Study 6	Field Study 7a	Field Study 7b
Device	Zorn, Keros, and Dynatest 3031			Zorn, Dynatest 3031, static PLT	
Testing Layer	Granular subgrade	Gravel road	Subgrade	Granular base	
c_u^*	23.54	262.08	—	—	85.4
c_c^*	7.97	1.94	—	—	0.8
LL (%)	Non-plastic	Non-plastic	30	NP	NP
PI	Non-plastic	Non-plastic	14	NP	NP
AASHTO Classification	A-2-4	A-1-b	A-6(6)	A-1-a	A-1-a
USCS Classification and Material Description (ASTM D2487-00)	SM Silty sand	SM Silty sand	CL Sandy lean clay	SP-SM Poorly graded sand with silt and gravel	SP-SM Poorly graded sand with silt and gravel

* c_u – coefficient of uniformity, c_c = coefficient of curvature

TABLE 2.6—Summary statistics of modulus measurements from different field studies.

Field Study	Measurement (MPa)	n	μ	σ	COV (%)
Field Study 1a	E _{LWD-Z2(63)}	13	50.9	31.0	61
	E _{LWD-K2(63)}	13	88.8	55.2	62
Field Study 1b	E _{LWD-Z2(63)}	124	33.5	18.0	54
	E _{LWD-K2(63)}	124	56.8	36.6	64
Field Study 2	E _{LWD-Z2(63)}	46	87.8	28.0	32
	E _{LWD-Z3(72)}	46	62.2	16.7	27
	E _{LWD-K3(72)}	46	140.1	58.8	42
Field Study 3a	E _{LWD-Z2(50)}	11	74.2	6.9	9
	E _{LWD-D2(50)}	11	139.8	33.0	24
Field Study 3b	E _{LWD-Z2(50)}	15	75.7	15.9	21
	E _{LWD-D2(50)}	15	117.0	22.3	19
Field Study 4	E _{LWD-Z2(50)}	20	23.2	5.3	23
	E _{LWD-D2(50)}	20	46.9	15.5	33
	E _{LWD-K2(50)}	20	42.9	12.5	29
Field Study 6	E _{LWD-Z2(50)}	14	14.7	4.2	29
	E _{LWD-D2(50)}	14	32.8	12.9	39
	E _{LWD-K2(50)}	14	30.2	9.8	33
Field Study 7a	E _{LWD-Z2(50)}	140	31.0	22.7	73
	E _{V1}	155	16.6	15.4	93
	E _{V2}	155	61.1	50.2	82
Field Study 7b	E _{LWD-Z2(50)}	273	42.3	11.7	28
	E _{LWD-D2(50)}	273	64.7	18.9	29

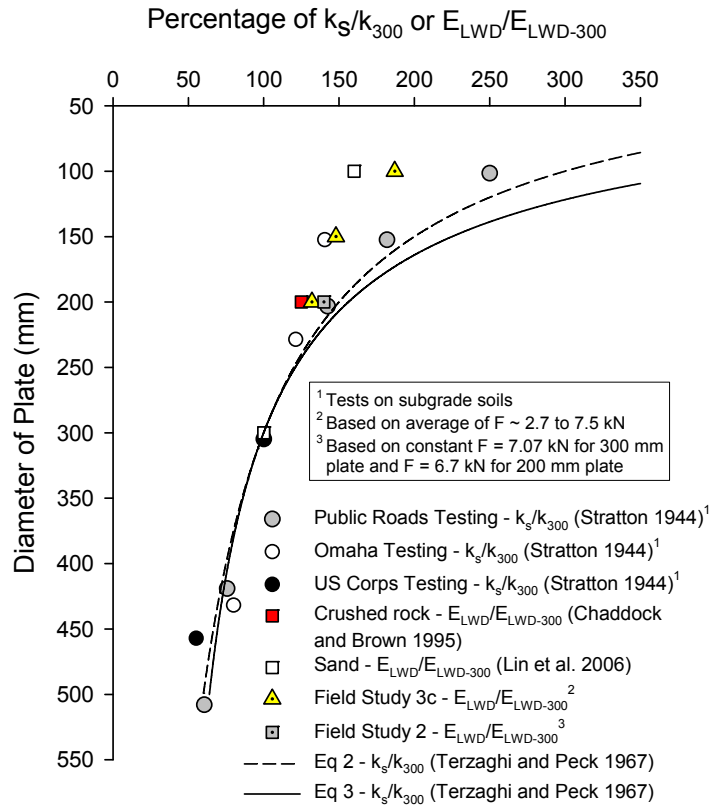


FIG. 2.1—Relationship between material stiffness and diameter of bearing plate

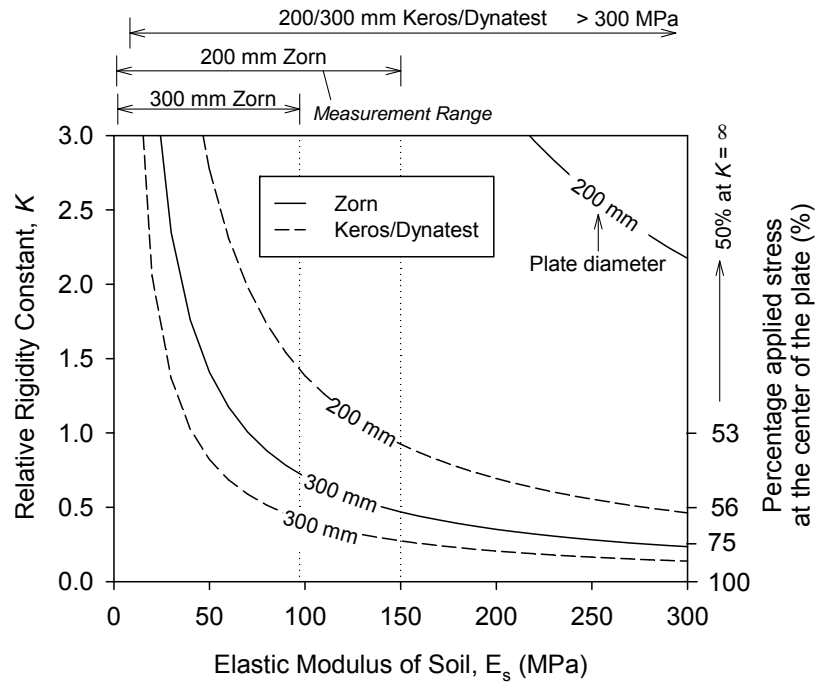


FIG. 2.2—Relationship between plate rigidity, modulus of soil, and contact stress distribution under a plate for elastic subgrade material (using Borowicka (1936) procedure)

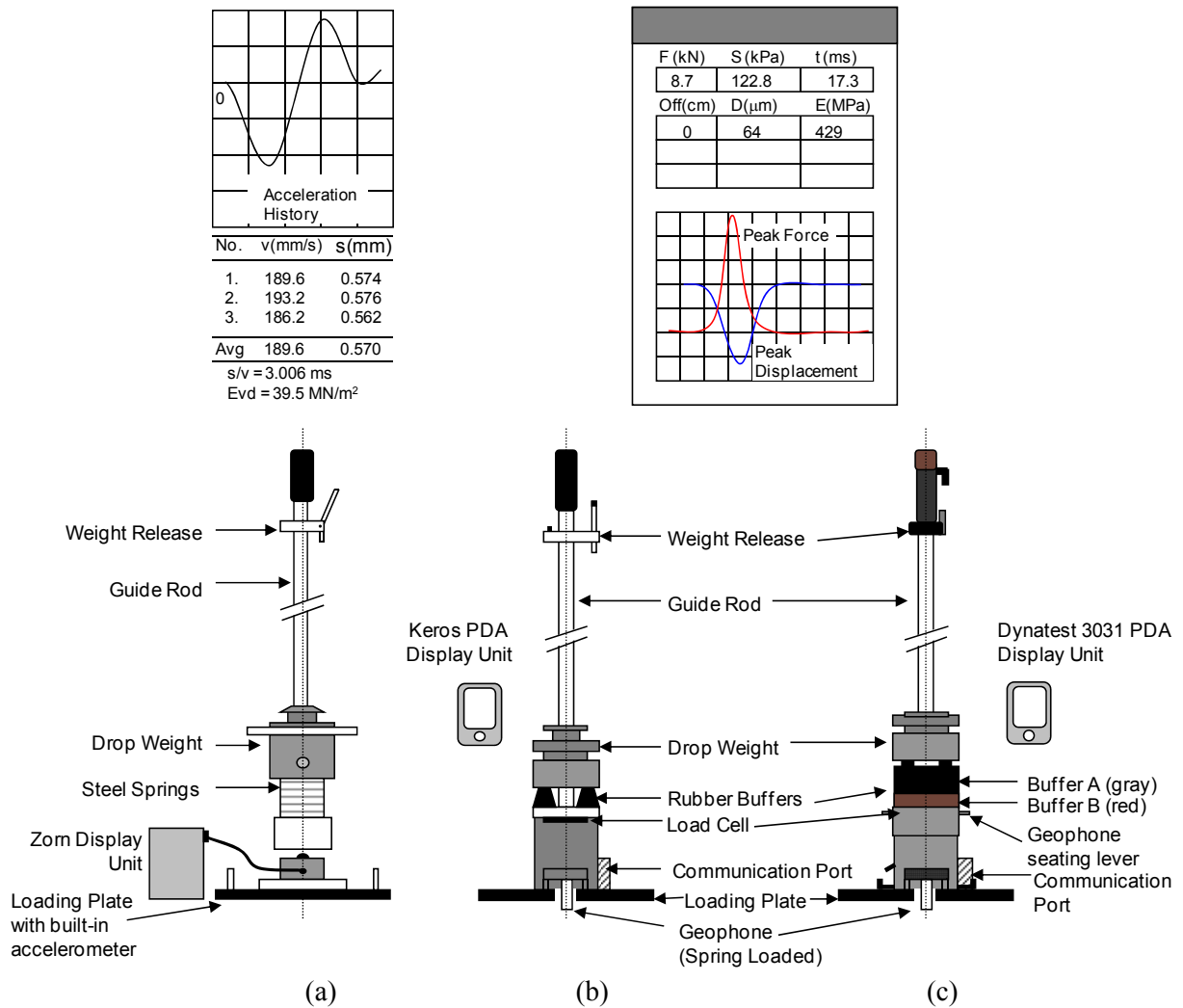


FIG. 2.3—Schematic with example output of LWD devices used in this study (a) Zorn ZFG 2000 (b) Keros (c) Dynatest 3031

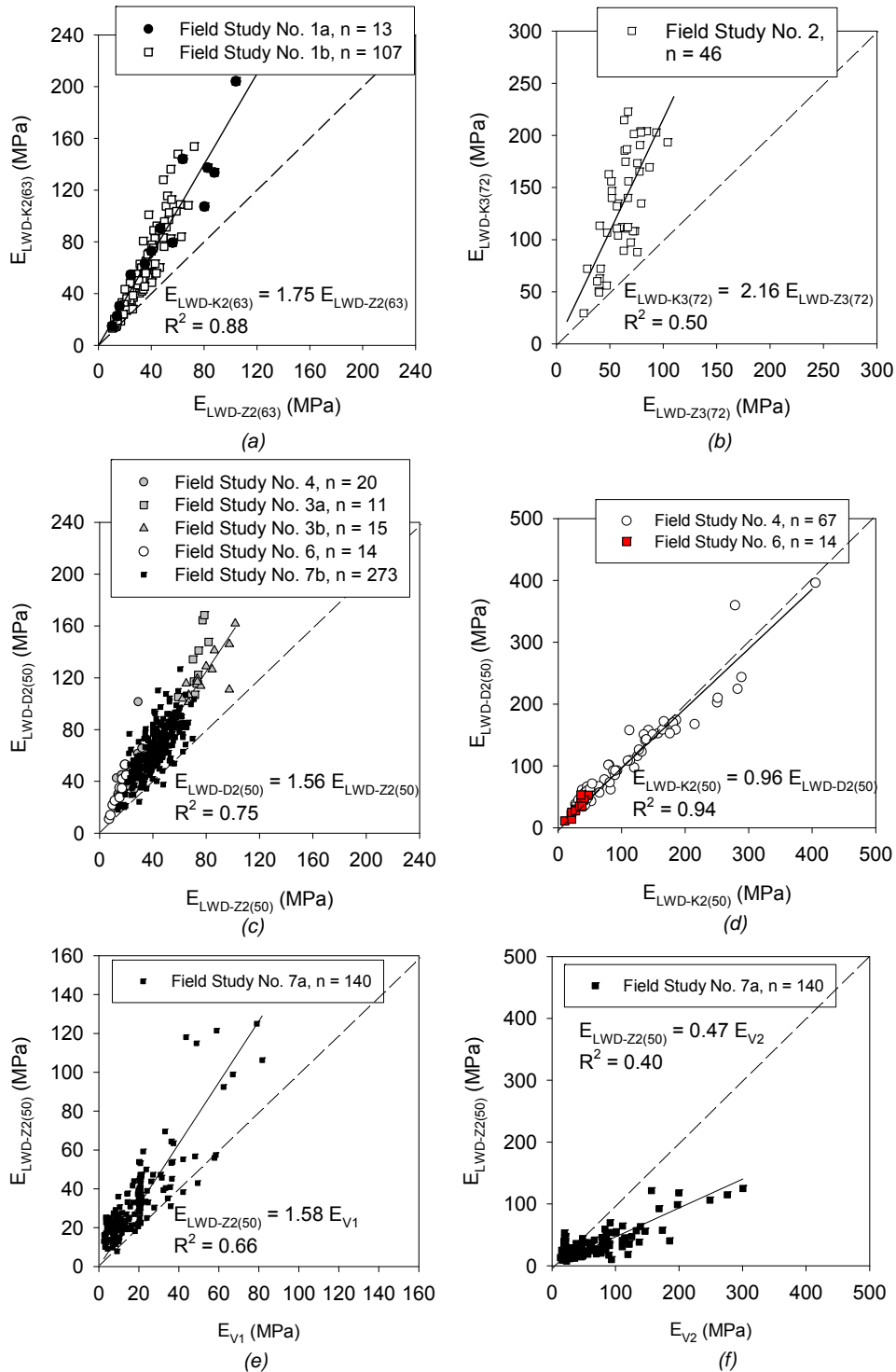


FIG. 2.4—Relationships between ELWD values from different devices: (a) 200-mm Keros and Zorn, (b) 300-mm Keros and Zorn, (c) 200-mm Dynatest and Zorn, (d) 200-mm Dynatest and Keros, (e) 200-mm Zorn and 300-mm static plate load test initial modulus, and (f) 200-mm Zorn and 300-mm static plate load test reload modulus

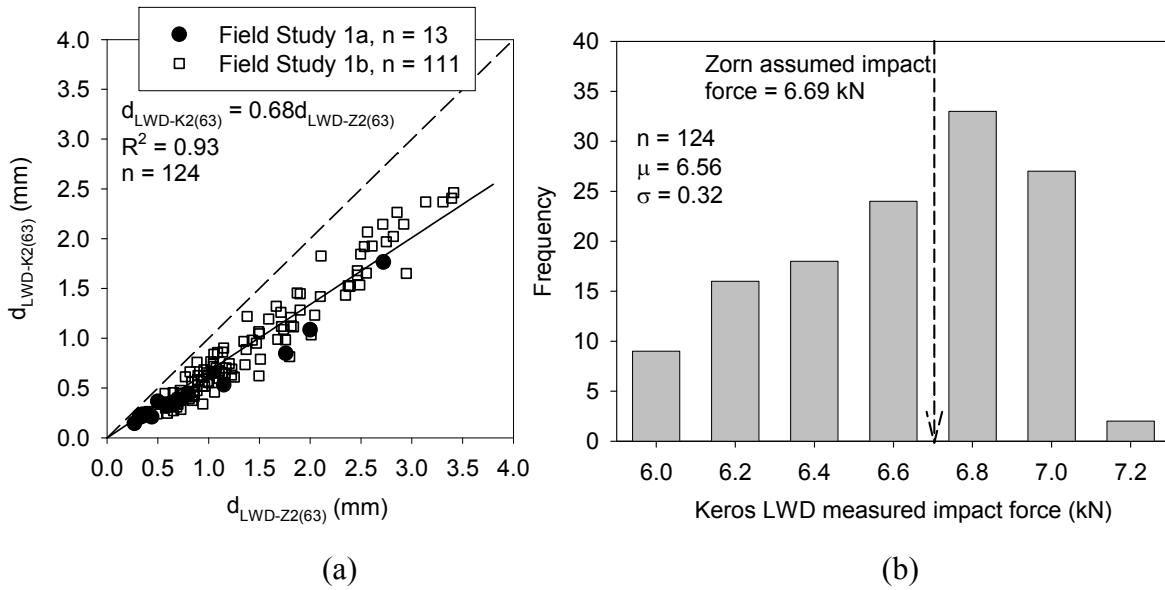


FIG. 2.5— Results from field study 1a and 1b: (a) Comparison between deflection measurements by Zorn and Keros devices, (b) Frequency distribution of impact force by Keros LWD device and comparison to Zorn assumed impact force

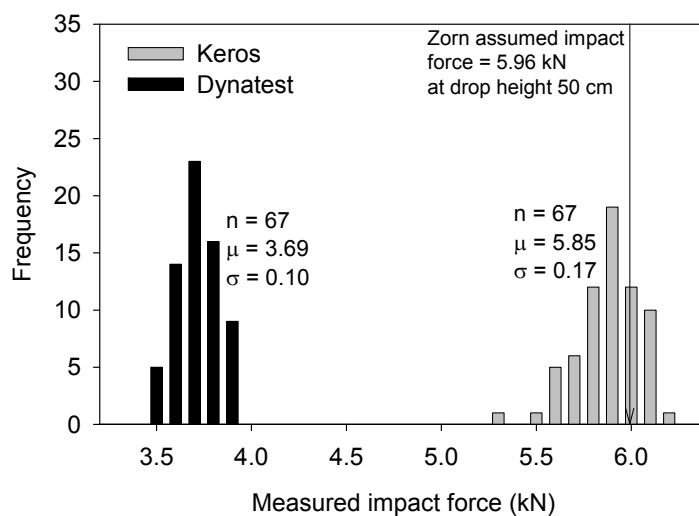


FIG. 2.6—Frequency distribution of impact force at drop height 50 cm by Keros and Dynatest LWD devices and comparison to Zorn assumed impact force (field study 4)

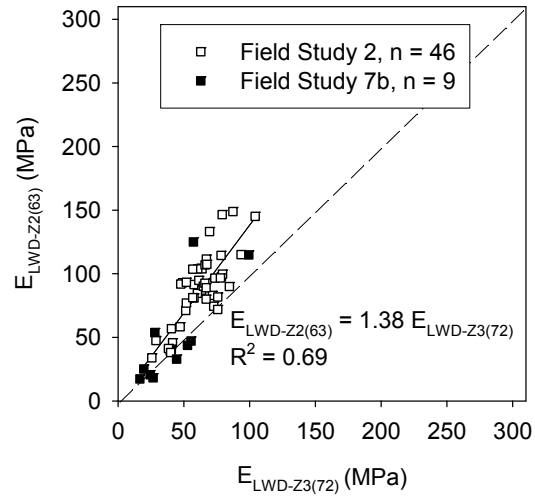


FIG. 2.7— Relationship between 200-mm and 300-mm plate Zorn E_{LWD}

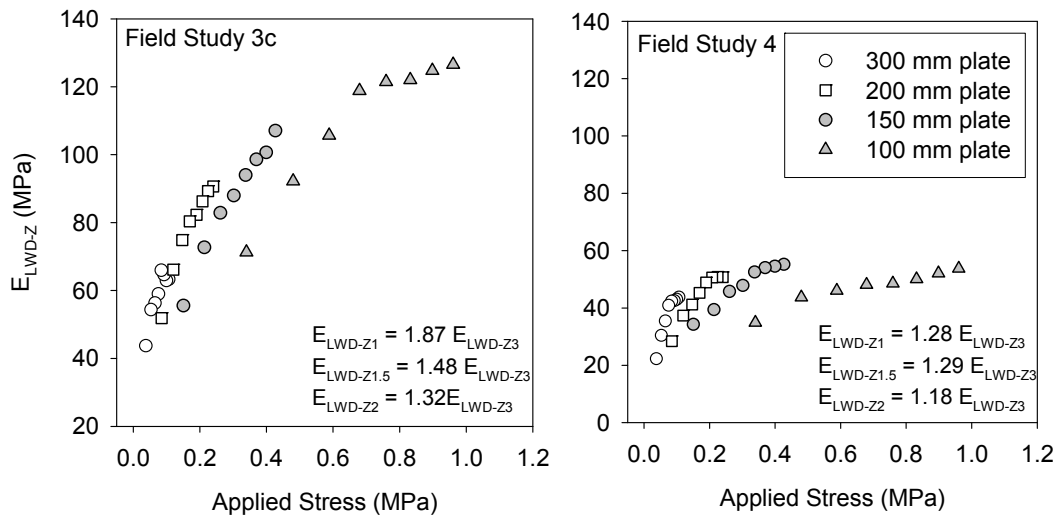


FIG. 2.8— Influence of plate diameter and applied stress on Zorn E_{LWD} from field studies 3 and 4

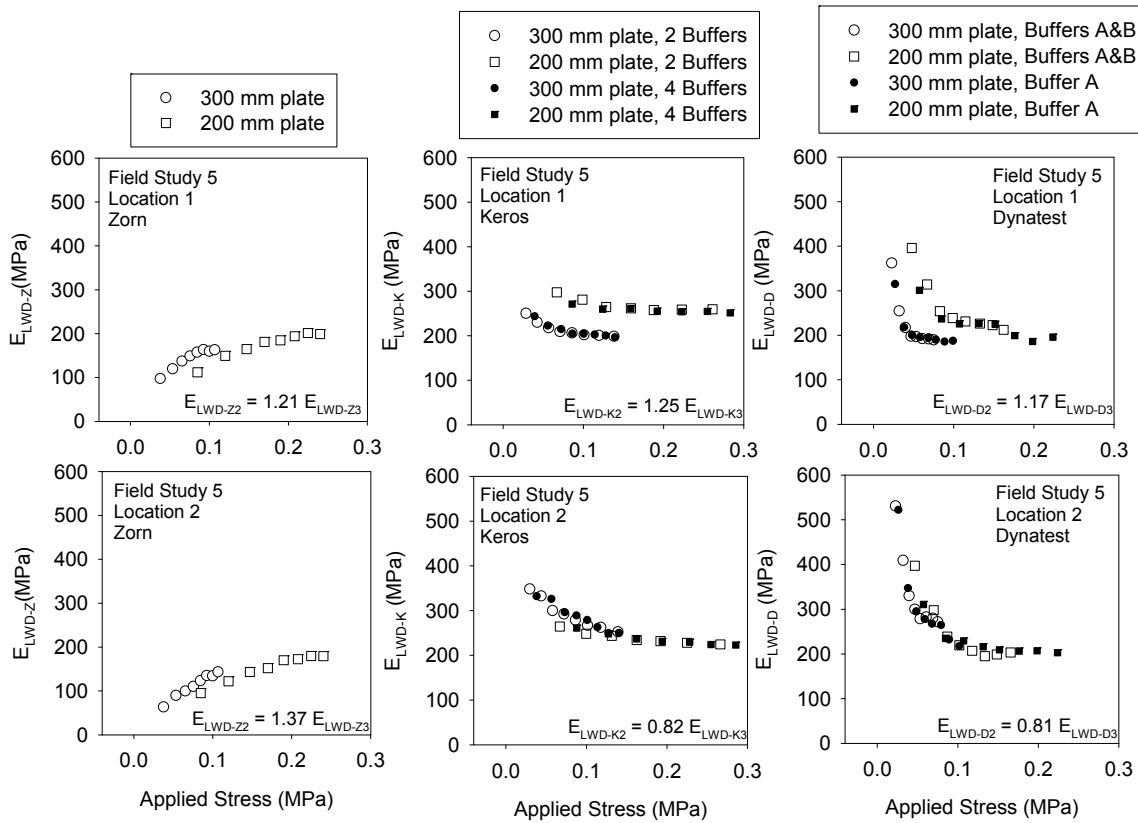


FIG. 2.9— Influence of applied stress and effect of buffer stiffness on ELWD with different plate diameters from field study 5

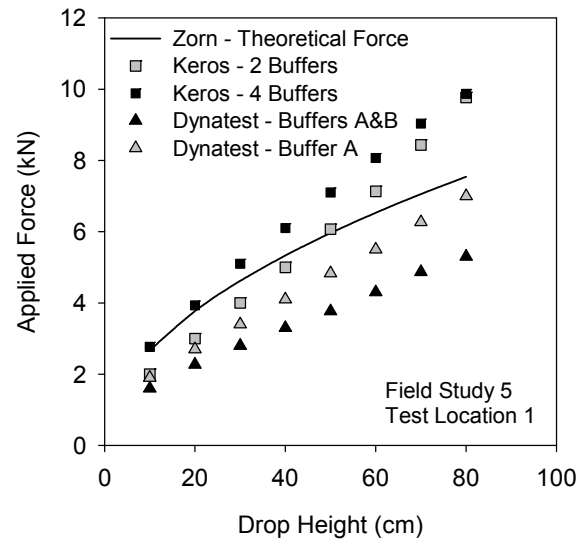


FIG. 2.10— Effect of buffer type and stiffness on applied force for different LWD devices

CHAPTER 3. GEOSTATISTICAL ANALYSIS FOR SPATIALLY REFERENCED ROLLER-INTEGRATED COMPACTION MEASUREMENTS

Pavana KR. Vennapusa, David J. White, and Max D. Morris

A paper submitted to Journal of Geotechnical and Geoenvironmental Engineering, ASCE.

3.1 Abstract

An approach to quantify non-uniformity of compacted earth materials using spatially referenced roller-integrated compaction measurements and geostatistical analysis is discussed. Measurements from two detailed case studies are presented in which univariate statistical parameters are discussed and compared to geostatistical semivariogram modeling parameters and analysis. The univariate and geostatistical parameter values calculated from the roller-integrated measurements are also compared to traditional spot test acceptance criteria. Univariate statistical parameter values based on roller-integrated measurement values provide significantly more information than traditional point measurements, while geostatistics can be used to identify regions of non-compliance and prioritize areas for rework.

3.2 Introduction

Roller-integrated compaction monitoring (RICM) technologies for earth materials provide spatially referenced compaction measurements in real time with 100% coverage, which is a significant improvement over conventional spot test density measurements. This is accomplished by instrumenting the roller with sensors (e.g., accelerometer, torque sensor) that evaluate machine-ground interactions, a global positioning system (GPS) for mapping, and a computer to record, analyze, and output the data. There are at least six RICM measurement values: *omega value* (ω), *compaction meter value* (CMV), *compaction control value* (CCV), roller-determine stiffness (k_s) and vibration modulus (E_{VIB}), and *machine drive power* (MDP) (see Mooney and Adam 2007, White et al. 2005). Measurements are commonly recorded every 0.1 to 0.5 m and are integrated over the width of the roller drum

(typically about 2.1 m). GPS coordinates are assigned to create spatially referenced maps of the measurements. The measurements have been correlated to a variety of in-situ spot test measurements (Floss et al. 1983, Samaras et al. 1991, Brandl and Adam 1997, White and Thompson 2008, Thompson and White 2008). Spatial comparisons between in-situ spot test measurements and roller-integrated measurements are documented by Thompson and White (2007) and White et al (2008b).

With the ability of real-time viewing of compaction data, the technology offers an opportunity to improve process control, construct more “uniform” foundation layers, and reduce rework and overwork in areas that have already met the specification. Although there are several identified benefits of implementing this technology, challenges exist with interpreting data and developing suitable specifications for acceptance. White et al. (2008b) reviewed five different RICHM specifications which showed that univariate statistics (i.e., mean and standard deviation) are typically used for quality control criteria (e.g., ZTVE-StB 1994, RVS 8S.02.6 1999, ATB Väg 2004, ISSMGE 2005, Mn/DOT 2006). Univariate statistics, however, do not address the issue of uniformity from a spatial standpoint. Two datasets with identical distributions of the data (having similar mean, standard deviation, etc.), can have significantly different spatial characteristics. Geostatistical analysis tools, such as a semivariogram model (Fig. 3.1), in combination with univariate statistics could potentially be utilized to effectively address the issue of uniformity, identify poorly compacted areas, and improve process control during earthwork operations.

Geostatistical analysis could also be beneficial in evaluating the performance of geotechnical structures like shallow foundations and pavement layers. Generally, pavement design considers the foundation layers as a layered medium with uniform material properties in each layer. However, in reality, soil engineering parameters generally show significant spatial variation. Spatial variation of strength, stiffness, and permeability properties of pavement foundation layers are documented by Vennapusa (2004) and White et al. (2004). Results of analysis by considering average values, i.e., by treating soil properties as uniform may vary considerably from actual performance (White et al. 2004, Griffiths et al. 2006). Influence of spatial variability in soil engineering properties on the performance of geotechnical structures are becoming increasingly popular over a wide range of geotechnical

applications (e.g., Mostyn and Li 1993, Phoon et al. 2000, White et al. 2004, Griffiths et al. 2006). The spatially referenced RICM data can provide better characterization of the spatial variability of selected engineering properties. If the data can be linked to suitable analytical/numerical models, new insights into spatial load-deformation analysis can be developed and is a subject of on-going research.

The main objectives of this paper are to: (a) provide an overview of geostatistical analysis procedures for spatially referenced RICM to characterize and model spatial variability using semivariogram analysis, (b) identify challenges involved in performing the analysis, (c) compare spatial statistics with univariate statistics in characterizing non-uniformity, and (d) demonstrate the practical significance of the analysis results. Detailed measurements from two case studies are analyzed for these purposes and presented in this paper. The analysis approach would be applicable to any of the RICMs referenced above.

3.2 Background

3.2.1 Roller-Integrated Compaction Measurement Values

Caterpillar's CS-533E and CS-563E smooth drum soil compaction rollers equipped with RICM technology were used in the two field studies documented in this paper. These rollers simultaneously calculated the vibratory-based *compaction meter value* (CMV) and *resonant meter value* (RMV), and static or vibratory-based *machine drive power* (MDP). A brief description of these technologies is provided below.

CMV is a dimensionless compaction parameter developed by Geodynamik that depends on roller dimensions, (i.e., drum diameter and weight) and roller operation parameters (e.g., frequency, amplitude, speed) and is determined using the dynamic roller response (Sandström 1994). It is calculated using Eq. 3.1, where C is a constant (300), $A_{2\Omega}$ = the acceleration of the first harmonic component of the vibration, A_{Ω} = the acceleration of the fundamental component of the vibration (Sandström and Pettersson 2004). Correlation studies relating CMV to soil dry unit weight, strength, and stiffness are documented in the literature (e.g., Floss et al. 1983, Samaras et al. 1991, Brandl and Adam 1997, Thompson and

White 2008, White and Thompson 2008).

$$CMV = C \cdot \frac{A_{2\Omega}}{A_{\Omega}} \quad (3.1)$$

RMV provides an indication of the drum behavior (e.g. continuous contact, partial uplift, double jump, rocking motion, and chaotic motion) and is calculated using Eq. 3.2, where $A_{0.5\Omega}$ = subharmonic acceleration amplitude caused by jumping (the drum skips every other cycle).

$$RMV = C \cdot \frac{A_{0.5\Omega}}{A_{\Omega}} \quad (3.2)$$

According to Adam and Kopf (2004), $RMV = 0$ theoretically indicates that the drum is in a continuous or partial uplift mode. When $RMV > 0$, drum enters double jump mode and transitions into rocking and chaotic modes. Based on numerical studies, Adam (1997) showed that as the soil stiffness increases CMV increases almost linearly for the roller drum in a continuous or partial uplift mode. With increasing soil stiffness, the drum transitions to double jump mode where RMV increases and CMV decreases rapidly. With further increase in ground stiffness, CMV decrease to a minimum value and then increases again. This relationship between drum operation mode, RMV, and ground stiffness is identified as a distinctive feature of CMV (Adam 1997 and Sandström 1994). The interpretation of CMV thus must not be absent of evaluating RMV. Although this effect has been identified by several researchers, to the authors' knowledge, it lacked attention in the literature on how to consider from a specification/quality assurance standpoint (data analysis using RMV measurements is presented in Case study II later in this paper). New developments in RICM technology with variable feedback control systems (referred to as intelligent compaction (IC)) help control the drum behavior to prevent double jump by automatic adjustment of frequency and/or amplitude (Adam and Kopf 2004).

MDP is a machine power-based technology that monitors and empirically relates mechanical performance of the roller during compaction to the properties of the compacted soil. It is calculated using Eq. 3.3 where P_g = gross power needed to move the machine, W = roller weight, a = machine acceleration, g = acceleration of gravity, θ = slope angle (roller

pitch), V = roller velocity, and m and b = machine internal loss coefficients specific to a particular machine. The use of roller machine power for indicating soil compaction is documented in the literature (e.g., White et al. 2005, White et al. 2006, Thompson and White 2008). MDP measurements can be made in static or vibratory mode.

$$MDP = P_g - WV \left(\sin \theta + \frac{a}{g} \right) - (mV + b) \quad (3.3)$$

The two rollers used in the case studies presented in this paper were equipped with a GPS system to spatially reference the RICM measurements. The mapped data is viewed in real time using an on-board compaction monitor.

3.3 Geostatistical Analysis

Geostatistics characterize and quantify spatial variability. The semivariogram $\gamma(h)$ is a common analysis tool to describe spatial relationships in many earth science applications and is defined as one-half of the average squared differences between data values that are separated at a distance h (Isaaks and Srivastava 1989). If this calculation is repeated for many different values of h , as the sample data will support, the result can be graphically presented as shown in Fig. 3.1 (shown as circles), which constitutes the experimental semivariogram plot. The mathematical expression to estimate the experimental semivariogram is given in Eq. 3.4 for reference, where $z(x_i)$ is a measurement taken at location x_i , and $n(h)$ is the number of pairs h units apart in the direction of the vector, and $\hat{\gamma}$ is an experimental estimate of the underlying variogram function γ (Olea, 2006).

$$\hat{\gamma}(h) = \frac{1}{2n(h)} \sum_{i=1}^{n(h)} [z(x_i + h) - z(x_i)]^2 \quad (3.4)$$

The three main characteristics, by which a semivariogram plot is often summarized, include the following (Isaaks and Srivastava 1989):

Range (a): As the separation distance between pairs increase, the corresponding semivariogram value will also generally increase. Eventually, however, an increase in the distance no longer causes a corresponding

increase in the semivariogram, i.e., where the semivariogram reaches a plateau. The distance at which the semivariogram reaches this plateau is called as *range*. Longer *range* values suggest greater spatial continuity or relatively larger (more spatially coherent) “hot spots”.

Sill (C_0+C): The plateau that the semivariogram reaches at the range is called the *sill*. A semivariogram (which is one-half of variogram) generally has a sill that is approximately equal to the variance of the data (Srivastava 1996).

Nugget Effect (C_0): Though the value of the semivariogram at $h = 0$ is strictly zero, several factors, such as sampling error and very short scale variability, may cause sample values separated by extremely short distances to be quite dissimilar. This causes a discontinuity at the origin of the semivariogram and is described as *nugget effect*.

Some important points to note are that a semivariogram model is stable only if the measurement values are stationary over an aerial extent. If the data values are non-stationary, spatial variability should be modeled only after appropriate transformation of the data (Clark and Harper 2002). If the values show a systematic trend, this trend must be modeled and removed prior to modeling a semivariogram (Gringarten and Deutsch 2001). An example with polynomial trend surface analysis is presented later in this paper.

In addition to quantifying spatial variability, geostatistics can be used as a spatial prediction technique, i.e., for predicting a value at unsampled locations based on values at sampled locations. Kriging is a stochastic interpolation procedure (Kriging 1951), by which the variance of the difference between the predicted and “true” values is minimized, using a semivariogram model. Kriging was used to create smoothed contour maps of RICM point data for analysis of non-uniformity and comparison to maps of different in-situ spot test measurement values. Kriging is further discussed later in this paper.

3.3.1 Fitting a Theoretical Model

The major purpose of fitting a theoretical model to the experimental semivariogram is to give an algebraic formula for the relationship between values at specified distances. There

are many possible models to fit an experimental semivariogram. Some commonly used models include linear, spherical, exponential, and Gaussian models. Mathematical expressions for these models are presented in Table 3.1. Detailed descriptions of these theoretical models can be found elsewhere in the literature (e.g., Isaaks and Srivastava 1989, Clark and Harper 2002).

The *range* is well defined in case of a spherical model, i.e., where the sill reaches its plateau. It cannot be interpreted, however, in the same manner for other models (Clark and Harper 2002). For example, exponential and gaussian models have only asymptotic sills, and approximate ranges for these models (distances at which the asymptotic sill is closely approximated) are three to five times larger than range values for closely matched spherical models. Some researchers used effective range as $3a$ for the exponential semivariogram (e.g., Erickson et al. 2005).

3.4 Case Studies

Roller-integrated compaction measurements obtained from two case studies were analyzed using geostatistical methods and are presented in this section. A brief summary of conditions for each case study is provided in 4.2. Exponential models were found to fit well with most of the experimental semivariograms, while spherical models fit less frequently. For purposes of comparing datasets, only exponential models were fit to the experimental semivariograms discussed in this paper. Models were checked for “goodness” using the modified Cressie goodness fit method, suggested by Clark and Harper (2002), and a cross-validation process. The nugget effect was modeled using the variance of the measured value from the nearest neighbor statistics as the upper bound of the nugget value. The best fit model was selected based on a combination of best possible Cressie goodness factor and cross-validation results.

3.4.1 Case Study I

The test area was prepared with two distinctly different subsurface conditions: relatively stiff, sandy lean clay subgrade (CL) and CA6 gravel base material (SW-SM),

underlain by sandy lean clay subgrade (see Fig. 3.2). Index properties of these two soil types are summarized in Table 3.3. The section with CA6 material was originally compacted using several roller passes to create a stable platform. A portion of this section adjacent to the subgrade was scarified to approximately 200 to 250 mm to create a loose condition and differences in the compaction measurements. The CS 533E smooth drum roller was used for mapping the test area in eight parallel roller lanes. CMV and MDP output from the roller are presented in Fig. 3.3. After mapping the test area, in-situ compaction test measurements, using a dynamic cone penetrometer (DCP) and 200-mm plate Zorn light weight deflectometer (LWD), were performed at 144 test locations shown on Fig. 3.2. DCP tests were performed in accordance with ASTM D6951. LWD tests were performed, following manufacturer recommendations to determine E_{LWD} (Zorn 2003). The spot tests were positioned such that the boundaries of non-stationary conditions (i.e., different subsurface conditions) were captured in the semivariogram modeling and interpolation process.

A frequency distribution plot and the semivariogram results for the test area are presented in Fig. 3.4 for CMV measurements. The frequency distribution is skewed to the right, and the semivariogram plot shows increasing variance above the theoretical sill (i.e., actual sample variance ~ 95) with separation distance. The findings from Fig. 3.4a are generally indicators of non-stationarity and trend (Gringarten and Deutsch 2001) in the CMV values. However, the semivariogram does not indicate the form of the trend in the values. A polynomial trend surface analysis, common to geological applications (e.g., Whitten 1963), was selected to remove the trend before modeling a semivariogram. This analysis assumes that the measured value is made up of a “trend” component, which is represented by a polynomial function of X and Y (spatial coordinates), and a residual or error component, ε (Clark and Harper 2002). The trend is modeled using linear (Eq. 3.6), quadratic (Eq. 3.7), or cubic models (Eq. 3.8). The best fit model was determined using the method of least squares.

$$g_i = b_0 + b_1X_i + b_2Y_i + \varepsilon_i \quad (6)$$

$$g_i = b_0 + b_1X_i + b_2Y_i + b_3X_i^2 + b_4X_iY_i + b_5Y_i^2 + \varepsilon_i \quad (7)$$

$$g_i = b_0 + b_1X_i + b_2Y_i + b_3X_i^2 + b_4X_iY_i + b_5Y_i^2 + b_6X_i^3 + b_7X_i^2Y_i + b_8X_iY_i^2 + b_9Y_i^3 + \varepsilon_i \quad (8)$$

If the trend is removed successfully, the residual values, ε , of the analysis parameter after detrending should be spatially stationary (Clark and Harper 2002). Analysis of variance (ANOVA) results were used to help judge the suitability of a representative least squares fit from the polynomial trend surface analysis. The F ratio statistic of a quadratic trend surface explained a greater significance over the linear and cubic trend surfaces. The CMV residuals after quadratic detrending approximate a normal distribution, and the semivariogram plot shows a clear spatial structure with well-defined sill and range (Fig. 3.4b). Similar polynomial trend surface analysis was used for the roller measurement value MDP and in-situ compaction test measurements DCP (blows/200mm) and E_{LWD} in developing distribution plots and semivariogram models (Fig. 3.5). The MDP, DCP, and E_{LWD} values exhibited a quadratic trend similar to CMV. Using the semivariogram models, kriged contour surface maps of roller-integrated measurement values and in-situ spot test measurements were created, as shown in Fig. 3.6.

Of the two roller-integrated compaction measurement values, CMV presented longer spatial continuity ($a = 2$ m) compared to MDP ($a = 0.5$ m). Also, MDP values showed greater short-scale variability than CMV, as evidenced by the nugget effect present in the MDP semivariogram model (Fig. 3.5a). The reason for this difference can be attributed to the influence depths of the two measurement values and the influence of the rear tires for MDP. MDP, which is a measure of rolling resistance and sinkage of the drum and rear tires combined, may be heavily affected by surficial characteristics of the compacting soil (White et al. 2007a), while CMV is a measure of dynamic roller drum-ground interaction that can be influenced by soil characteristics below the compaction layer. Reportedly, the measurement influence depths for smooth drum vibratory rollers range from 0.4 to 0.6 m for a 2-ton roller to 0.8 to 1.5 m for a 12-ton roller (ISSMGE 2005).

The de-trended semivariograms of DCP index (Fig. 3.5b) and E_{LWD} (Fig. 3.5c) showed reasonable spatial structure but with more scatter than CMV or MDP. The kriged contour plots of DCP index and E_{LWD} showed comparable spatial distributions with CMV (Fig. 3.6). Some differences should be expected as the DCP values are averaged for the upper 200 mm, and the LWD measurements are taken at the surface. The LWD measurements have a measurement influence depth approximately equal to one plate

diameter (Sulewska 1998), which in this case was 200 mm.

3.4.2 Case Study II

This case study was conducted at the TH 64 reconstruction project located south of Akeley, Minnesota, USA. The CS-563E smooth drum IC roller was used at the project site. Roller-integrated CMV was used as the primary quality control measurement during earthwork compaction process (White et al. 2008a). Calibration strips were constructed prior to production compaction for several soil types and fill sections encountered at the project. Target values were established from these calibration strips and used as reference for quality control in the production areas. Acceptance in production compaction was achieved, such that at least 90% of a proof area reached at least 90% of the target value, and if significant portion of the area exceed 130% of the target value, the project engineer re-evaluated the use of an appropriate calibration strip. Index properties of the fill material are summarized in 4.3. Two calibration strips and a proof area were analyzed using geostatistics and are described in the following subsections.

3.4.2.1 Analysis of Calibration Strips

Subsurface conditions for calibration strip 1 consisted of approximately 1.1-m thick fill material placed in four successive lifts, and the final surface layer was compacted using seven roller passes. Calibration strip 2 consisted of 0.25-m thick fill material placed in one lift and compacted using eleven roller passes. Compaction operations for both strips were performed in north-south directions and along three and six adjacent roller lanes for strips 1 and 2, respectively. A summary of spatial and univariate statistics and comparison to the quality assurance criteria are presented in Table 3.4. Sill and range values for omnidirectional semivariograms and directional semivariograms with orientation in the roller direction (north-south, N-S) and perpendicular to the rolling lanes (east-west, E-W) are also presented in Table 3.4.

Analysis of directional semivariograms can help determine principle directions of anisotropy in the data. Results show that the sill values in E-W direction were consistently lower than in N-S direction, which indicates less variability in E-W direction. Longer range

values were observed in N-S direction semivariogram, which suggests greater spatial continuity along the direction of roller travel than in the transverse direction. Comparison between omnidirectional and N-S directional semivariogram statistics from the two calibration strips did not reveal significant differences in their spatial statistics. This is expected, as the omnidirectional semivariograms are composed of more data that is oriented in the N-S direction than in the E-W direction. Because the compaction was performed in only 3 to 6 adjacent lanes, only a limited number of data points were available to construct the E-W directional semivariograms. This case was true for all other areas of production compaction for this project and is typical of road construction projects. The omnidirectional semivariograms account for data in all directions, and as long as the semivariogram presented a clearly interpretable structure, it did not appear critical to model anisotropy in the semivariogram analysis for this project. Nevertheless, difference between N-S and E-W semivariograms is to be expected due to the spatial nonsymmetry of the measurements as the values are located at points in N-S direction but are integrated over the roller length in E-W direction.

A summary of changes in univariate and spatial statistics for calibration strip 1 as a function of roller passes is presented in Fig. 3.7a. The mean CMV increased from approximately 41 to 48, and coefficient of variation (COV) decreased from approximately 17% to 12% with increasing roller passes. The percent CMV value in 90% to 130% bin for the project acceptance criteria increased from about 71% to 89% (see Table 3.4), indicating increased compaction and decreased variability of CMV from pass 2 to 7. The sill value for all semivariograms (omnidirectional, N-S, and E-W) generally decreased with increasing roller passes, thus indicating increasing uniformity. No significant changes in range values are observed.

A summary of changes in univariate and spatial statistics for calibration strip 2 as a function of roller passes is presented in Fig. 3.7b. The mean CMV increased slightly from about 61 to 66, and COV decreased from about 17% to 11% from passes 2 to 11. The percent CMV value in the 90% to 130% bin increased from about 75% to 93% (see Table 3.4), which is an indication of decreasing variability and increasing compaction. No definite trend in sill was observed with increasing roller passes. However, the range value showed a

strong second-order polynomial increasing trend with R^2 of 0.75 with increasing passes. Increasing range with roller passes indicates increasing spatial continuity in CMV.

3.4.2.2 Analysis of Proof Area

The subgrade conditions in the proof area consisted of fill material varying from about 0.4 m to 1.2 m in thickness, underlain by native sand. Compaction operations were performed longitudinally in N-S direction, along six adjacent lanes. CMV target value of 42 established from calibration strip 1 was used as reference for acceptance on this proof area.

Semivariograms and CMV/RMV kriged contour maps for the proof area, along with comparison to calibration strip 1, are presented in Fig. 3.8. The influence of RMV on CMV was discussed earlier in the background section of the paper. A review of CMV-RMV data from the proof area indicated that when CMV reached approximately 60, RMV increased indicating a transition in drum behavior from partial uplift to double jump mode. Although double jump mode is theoretically defined as $RMV > 0$ (Adam and Kopf 2004), based on spatial distribution of RMV in the proof area (Fig. 3.8), a value of $RMV > 2$ was considered a practical cutoff value for further analysis. To filter the resulting low CMV measurements in areas with $RMV > 2$, the CMV measurements were assigned a value of 60 as an indication of stiff ground conditions and no additional need of compaction. The CMV kriged contour map in Fig. 3.8 is based on the filtered and modified measurements.

Comparison of univariate statistics of CMV-measurements and acceptance criteria is presented in Fig. 3.8. Results indicate that this proof area “passed” the quality acceptance criterion of achieving 90% of IC-TV in 90% of the evaluated area. However, if spatial statistics between the proof and the calibration strip are compared, the proof area failed to achieve the “sill” and “range” values achieved in the referenced calibration strip. The production area consisted of localized areas of soft ground conditions or “hot spots” that have $CMV < 30$, especially along the centerline of the alignment. These locations generally match with the locations of grade stakes in the field and were not subjected to construction traffic like the outside lines. Although the proof area meets the acceptance criteria specified for the project based on average values, geostatistical spatial analysis reveals localized areas that perhaps could benefit from additional compaction to improve spatial uniformity.

Fig. 3.9 illustrates an example approach to select localized areas within the proof to target for additional compaction or other treatment that would contribute to improved uniformity. The area shown in Fig. 3.9 is a section from the proof area about 94 m long, which is of similar length to the calibration strip. If proof areas are checked for quality control with reference to a calibration area, then ideally, any given portion of the production area with dimensions equal to that of the calibration area should meet the spatial statistics established from the calibration. In Fig. 3.9, kriged surface maps of the original and modified CMV data are presented (i.e., $CMV < 45 = 45$; represents data that are less than 45 and have been set to 45). The low CMV data were incrementally increased to represent targeted additional compaction. Also, the semivariograms associated with each CMV data set are presented in Fig. 3.9, along with the semivariogram of the calibration strip. Comparatively, the semivariogram for modified CMV data – $CMV < 48 = 48$ closely follows the semivariogram of the target calibration strip with similar sill values. The semivariogram of $CMV < 52 = 52$ modified dataset shows increased uniformity with a lower sill value, relative to the calibration strip.

This approach combined with correction of CMV measurements in areas with high RMV provides an optimized solution to target areas that need additional compaction. It also provides quantitative parameters to establish uniformity based on spatial statistics criteria. Geostatistical analysis and spatially referenced roller-integrated compaction monitoring represent a paradigm shift in how compaction analysis and specifications could be implemented in the future.

3.5 Concluding Remarks

Geostatistical analysis using semivariogram modeling provide a unique opportunity to characterize and quantify non-uniformity of compacted earth fill materials, which is often considered a key element for geotechnical structures like pavements. Geostatistical analysis and spatially referenced roller-integrated compaction monitoring represent a paradigm shift in how compaction analysis and specifications could be implemented in the future.

However, there are some important steps during semivariogram modeling that need particular

attention, which include: (a) performing exploratory data analysis to examine the distribution and assess the need for transformation, (b) determining non-stationarity in the data that may require polynomial trend surface analysis, (c) modeling anisotropy (directional semivariograms herein showed that this is generally not an issue because of limited data points in the transverse direction), and (d) understanding and exercising the semivariogram model fitting process. This paper provided two case study examples which emphasized these issues during semivariogram modeling. If automated, the described use of geostatistics could aid the contractor in identifying localized, poorly compacted areas or areas with highly non-uniform conditions that need additional compaction or other modification and would contribute to improved uniformity. This information could also be used to target quality assurance testing by the field engineers.

3.6 Acknowledgments

The authors would like to acknowledge to support of the Minnesota Department of Transportation (Mn/DOT), the Federal Highway Administration (FHWA), and Caterpillar Inc. (CAT) for funding these studies. Numerous people from Mn/DOT provided assistance in identifying and providing access to grading projects. John Siekmeier and Ruth Roberson from Mn/DOT and several Mn/DOT field engineers provided assistance in organizing the compaction data. The authors would like to thank Mark Thompson, Heath Gieselman, Michael Kruse, Amy Heurung, and Michael Blahut at Iowa State University and Paul Corcoran, Tom Congdon, Donald Hutchen, Allen Declerk, and Glen Feather at CAT for providing assistance with the field and lab testing.

3.7 Notations

a	=	Machine acceleration
a	=	Range of influence (semi-variogram)
A_{Ω}	=	Acceleration of the fundamental component of the vibration
$A_{2\Omega}$	=	Acceleration of the first harmonic component of the vibration

b	=	machine internal loss coefficient specific to a particular machine.
C_0+C	=	Sill (semi-variogram)
C_0	=	Nugget effect (semi-variogram)
COV	=	Coefficient of variation
CMV	=	Compaction meter value
E_{LWD}	=	Elastic modulus determined by the light weight deflectometer
g	=	Acceleration due to gravity
h	=	Lag or separation distance
m	=	Machine internal loss coefficient specific to a particular machine
MDP	=	Machine drive power
P_g	=	Gross power needed to move the machine
V	=	Roller velocity
W	=	Weight of the roller
μ	=	Statistical mean
σ	=	Standard deviation
θ	=	Slope angle (roller pitch)
$\hat{\gamma}$	=	Experimental estimate of the underlying variogram function γ

3.8 References

- Adam, D. 1997. "Continuous compaction control (CCC) with vibratory rollers," *GeoEnvironment 97: Proceedings of 1st Australia-New Zealand Conference on Environmental Geotechnics*. Rotterdam, Netherlands: A.A. Balkema, 245–250.
- Adam, D., and Kopf, F. (2004). "Operational devices for compaction optimization and quality control (Continuous Compaction Control & Light Falling Weight Device)."

- Proc., of the Intl. Seminar on Geotechnics in Pavement and Railway Design and Construction*, December, Athens, Greece (Invited paper), 97-106.
- ASTM D6951. (2003). “Standard test method for use of the dynamic cone penetrometer in shallow pavement application.” American Standards for Testing Methods (ASTM), West Conshohocken, PA.
- ASTM D698. (2003). “Standard test methods for laboratory compaction of soil using standard effort.” American Standards for Testing Methods (ASTM), West Conshohocken, PA.
- ATB Väg. (2004). “Kapitel E - Obundna material VV Publikation 2004:111,” *General technical construction specification for roads*, Road and Traffic Division, Sweden.
- Adam, D. (1997). “Continuous compaction control (CCC) with vibratory rollers.” *Proc., 1st Australia-Newzealand Conf. on Environmental Geotechnics – GeoEnvironment 97*, Melbourne, Australia, 26-28 November.
- Brandl, H., and Adam, D. (1997). “Sophisticated continuous compaction control of soils and granular materials.” *Proc. 14th Intl. Conf. Soil Mech. and Found. Engrg.*, Hamburg, Germany, 1–6.
- Clark, I., and Harper, W. (2002). *Practical geostatistics 2000*. 3rd reprint, Ecosse North America Llc, Columbus, Oh.
- Erickson, T. A., and Williams, M. W., and Winstal, A. (2005). “Persistence of topographic controls on the spatial distribution of snow in rugged mountain terrain, Colorado, United States.” *Water Resources Res.*, 41, W0414.
- Floss, R., Gruber, N., Obermayer, J. (1983). “A dynamical test method for continuous compaction control.” *Proc. 8th European Conf. on Soil Mech. and Found. Engg.*, H.G. Rathmayer and K. Saari, eds., May, Helsinki, 25-30.
- Griffiths, D. V., Fenton, G. A., and Manoharan, N. (2006). “Undrained bearing capacity of two-strip footings on spatially random soil.” *Intl. J. Geomech.*, 6 (6), 421–427.
- Gringarten, E., Deutsch, C. V. (2001). “Variogram interpretation and modeling – Teacher’s

- Aide.” *Mathematical Geol.*, 33(4), 507–534.
- Isaaks, E. H., and Srivastava, R. M. (1989). *An introduction to applied geostatistics*. Oxford University Press, New York.
- ISSMGE. (2005). *Roller-Integrated continuous compaction control (CCC): Technical Contractual Provisions, Recommendations*, TC3: Geotechnics for Pavements in Transportation Infrastructure. International Society for Soil Mechanics and Geotechnical Engineering.
- Krige, D. G. (1951). *A statistical approach to some mine valuations and allied problems at the Witwatersrand*. M.S. Thesis, University of Witwatersrand, Johannesburg, South Africa.
- Mn/DOT. (2006). *Excavation and embankment – (QC/QA) IC quality compaction (2105) pilot specification*. Minnesota Department of Transportation, St. Paul, Mn.
- Mooney, M. A., and Adam, D. (2007). “Vibratory roller integrated measurement of earthwork compaction: An overview.” *Proc., 7th Intl.Symp. on Field Measurements in Geomechanics: FMGM 2007*, ASCE, Boston, Ma.
- Mostyn, G. R., and Li, K. S. (1993). “Probabilistic slope analysis: State-of-play.” *Probabilistic methods in geotechnical engineering*, K. S. Li and S-C. R. Lo, eds., Balkema, Rotterdam, The Netherlands, 89–109.
- Olea, R. A. (2006). “A six-step practical approach to semivariogram modeling – Teaching Aid.” *Stoch. Environ. Res. Risk Assess.*, 20, 307–318.
- Phoon, K-K., Kulhawy, F. H., and Grigoriu, M. D. (2000). “Reliability based design for transmission line structure foundations.” *Comput. Geotech.*, 26(3–4), 169–346.
- RVS 8S.02.6. (1999). “Continuous compactor integrated compaction – Proof (proof of compaction),” *Technical Contract Stipulations RVS 8S.02.6 – Earthworks*, Federal Ministry for Economic Affairs, Vienna.
- Samaras, A.A., Lamm, R., Treiterer, J. (1991). “Application of continuous dynamic compaction control for earthworks in railroad construction.” *Transportation Research*

- Record*, 1309, 42–46.
- Sandström, Å. (1994). *Numerical simulation of a vibratory roller on cohesionless soil*, Internal Report, Geodynamik, Stockholm, Sweden.
- Sandström A. J., Pettersson, C. B., (2004). "Intelligent systems for QA/QC in soil compaction", *Proc. TRB 2004 Annual Meeting* (CD-ROM), Transportation Research Board, Washington, D. C.
- Srivastava, R. M. (1996). "Describing spatial variability using geostatistical analysis." *Geostatistics for Environmental and Geotechnical Applications, ASTM STP 1283*, R. M. Srivastava, S. Rouhani, M. V. Cromer, A. J. Desbarats, A. I. Johnson, eds., ASTM, West Conshohocken, Pa, 13–19.
- Sulewska, M. J. (1998) "Rapid quality control method of compaction of non-cohesive soil embankment", *Geotechnical Hazards*, L. Marić, and N. Szavits, eds., Balkema, Rotterdam, May.
- Thompson, M., and White, D. (2007). "Field calibration and spatial analysis of compaction-monitoring technology measurements." *Transportation Research Record*, 2004, 69 – 79.
- Thompson, M., and White, D. (2008). "Estimating compaction of cohesive soils from machine drive power." *J. of Geotech. and Geoenviron. Engg*, ASCE (accepted).
- Vennapusa, P. (2004). "Determination of the Optimum Base Characteristics for Pavements," M.S. Thesis, Department of Civil Construction and Environmental Engineering, Iowa State University, Ames, Iowa.
- White, D. J., Rupnow, T., and Ceylan, H. (2004). "Influence of subgrade/subbase nonuniformity on pavement performance." *Proc., Geo-Trans 2004 – Geotechnical Engineering for Transportation Projects*, Geotechnical Special Publication No. 126, ASCE, Los Angeles, Ca., 1058–1065.
- White, D. J., Jaselskis, E., Schaefer, V., Cackler, T. (2005). "Real-time compaction monitoring in cohesive soils from machine response." *Transp. Res. Rec.*, 1936, Transportation Research Board, Washington D.C., 173–180.

- White, D. J., Morris, M. D., Thompson, M. (2006). "Power-based compaction monitoring using vibratory padfoot roller." *Proc. GeoCongress 2006: Geotechnical Engineering in the Information Technology Age*, ASCE Geo-Institute, Atlanta, CD-ROM.
- White, D. J., Thompson, M., Vennapusa, P. (2007a). *Field study of compaction monitoring systems – Tamping foot 825 and vibratory smooth drum CS-533E rollers*. Final Report, Center of Transportation Research and Education, Iowa State University, Ames, Ia.
- White, D., and Thompson, M. (2008). "Relationships between in-situ and roller-integrated compaction measurements for granular soils." *J. of Geotech. and Geoenviron. Engg* (accepted).
- White, D., Thompson, M., Vennapusa, P., and Siekmeier, J. (2008a). "Implementing intelligent compaction specifications on Minnesota TH 64: Synopsis of measurement values, data management, and geostatistical analysis." *Transp. Res. Rec.*, Journal of the Transportation Research Board, Washington, D.C (in press).
- White, D., Vennapusa, P., Gieselman, H. (2008b). "Roller-integrated compaction monitoring technology: Field evaluation, spatial visualization, and specifications." *Proc., 12th Intl. Conf. of Intl. Assoc. for Computer Methods and Advances in Geomechanics (IACMAG)*, 1-6 October, Goa, India (accepted).
- Whitten, E. H. T. (1963). *A Surface-fitting Program Suitable for Testing Geological Models which Involve Areal-distributed Data*. Geography Branch, Office of Naval Research, Northwestern University, Evanston, Illinois, Technical Report 2, ONR Task No. 389–135.
- ZTVE-StB. (1994). "Flächendeckende dynamische Prüfung der Verdichtung," *Technische Prüfvorschriften für Boden und Fels im Straßenbau*, FGSV-Nr 599, FGSV Verlag GmbH, Köln (in German).
- Zorn, G., 2003, *Operating manual: Light drop-weight tester ZFG2000*, Zorn Stendal, Germany.

TABLE 3.1—Commonly used theoretical semivariogram models

Model Name	Mathematical Expression
Linear	$\gamma(0) = 0$ $\gamma(h) = nC_0 + ph, \text{ when } h > 0$
Spherical	$\gamma(0) = 0$ $\gamma(h) = C_0 + C \left[\frac{3h}{2a} - \frac{h^3}{2a^3} \right] \text{ when } 0 < h < a$ $\gamma(h) = C_0 + C \text{ when } h > a$
Exponential	$\gamma(0) = 0$ $\gamma(h) = C_0 + C \left[1 - \exp\left(-\frac{h}{a}\right) \right] \text{ when } h > 0$
Gaussian	$\gamma(0) = 0$ $\gamma(h) = C_0 + C \left[1 - \exp\left(-\frac{h^2}{a^2}\right) \right] \text{ when } h > 0$

p = slope of the line

a = range

C_0 = nugget effect

$C+C_0$ = sill

TABLE 3.2—Case studies summary

ID	Case Study I	Case Study II
Roller	CS 533 E (smooth drum)	CS 563E (smooth drum)
Location	Edwards, IL	Ackeley, MN
Fill Material (USCS)	SW-SM, CL	SP
Roller Measurement Value	CMV, RMV, MDP	CMV, RMV
Amplitude (mm)	2.00	2.02
Frequency (Hz)	27.0	31.0

TABLE 3.3—Summary of soil index properties

Soil property	Fill materials		
	Case study I	Case study II	
Unified Soil Classification (USCS)	SW-SM	CL	SP
AASHTO Classification	A-1-b	A-2-6	A-3
Gravel size (%) (> 4.75mm)	29.5	3.1	4.0
Sand size (%) (4.75 to 0.075mm)	61.0	28.9	93.0
Silt + Clay size (%) (< 0.075 mm)	9.5	68.0	3.0
Liquid Limit, LL (%)	non-plastic	29	non-plastic
Plasticity Index, PI (%)	non-plastic	12	non-plastic
Optimum moisture content, w_{opt} (%) (ASTM D 698)	8.0	13.0	11.8
Maximum dry unit weight, γ_{dmax} (kN/m ³) (ASTM D 698)	21.40	18.40	17.83

TABLE 3.4—Comparison of spatial and univariate statistics of CMV with quality assurance criteria for calibration strips – case study II

IC-TV	Pass	Univariate Statistics of CMV		Spatial Statistics of CMV						QA Criteria (Percent of IC-TV)			
		μ	σ	Omni-Directional	North - South	East - West	a (m)	$C+C_0$ (CMV) ²	a (m)	$C+C_0$ (CMV) ²	a (m)	$C+C_0$ (CMV) ²	> 130%
42	2	41.0	6.9	5.0	45.0	5.0	45.0	1.0	40.0	1.0	71.2	27.9	
	3	42.6	6.2	5.0	38.0	5.0	38.0	0.5	30.0	1.2	81.5	17.4	
	4	44.7	6.3	5.0	36.0	5.0	36.0	1.0	23.0	1.4	87.7	10.9	
	6	45.9	6.3	5.0	38.0	5.0	38.0	1.0	26.0	3.8	87.0	9.1	
	7	47.6	5.6	6.0	30.0	6.0	30.0	2.0	20.0	6.0	89.0	5.0	
60	2	61.0	10.0	4.5	91.0	5.5	92.0	2.0	120.0	3.7	75.1	21.2	
	3	60.8	9.8	8.0	105.0	7.0	100.0	2.0	100.0	0.8	82.1	17.1	
	4	64.1	7.8	4.5	62.0	4.5	62.0	0.5	50.0	1.6	88.7	9.7	
	5	64.2	7.6	10.0	74.0	11.0	74.0	1.5	50.0	2.6	87.1	10.3	
	6	64.1	7.7	9.0	71.0	10.0	73.0	1.5	45.0	2.4	86.9	10.7	
	7	63.7	8.7	9.0	95.0	10.0	98.0	2.0	70.0	2.4	87.9	9.7	
	8	65.4	9.2	11.0	105.0	11.0	105.0	1.5	100.0	4.5	88.1	7.4	
	9	64.3	8.2	13.0	90.0	13.0	90.0	1.5	40.0	3.2	88.6	8.1	
	10	64.4	8.4	11.0	94.0	11.0	94.0	1.5	50.0	4.1	85.4	10.5	
	11	65.9	7.4	12.0	80.0	12.0	80.0	1.5	40.0	4.9	92.7	2.3	

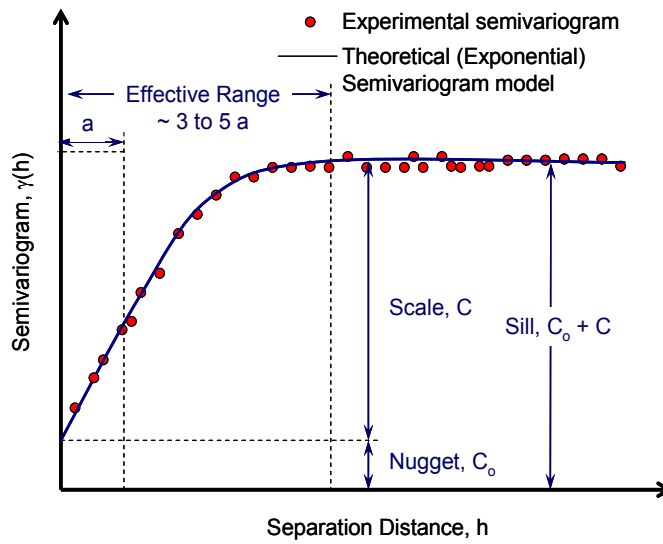


FIG. 3.1—Typical sample semivariogram. Comparatively, a semivariogram with a lower sill and longer range represents improved uniformity and spatial continuity.

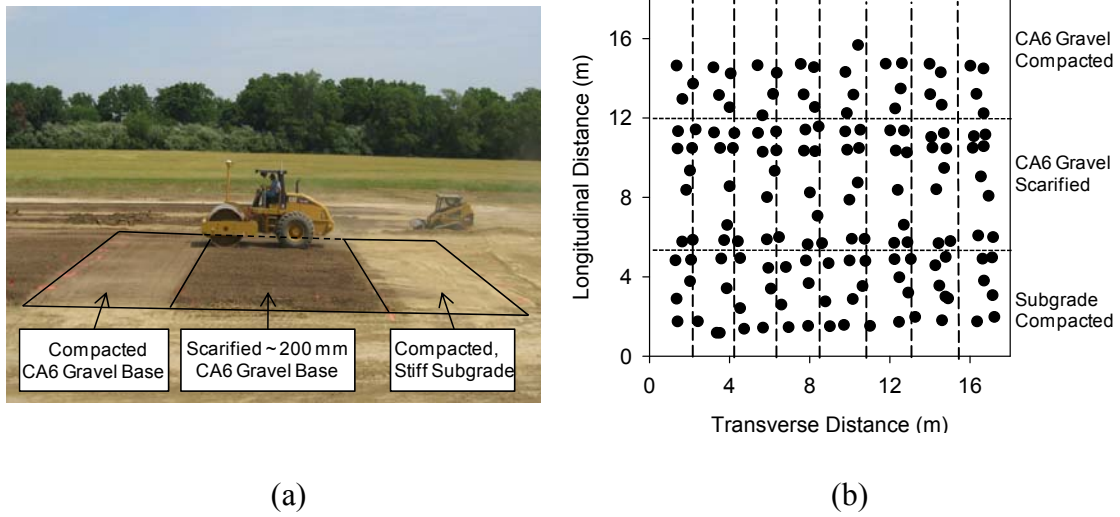


FIG. 3.2— (color) Figures for case study I showing (a) in-situ subsurface conditions and spot test locations, (b) picture of compaction process using the Caterpillar's CS 533E roller

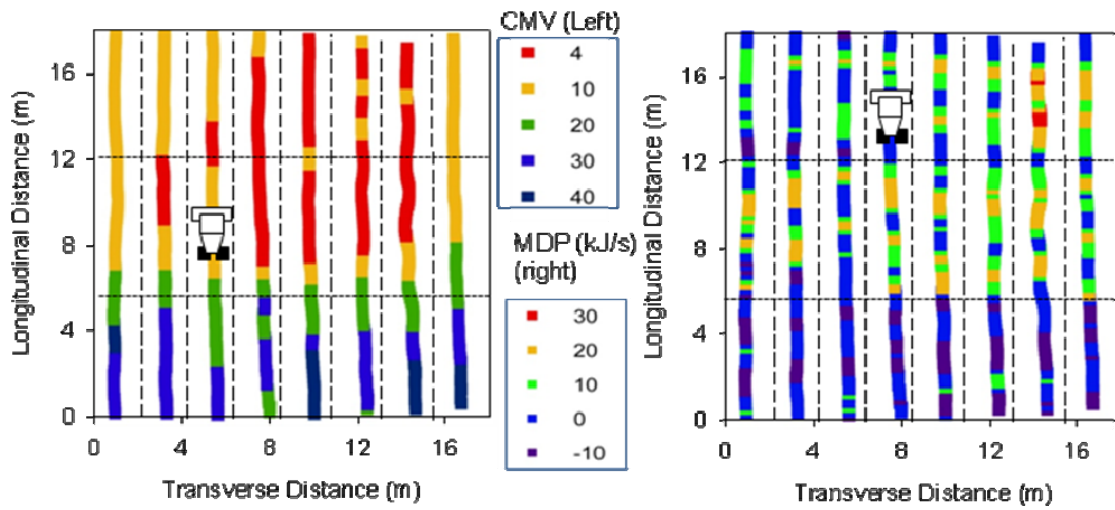


FIG. 3.3— (color) CMV (left) and MDP (right) data for case study I represented as points

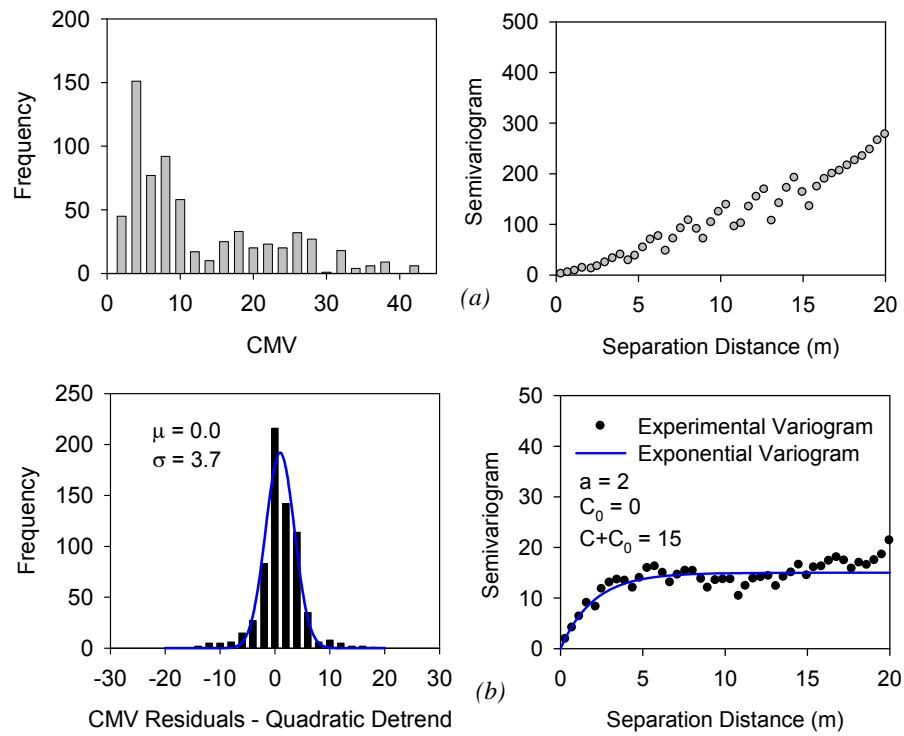


FIG. 3.4—Histogram (on left) and omni-directional semivariogram plots (on right) of CMV (a) actual data and (b) residuals after quadratic detrending from case study I

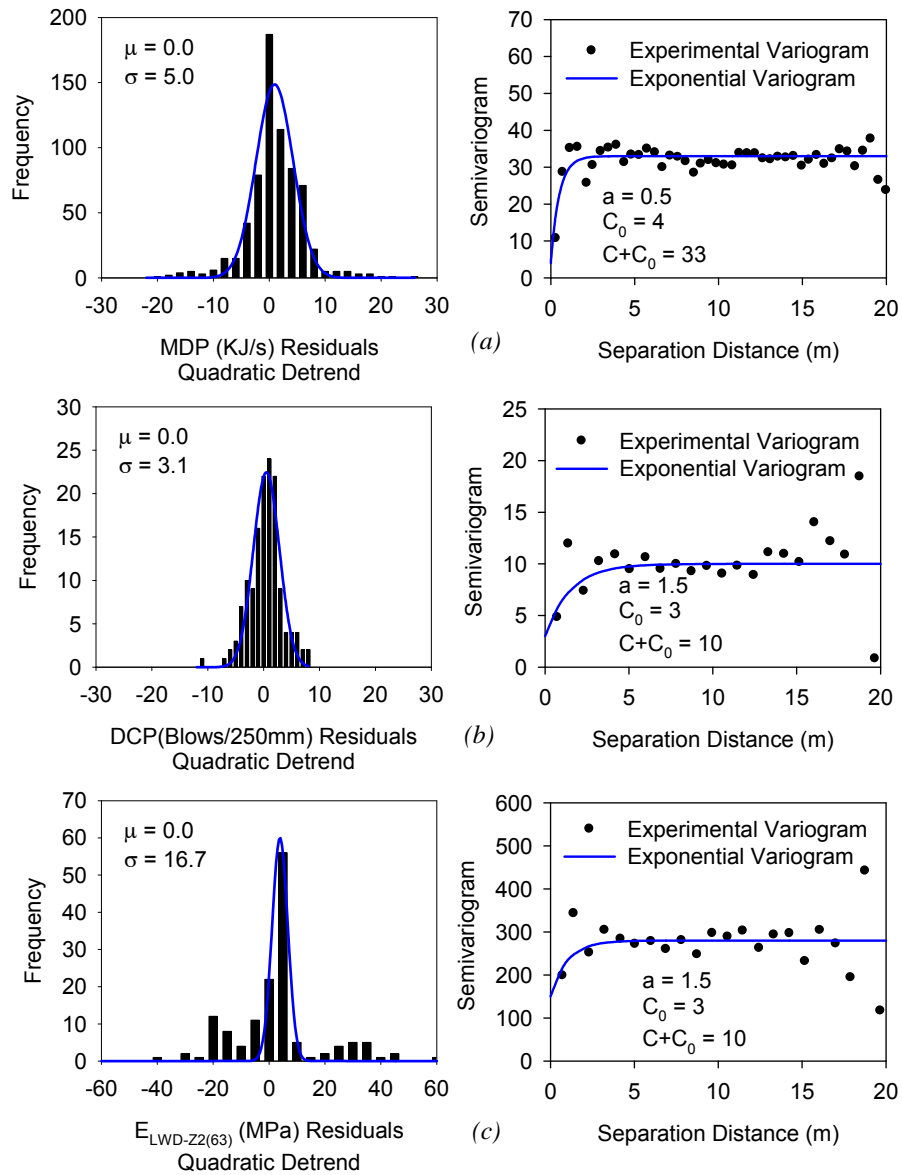


FIG. 3.5—Histogram (on left) and omni-directional semivariogram plots (on right) of residuals of (a) MDP, (b) DCP values (blows/250mm), and (c) ELWD after quadratic detrending in case study I

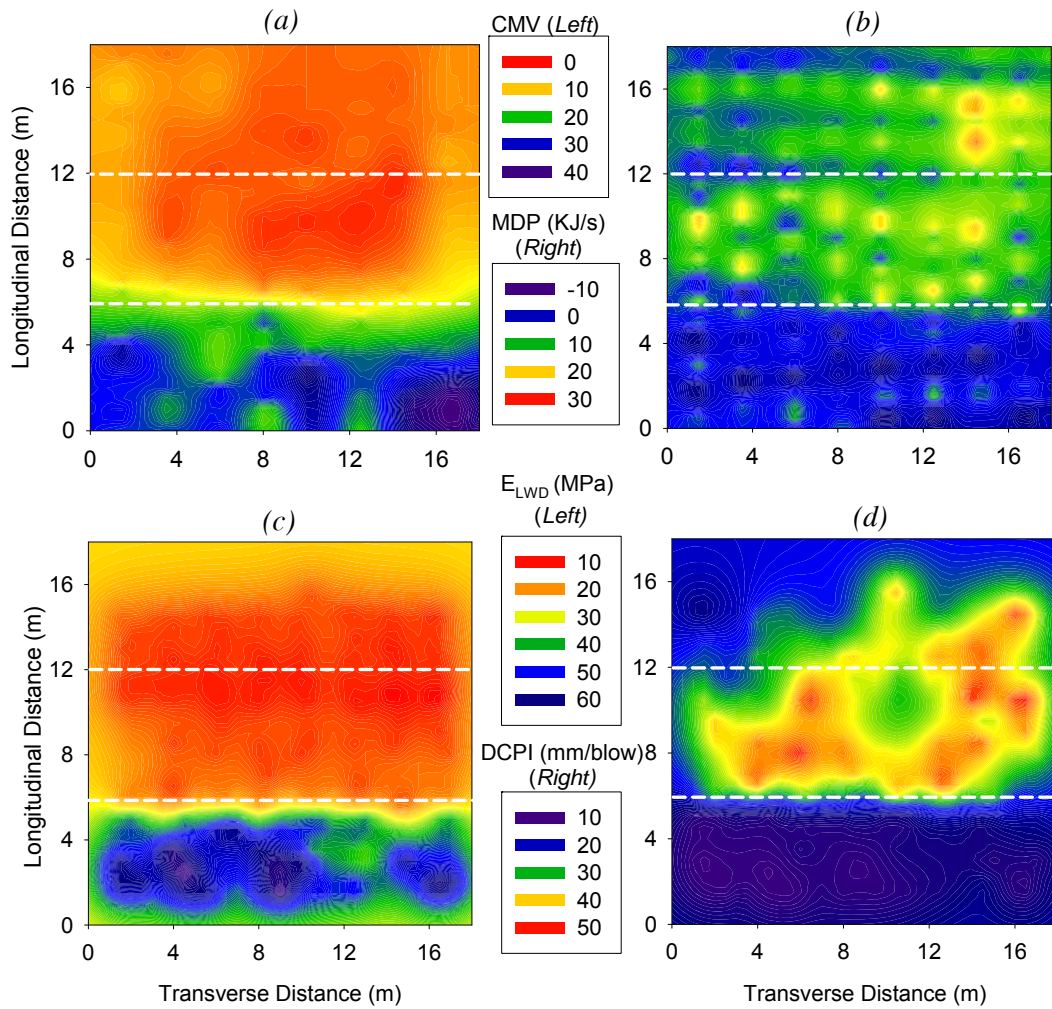


FIG. 3.6—(color) Kriged contour maps of (a) CMV (b) MDP, (c) DCPI, and (d) ELWD in case study I

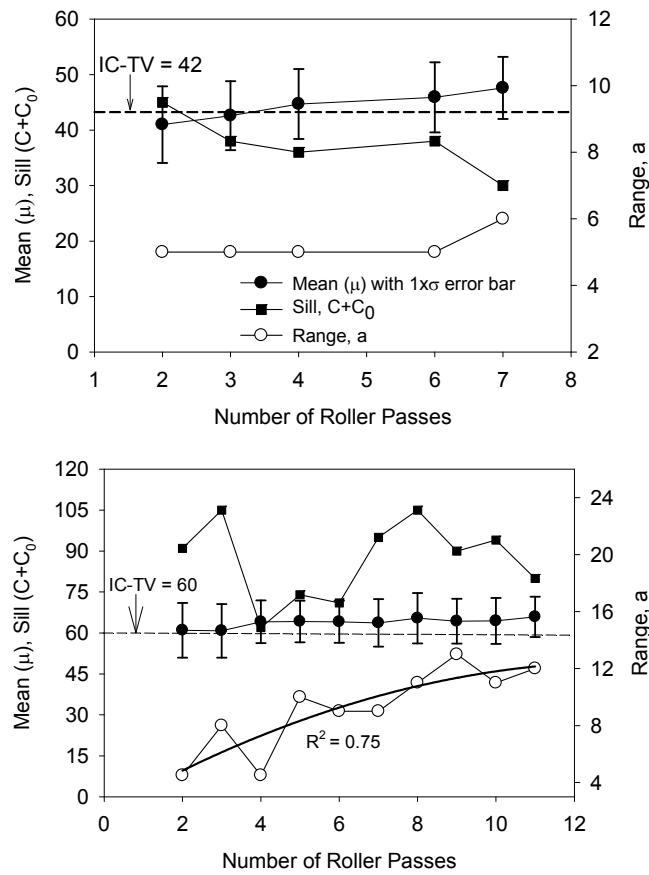


FIG. 3.7—Change in univariate (μ , σ) and spatial statistics (a , $C+C_0$) of CMV with roller passes for calibration strip 1 (on left) calibration strip 2 (on right) in case study II

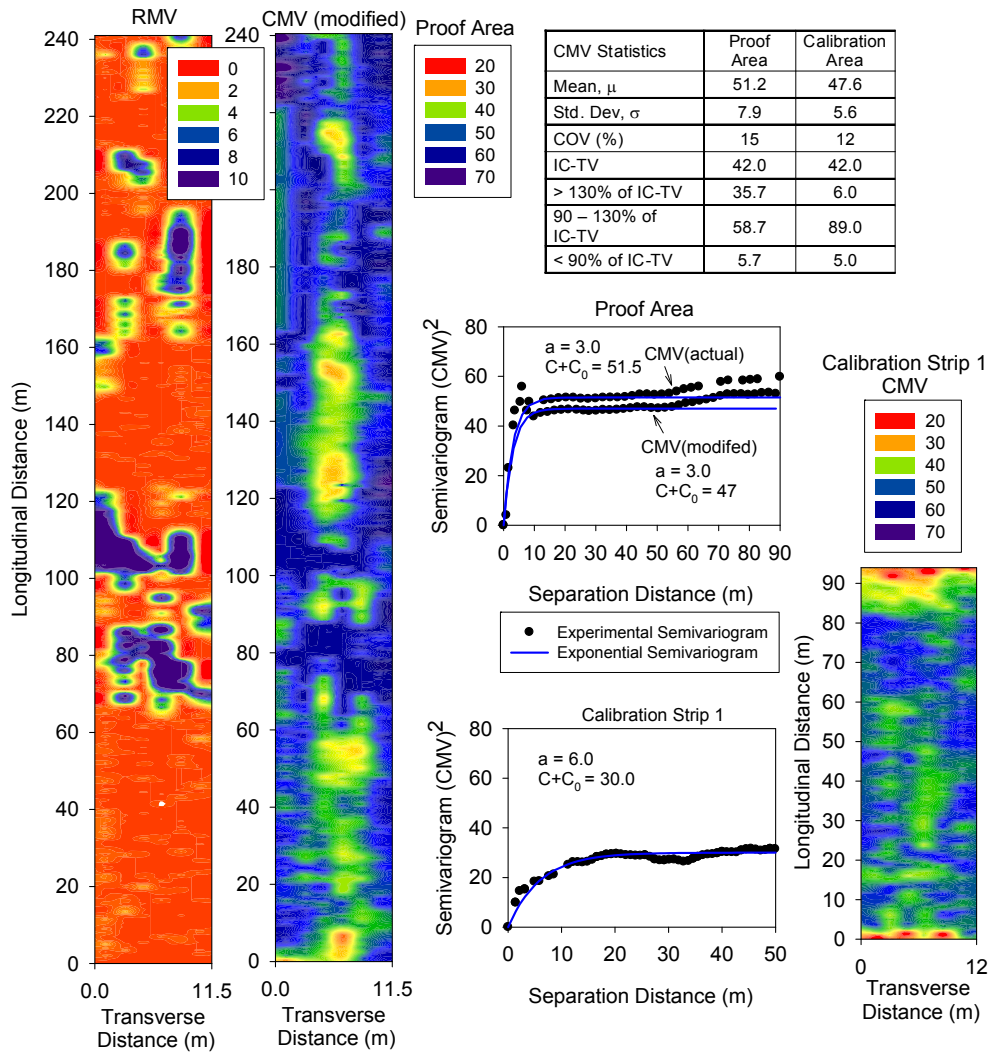


FIG. 3.8— Comparison between calibration and proof areas with univariate and spatial statistics for acceptance criteria

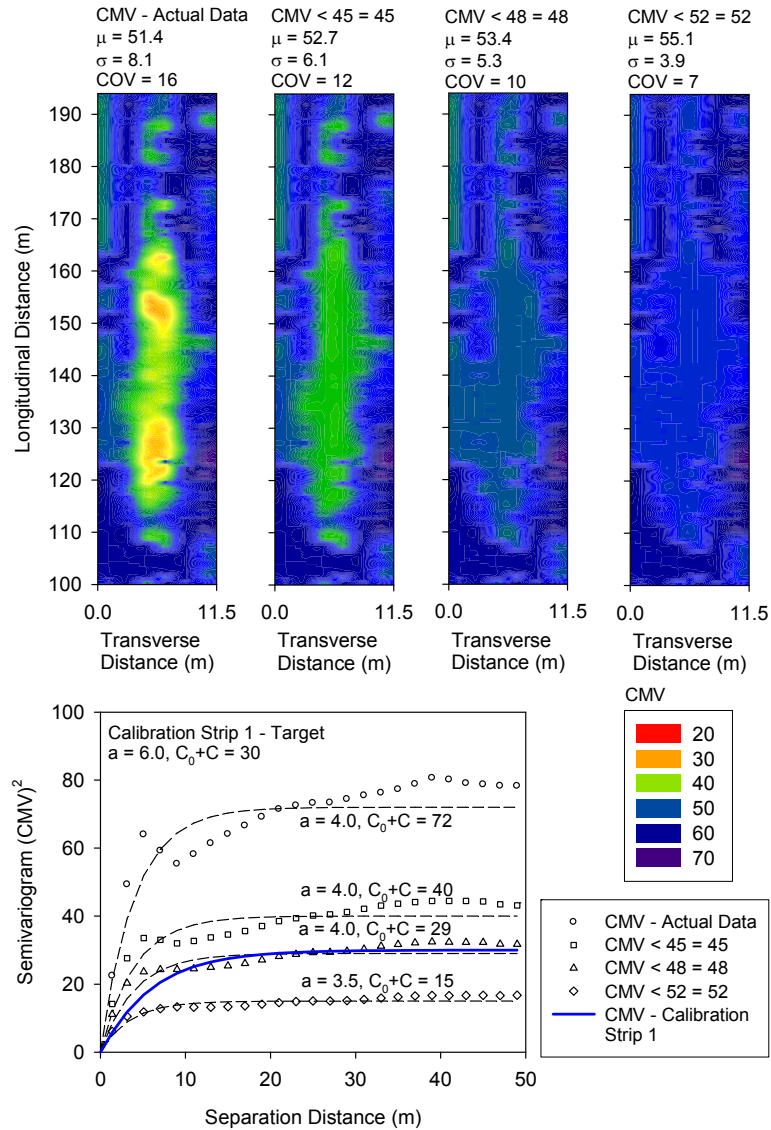


FIG. 3.9— Kriged surface maps and semivariograms of a selected portion of the proof showing variations with modifications in the actual CMV data

CHAPTER 4. ALTERNATIVES TO HEAVY TEST ROLLING FOR COHESIVE SUBGRADE ASSESSMENT

David J. White, Pavana KR. Vennapusa, Heath Gieselmann, Luke Johanson, John Seikmeier

A paper submitted to the Eight International Conference on Bearing Capacity of Roads, Railroads and Airfields, The University of Urbana-Champaign, June 29-July 2, 2009.

4.1 Abstract

This paper describes comparison measurements to assess support conditions of compacted cohesive subgrade materials using heavy test rolling, roller-integrated compaction measurements, and light weight deflectometer (LWD) and dynamic cone penetrometer (DCP) point measurements. Results indicate that many of these measurements are empirically related. Further, roller measurement values and LWD/DCP point measurements can reliably indicate the rut depth under test rolling. Target values for QA are developed for these different measurements with respect to the Mn/DOT heavy test rolling criteria for rut depth < 50 mm. DCP profiles on compacted subgrade layers show vertical non-uniformity typically with a stiff layer underlain by a soft layer. Support capacities of the subgrade under the heavy test roller were analyzed using a layered bearing capacity solution and compared to measured rut depths at the surface. A simple chart solution is presented to determine target shear strength properties of compacted subgrades from DCP profiles to ensure heavy test rolling rut depths are less than the acceptable limit.

4.2 Introduction

The performance and durability of pavement structures depend heavily on the foundation layer support conditions. Several in-situ testing methods have been developed over the past five decades to evaluate the support capacities of the subgrade layers in-situ during construction. Recently, there has been growing interest in evaluating alternatives to traditional quality assurance (QA) point measurements and to heavy test rolling for Mn/DOT

projects. Two different roller-integrated compaction measurement technologies along with comparisons to dynamic cone penetrometer (DCP) and light weight deflectometer (LWD) point measurements are discussed in this paper.

Heavy test rolling is a widely used quality assurance (QA) technique on earthwork construction projects in Minnesota for the subgrade pavement foundation (Mn/DOT 2000). Test rolling is performed using a pneumatic wheel roller on a compacted surface and the ruts observed beneath the wheels are measured to assess the support conditions. Test rolling has the advantage of providing a continuous visual record; however, it can be difficult and expensive to setup and operate.

Roller-integrated compaction monitoring (also referred to as continuous compaction control or intelligent compaction) aided with global positioning system (GPS) were investigated as alternatives to test rolling because the measurements can be viewed in real-time during the compaction process and the data provides 100% coverage. Two different roller-integrated compaction measurement technologies are discussed in this paper: (1) Geodynamik compaction meter value (CMV) and (2) machine drive power (MDP). Regardless of the type of measurement technology, by making the compaction machine a measuring device, the compaction process can be better controlled to improve quality, reduce rework, maximize productivity, and minimize costs, etc. While compaction monitoring technologies offer significant advantages, to successfully implement the technology it is necessary to develop an understanding of their relationships to conventionally used test measurements – in this case heavy test rolling. The approach for implementation in Minnesota has been to develop material and site specific target roller measurement values and LWD values (see Mn/DOT 2006, White et al. 2008).

LWD and DCP are rapid in-situ quality control/assurance (QC/QA) testing tools that are being widely evaluated by several agencies across the globe in earthwork construction practice. LWD testing is relatively rapid compared to DCP testing and has the advantage of determining elastic modulus which is a primary input in pavement design. The measurements are typically influenced by material beneath the plate up to a depth equal to the diameter of the loading plate (Kudla et al. 1991). Dynamic cone penetration index (DPI) measured from

DCP test is inversely related to soil strength/stiffness properties and is well discussed in the literature (e.g., McElvanet & Djatnika, 1991, Konrad & Lachance, 2001). Correlations developed between DPI and undrained shear strength properties are presented later in this paper. A major advantage of the DCP test is that it creates a near continuous vertical record of soil mechanical properties typically up to a depth of about 1 m, which is critical in detecting vertical non-uniformity in compacted fill materials. In this paper, support capacities of the subgrade under a test roller is analyzed using DCP profiles and classical layered bearing capacity solution proposed by Meyerhof & Hanna (1978).

Recent field studies assessing compaction quality for cohesive embankment subgrades in Minnesota and Iowa (see White et al. 2007a, Larsen et al. 2008) documented significant vertical non-uniformity in soil strength/stiffness properties. This condition is generally a result of poor moisture control and overly thick lift placement. An example of vertical non-uniformity from US14 construction project in Janesville, MN on compacted glacial till material is presented in Figure 4.1 (White et al. 2007). DCP tests conducted at five select locations in an area of compacted subgrade showed significant vertical non-uniformity based on undrained shear strength profiles at each point (undrained shear strength s_u values estimated from DPI using a correlation presented later in this paper). Heavy test rolling performed in this area using a 133.5 kN (15 ton) pneumatic tire roller showed rutting on the order of 50 mm at points 1, 2, and 4 and minimal rutting at points 3 and 5. The comparatively-wet moisture content at the surface and low undrained shear strength conditions are believed to have contributed to poor stability under the test roller at points 1, 2, and 4. The presence of vertical non-uniformity in the support conditions of subgrades is of consequence as it can potentially affect the performance of the overlying pavement structures.

In brief, the key objectives of this paper are to: (a) evaluate empirical relationships between rut depth measurements from heavy test rolling and roller integrated measurement values, and LWD/DCP point measurement values, (b) demonstrate an approach to develop target values for roller and point measurement values relating to conventionally accepted rut depth measurements, and (c) evaluate the effect of vertical non-uniformity in soil shear strength properties on bearing capacity under the test roller.

4.3 Background

4.3.1 Roller-Integrated compaction measurements

A CP-563 12-ton padfoot roller equipped with MDP system (Figure 4.2a) and a CS-683 19-ton smooth drum roller equipped with Geodynamik CMV system were used in this study (Figure 4.2b). Controlled field studies documented by White & Thompson (2008) and Thompson & White (2008) verified that roller-integrated machine drive power (MDP) can reliably indicate soil compaction for granular and cohesive soils. The basic premise of determining soil compaction from changes in equipment response is that the efficiency of mechanical motion pertains not only to the mechanical system but also to the physical properties of the material being compacted. MDP is calculated using Equation 4.1.

$$\text{MDP} = P_g - WV \left(\sin \alpha + \frac{a}{g} \right) - (mV + b) \quad (4.1)$$

where P_g = gross power needed to move the machine (kJ/s), W = roller weight (kN), a = machine acceleration (m/s^2), g = acceleration of gravity (m/s^2), α = slope angle (roller pitch from a sensor), V = roller velocity (m/s), and m (kJ/m) and b (kJ/s) = machine internal loss coefficients specific to a particular machine (White et al. 2005). MDP is a relative value referencing the material properties of the calibration surface, which is generally a hard compacted surface ($\text{MDP} = 0$ kJ/s). Positive MDP values therefore indicate material that is less compact than the calibration surface, while negative MDP values would indicate material that is more compacted than the calibration surface (i.e. less roller drum sinkage). The MDP results presented in this paper (here after referred to as MDP^*) are adjusted on a 1 to 150 scale. The calibration surface with $\text{MDP} = 0$ (kJ/s) is scaled to $\text{MDP}^* = 150$, and a soft surface with $\text{MDP} = 111.86$ (kJ/s) is scaled to $\text{MDP}^* = 1$ (from email communication with Mario Souraty, Caterpillar, Inc. October 2007). The relationship to calculate MDP^* from MDP is provided in Equation 3.2 (note that as compaction increases MDP decreases and MDP^* increases).

$$\text{MDP}^* = 119.7 - 0.798 \times (\text{MDP}) \quad (4.2)$$

The CMV technology uses accelerometers to measure drum accelerations in response to soil behavior during compaction operations. The ratio between the amplitude of the first

harmonic and the amplitude of the fundamental frequency provides an indication of the soil compaction level (Thurner & Sandström, 1980). An increase in CMV indicates increasing compaction. CMV is calculated using Equation 4.3.

$$\text{CMV} = C \cdot \frac{A_1}{A_0} \quad (4.3)$$

where C = constant (300), A_1 = acceleration of the first harmonic component of the vibration, and A_0 = acceleration of the fundamental component of the vibration (Sandström & Pettersson, 2004). CMV is a dimensionless parameter that depends on roller dimensions (i.e., drum diameter, weight) and roller operation parameters (i.e., frequency, amplitude, speed). CMV at a given point indicates an average value over an area whose width equals the width of the drum and length equal to the distance the roller travels in 0.5 seconds (Geodynamik ALFA-030).

4.3.2 Test rolling

Test rolling was performed using a pneumatic tire two-wheeled trailer with each wheel weighing 133.5 kN and is towed behind a tractor (Figure 4.2c) in accordance with Mn/DOT specifications (Mn/DOT 2000). The two wheels on the trailer were spaced 1.8 m apart, and the wheels were inflated to approximately 650 kPa. The contact width and length of the wheel were specified as 0.46 m (width) x 0.45 m (length). The depth of the rut beneath the roller wheels was measured from the top of the subgrade. If measured rut depths are ≥ 50 mm, the subgrade is considered unstable and it is specified to treat the subgrade appropriately (Mn/DOT 2000).

4.3.3 In-situ point measurements

Four different in-situ test methods were employed in this study to evaluate the in-situ support conditions: (1) undisturbed Shelby tube (ST) samples, (2) dynamic cone penetrometer (DCP), (3) light weight deflectometer (LWD), and (4) static plate load test (PLT). Undisturbed samples of compacted subgrade material were obtained by hydraulically pushing 71 mm diameter Shelby tube samples (Figure 4.2d). The tube samples were sealed and transported to the laboratory for unconfined compression testing in accordance with ASTM D2166-91 to determine undrained shear strength, s_u . DCP tests were performed in

accordance with ASTM D6951-03 to measure DPI (Figure 4.2e). DPI values determined for correlations presented later in this paper are determined as the ratio of 200 mm penetration depth and cumulative number of blows to reach that penetration depth. Zorn LWD tests were performed using a 200-mm diameter bearing plate setup with a 10-kg weight dropped from a height of 50 cm in accordance with manufacturer recommendations. ELWD-Z2 was determined following manufacturer recommendations (Zorn 2003) (assuming Poisson's ratio $\nu = 0.4$ and shape factor $f = \pi/2$). For surfaces with padfoot indentations, a level surface was prepared for testing by removing the material to the bottom of padfoot penetration to ensure repeatable results. Static PLT's were conducted by applying a static load on 300 mm diameter plate against a 6.2kN capacity reaction force. The applied load was measured using a 90-kN load cell and deformations were measured using three 50-mm linear voltage displacement transducers (LVDTs). The load and deformation readings were continuously recorded during the test using a data logger.

4.4 Experimental Testing

Tests reported in this paper were collected from two cohesive embankment subgrade construction projects: (1) US14 located near Janesville, MN and (2) TH60 located near Bigelow, MN. Results from US14 are shown in Figure 4.1, and soil index properties are presented in Table 4.1. Four sites (Site A, B, C, and D) were tested on the TH60 project. A summary of soil index properties are provided in Table 4.1, and a brief summary of site conditions are provided below.

Sites A and B consisted of one-dimensional test strips with uncompacted fill material of thickness in the range of about 0.25 to 0.50 m. The fill material was placed with average moisture contents of about 20.0% and 19.2%, respectively. The test strips were compacted using the CP 563 padfoot roller using constant machine operation settings $a = 1.87$ mm, $f = 30$ Hz, and $v = 3.2$ km/h. In-situ point measurements (DPI and E_{LWD-Z2}) were obtained in conjunction with the roller compaction measurements. ST samples were obtained after the final pass from the compacted subgrade layer at site A for unconfined compression testing. Site C consisted of a compacted subgrade material with plan dimensions of about 7.5 m x 30

m. The compaction layer was placed at an average moisture content of about 12.5%. The area was test rolled and rut depth measurements were obtained from 11 test locations. LWD and DCP point measurements were obtained at the rut depth locations. ST samples were obtained from select point measurement locations for unconfined compression testing. The area was then mapped using the CS 683 smooth drum roller using constant machine operation settings $a = 0.85$ mm, $f = 30$ Hz, and $v = 3.2$ km/h. Site D was located in a median area with dark brown topsoil material. LWD, DCP, and static PLT measurements were obtained from this site.

4.4.1 Correlations between different QA test measurements

Relationships derived from experimental testing described above are summarized in Figure 4.3. The relationships are first discussed below and then target values are derived based on the relationships and compared with target values used on the project. A non-linear relationship was found between DPI and undrained shear strength, s_u (Figure 4.3a). This relationship was developed based on unconfined compression tests performed on samples obtained from different depths at the DCP test locations. The relationship showed good correlation with $R^2 = 0.6$. A similar relationship was published by McElvanet & Djatnika (1991) for lime-stabilized materials as shown in Figure 4.3a. Data obtained from this project fall slightly below the trend observed by McElvanet & Djatnika (1991). E_{LWD} and DPI showed a non linear relationship with $R^2 = 0.7$ (3.3b). Similar non-linear relationships between elastic modulus and DPI are reported by others (e.g. Chai & Roslie 1998).

Relationships between rut depth measurements with E_{LWD} produced $R^2 = 0.6$ (3.3c). Some scatter was evident at rut depths $<$ about 40 mm and the reason is attributed to the differences in the influence depths of the two measurements. A stiff compaction layer of at least 200 mm in thickness typically results in a high E_{LWD} value (determined from a 200 mm diameter plate), while ruts beneath the test roller wheel are a result of subgrade conditions well below the compaction layer. An approach to analyze support capacities of the subgrade under the roller wheel using layered bearing capacity analysis is described later in this paper.

Relationships between roller-integrated CMV/MDP and in-situ point measurements are developed by spatially paring the nearest point data using GPS measurements.

Correlation between CMV – rut depth and E_{LWD} produced $R^2 = 0.6$ and 0.7 , respectively (Figure 4.3e, 4.3f). MDP* and E_{LWD} correlation showed two different trends for the two sites (Figure 4.3d). The MDP* values tend to reach an asymptotic value of about 150 which is the maximum value on the calibration hard surface.

The correlations for roller-integrated CMV and MDP with conventional test measurements (e.g. rut depth, E_{LWD}) showed correct trends but with varying degree of uncertainty (assessed by R^2 values) in the relationships. This scatter is expected because of the various factors that influence the relationships which include: (a) differences in measurement influence depths, (b) range over which measurements were obtained, (c) influence of moisture content, (d) intrinsic measurement errors associated with the roller MVs and point measurements, (d) position error from pairing point test measurements and roller MV data, and (f) soil variability.

4.4.2 Bearing capacity analysis on layered cohesive soil stratum

DCP profiles were analyzed for bearing capacity under the test roller wheel using analytical layered bearing capacity solutions proposed by Meyerhof & Hanna (1978). For the analysis, the contact area under the tire is assumed a rigid rectangular flat footing of size 0.46 m x 0.64 m (contact dimensions from Mn/DOT 2000), the contact pressure under the tire is assumed to be uniform, and the load application is assumed to be vertical. The behavior of soil beneath a wheel is assumed analogous to soil behavior beneath a footing under undrained loading conditions. The footing is assumed to be rigid to simplify the analysis and is considered a reasonable assumption with the relatively high tire inflation pressure and tire carcass stiffness compared to the deformability of the soil (see Bekker 1960). The analysis can be fine tuned by solving theoretical equations to determine contact area under the roller, considering a possible inclination in footing shape and load, and accounting for flexibility of the rubber tire (see Hambleton & Drescher 2008). Hambleton & Drescher 2008 summarized theoretical solutions to determine contact area as a function of wheel sinkage which is a sum of both elastic (rebound after the load application) and plastic deformations (measured rut depth) under the wheel. Although plastic deformation is predominant at locations with greater rut depths, locations with minimal rut depths can have considerable elastic rebound,

but is difficult to measure. The analysis is simplified herein with an objective of analyzing the effect of vertical non-uniformity on the subgrade bearing capacity under the wheel and obtaining insights on approximate target shear strength properties required to overcome rut failures under the test roller.

Meyerhof & Hanna (1978) proposed analytical solutions to estimate bearing capacity of a two-layered soil stratum with stronger soil overlaid by a weaker soil of known soil mechanical properties. If the thickness of the stronger layer (H) is relatively small, a punching shear failure is expected in the top stronger soil layer, followed by a general shear failure in the bottom weaker soil layer. In that case the ultimate bearing capacity q_{ult} is a function of the s_u properties (for $\phi' = 0$ condition) of both top and bottom layers and is calculated using Equation 4.4. If the thickness H is relatively large, then the failure envelope lies within the top layer only. For that case, q_{ult} is a function of top layer s_u using Equation 4.5.

$$q_{ult} = \left(1 + 0.2 \frac{B}{L}\right) 5.14 s_{u2} + \left(1 + \frac{B}{L}\right) \left(\frac{2c_a H}{B}\right) \leq q_t \quad (4.4)$$

$$q_t = \left(1 + 0.2 \frac{B}{L}\right) 5.14 s_{u1} \quad (4.5)$$

where B = contact width, L = contact length, s_{u1} = undrained shear strength of the top layer, s_{u2} = undrained shear strength of the bottom layer, c_a = adhesion determined using theoretical relationship between c_a/s_{u1} and s_{u2}/s_{u1} by Meyerhof & Hanna (1978).

Rut depth measurements at 11 test locations in comparison with DCP- s_u profiles at each location are presented in Figure 4.4. The s_u values were determined using the DPI- s_u relationship presented in Figure 4.3a. As described earlier and similar to previous findings by White et al. (2007a) and Larsen et al. (2008), significant vertical non-uniformity in soil shear strength properties is evident from the DCP- s_u profiles. The reason for this non-uniformity at this project is attributed to variable and thick lifts and variable moisture content.

The soil profile at each test location was analyzed as a two-layered soil system using

weighted average s_u values for each layer to determine the q_{ult} value at each location. The relationship between calculated q_{ult} values and measured rut depth measurements from the test locations is shown in Figure 4.5 and show a strong non-linear correlation with $R^2 = 0.9$. Based on the acceptable rut depth value = 50 mm, a target $q_{ult} = 1050$ kPa was calculated. This target value can be interpreted as the minimum value required at a location with a two-layered cohesive soil stratum to avoid rut depth failures, i.e., rut depths ≥ 50 mm.

The graph presented in Figure 4.5b shows relationship between s_{u1} and s_{u2} at different H values to achieve the target q_{ult} value. The advantage of viewing the results in this manner is that if s_u values of the two layers (s_{u1} and s_{u2}) are known (for example from DCP test), one can readily determine if one would or would not expect rut depth failures at a given location. An alternate way of interpretation is that if s_{u2} is known, then one can estimate the minimum required s_{u1} to avoid rut depth failures (as shown in the calculation in Figure 4.5b). A target s_u value for a homogenous condition (i.e. $H = 0$, $s_{u1} = s_{u2}$) can be readily determined from Figure 4.5b which is = 170 kPa.

q_{ult} values calculated from DCP- s_u profiles shown in Figure 4.4 are plotted on Figure 4.5 to demonstrate the use of the graphical “pass”/“fail” evaluation procedure. A test location is determined as “fail” if the measured rut depth was ≥ 50 mm and checked if the calculated q_{ult} value was $<$ target q_{ult} . Nine out of eleven test locations complied with the pass/fail criteria, and the two test locations that did not comply showed $q_{ult} = 969$ kPa with a rut depth = 23 mm and $q_{ult} = 1093$ kPa with a rut depth = 84 mm. Similarly, q_{ult} determined from DCP- s_u profiles from the TH 14 project (results presented in Figure 4.1) are also plotted in Figure 4.5 for comparison. The test points from that project did not have corresponding rut depth measurements but had visual confirmation of whether or not significant rutting was observed at the test locations. Three out of five test locations from that project complied with the pass/fail criteria. Considering the simplifications and assumptions made in the analysis and inevitable statistical uncertainty associated with empirical relationships used in the analysis, the pass/fail estimations are considered practically acceptable and useful for establishing alternative method for QA target values. As with any geotechnical engineering application, a chart like this cannot replace thorough testing/analysis and engineering judgment but it can serve as a quick reference guide for the field engineers.

The validity of the layered bearing capacity analysis analytical solutions was verified by performing 300-mm plate diameter static plate load tests at several test locations. Data from two test locations are presented in Figure 4.6. One test location was relatively soft (Point B, $E_{LWD} = 3.2$ MPa) and the other location was relatively stiff (Point A, $E_{LWD} = 26.1$ MPa) as shown in Figure 4.6. The applied load was increased at point B until a bearing capacity failure was induced and at point A until the maximum capacity of the PLT system was reached. DCP- s_u profile data was used to determine q_{ult} under the plate (assuming $B = L = 0.3$ m). The calculated $q_{ult} = 0.12$ MPa at point B was close to the measured $q_{ult} = 0.13$ MPa. The calculated $q_{ult} = 0.98$ MPa at point A appears to fall in line with the trend observed in the load-deformation curve up to an applied stress of about 0.65 MPa (tire contact pressure).

4.5 Implementation Aspects

An alternate approach to heavy test rolling is to develop regression relationships (as presented above) and target values for other measurements. A summary of QA target values developed based on the empirical relationships presented in Figure 4.3 are shown in Table 4.2. The target E_{LWD} and CMV measurement values were derived from relationships with rut depth measurements corresponding to a rut depth of 50 mm. The MDP* target value was derived from the relationship developed with E_{LWD} from site A (Figure 4.3d) for $E_{LWD} = 27$ MPa. The target s_u value was determined based on the layered bearing capacity analysis. The regression relationships, however, have some uncertainty which can be accounted for using statistical prediction limits at a selected percent confidence. For example, values in a relationship corresponding to the least-squared fit regression line will provide about 50% confidence in the predicted target value.

4.6 Concluding Remarks

Use of roller-integrated compaction measurement technologies (CMV and MDP) and DCP/LWD point measurements to evaluate the support capacities of subgrade layers in-situ are discussed in this paper. Comparisons were made to heavy test roller rut depth QA criteria

specified by Mn/DOT for the upper subgrade layer of a pavement foundation. Correlations developed between roller-integrated CMV and MDP and point measurements show positive trends but with varying degrees of uncertainty in relationships.

DCP- s_u profiles on compacted subgrades showed significant vertical non-uniformity with depth. Test rolling identified deep soft layers with excessive rutting (rut depths ≥ 50 mm) at the surface. Bearing capacities under the heavy roller wheel were evaluated using layered bearing capacity analytical solutions and DCP- s_u profiles. The ultimate bearing capacities determined were empirically related to the measured rut depths at the surface. A chart solution was developed for using the layered bearing capacity analysis to determine target shear strength properties of a layered soil to avoid rut failures under the test roller.

Considering the significant advantage of roller-integrated compaction monitoring technologies with 100% coverage of compacted areas and positive trends in the relationships, it is concluded that the measurements can serve as a reliable indicator of compaction quality of cohesive subgrades and provide a good alternative to heavy test rolling. A summary of QA target values for the different measurements based on the empirical relationships are provided.

4.7 Acknowledgements

The Minnesota Department of Transportation (Mn/DOT) and the Federal Highway Administration (FHWA) sponsored this study under Mn/DOT Contract No. 89256, Work Order No. 2. Numerous Mn/DOT district staff and Mathiowetz Construction Co. personnel assisted the authors in identifying and providing access to grading projects for testing. The authors would like to thank several graduate and undergraduate research assistants who provided assistance with the ISU Geotechnical Mobile Lab in field and lab testing.

4.8 References

Bekker, M.G. (1960). *Off the Road Locomotion*. University of Michigan Press, Ann Arbor, MI.

- Chai, G. and Roslie, N. (1998). "The structural response and behavior prediction of subgrade soils using falling weight deflectometer in pavement construction." *Proceedings of 3rd International Conference on Road and Airfield Pavement Technology*, Beijing, China.
- Geodynamik ALFA-030. *Compactometer, Compaction Meter for Vibratory Rollers*, ALFA-030-051E/0203, Geodynamik AB, Stockholm (Sweden).
- Hambleton, J.P. and Drescher, A. 2008. *Development of improved test rolling methods for roadway embankment construction*. Final Report MN/RC 2008-08. Minnesota Department of Transportation, St. Paul, MN.
- Konrad, J. and Lachance, D. 2001. "Use of in-situ penetration tests in pavement evaluation." *Canadian Geotechnical Journal*, 38(5), 924–935.
- Kudla, W., Floss, R. and Trautmann, C. (1991). Dynamic test with plate – Quick method of quality assurance of road layers without binder. *Streets and Highways (Strasse and Autobahn)*, 2: 66–71, Bonn (in German).
- Larsen, B.W., White, D.J. and Jahren, C.T. (2008). "Pilot project to evaluate dynamic cone penetration QC/QA specification for cohesive soil embankment construction." *Transportation Research Record*, Journal of the Transportation Research Board (in press).
- McElvaney, J. and Djatnika, I. (1991). "Strength evaluation of lime-stabilized pavement foundations using the dynamic cone penetrometer." *Australian Road Research*, 21(1), 40–52.
- Meyerhof, G.G. and Hanna, A.M. (1978). "Ultimate bearing capacity of foundations on layered soil under inclined load." *Canadian Geotechnical Journal*, 15(4), 565–572.
- Mn/DOT. (2000). *Standard Specifications for Construction – Specification 2111 Test Rolling*. Minnesota Department of Transportation (Mn/DOT), St. Paul, MN.
- Mn/DOT. (2006). *Excavation and Embankment – Quality Compaction by IC, LWD, and Test Rolling (Pilot Specification for Embankment Grading Materials)*. S.P. 5305-55, Minnesota Department of Transportation (Mn/DOT), St. Paul, MN.

- Sandström A.J. and Pettersson, C.B. (2004). “Intelligent systems for QA/QC in soil compaction.” *Proceedings of the 83rd Annual Transportation Research Board Meeting*, January 11–14. Washington, D.C.
- Thompson, M. and White, D.J. (2008). “Estimating compaction of cohesive soils from machine drive power.” *Journal of Geotechnical and Geoenvironmental Engineering*, ASCE, (in press).
- Thurner, H. and Sandström, Å. (1980). “A new device for instant compaction control.” *Proceedings of the International Conference on Compaction*, Vol II: 611–614, Paris.
- White, D.J., Jaselskis, E.J., Schaefer, V.R. and Cackler, E. T. (2005). “Real-time compaction monitoring in cohesive soils from machine response.” *Transportation Research Record*, Journal of the Transportation Research Board, 1936, 173–180.
- White, D.J., Thompson, M. and Vennapusa, P. (2007a). *Field validation of intelligent compaction monitoring technology for unbound materials*. Final Report MN/RC-2007-10, Minnesota Department of Transportation, St. Paul, MN.
- White, D.J. and Thompson, M. (2008). Relationships between in-situ and roller-integrated compaction measurements for granular soils. *Journal of Geotechnical and Geoenvironmental Engineering*, ASCE (in press).
- White, D.J. Thompson, M., Vennapusa, P., and Siekmeier, J.(2008). “Implementing intelligent compaction specification on Minnesota TH64: Synopsis of measurement values, data management, and geostatistical analysis.” *Transportation Research Record*, Journal of the Transportation Research Board, 2045: 1–9.
- Zorn, G. (2003). *Operating manual: Light drop-weight tester ZFG2000*, Zorn Stendal, Germany.

TABLE 4.1— Summary of soil index properties.

Parameter	Test Method	US14	TH60			
		Janesville, MN	Bigelow, MN			
			Site A	Site B	Site C	Site D
Material Description	—	Brown glacial till	Brown glacial till	Brown glacial till	Brown glacial till	Dark Brown topsoil
Standard Proctor γ_{dmax} (kN/m ³)	ASTMD 698-00	—	16.35	17.19	18.24	16.72
Optimum w (%)		—	19.3	17.3	13.3	17.3
Liquid Limit, LL	ASTMD	—	43	39	36	39
Plasticity Index, PI	4318-93	—	16	19	15	11
USCS group symbol	ASTMD	CL	CL	CL	CL	OL
USCS group name	2487-93/ 2488-93	Sandy lean clay	Lean clay with sand	Sandy lean clay	Sandy lean clay	Sandy organic clay

TABLE 4.2—Summary of QA target values as an alternative to heavy testing rolling rut depth of 50 mm.

Measurement Value	Target values from empirical relationships
E_{LWD-22} (MPa)	27
CMV	23
MDP*	149
DPI	12
s_u (kPa)	170

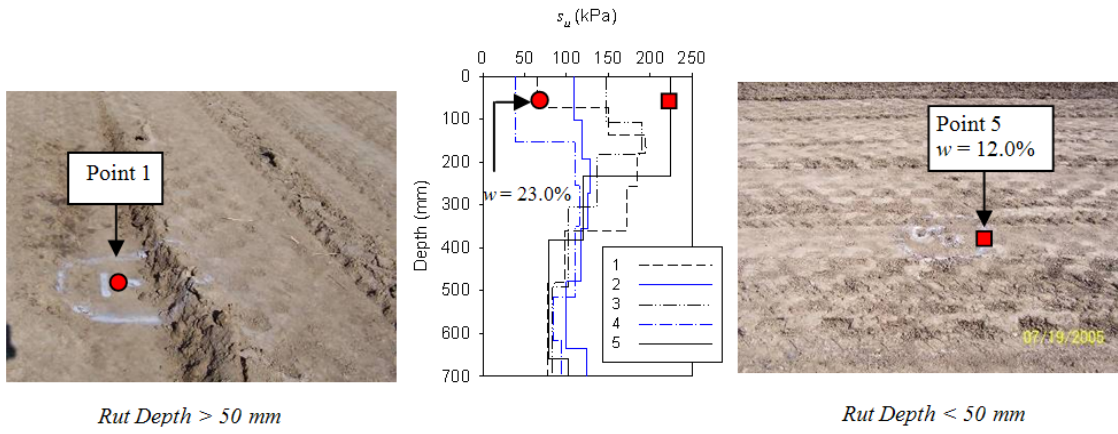


FIG. 4.1—DCP- s_u profiles from compacted glacial till subgrade at US14 (White et al. 2007a)



FIG. 4.2— (a) CP-563 roller, (b) CS-563 roller, (c) Towed pneumatic dual-wheel test roller with 650 kPa contact tire pressure, (d) Shelby tube sampler, (e) DCP, (f) Zorn 200-mm diameter plate LWD, (g) 6.2 kN capacity static plate load test setup.

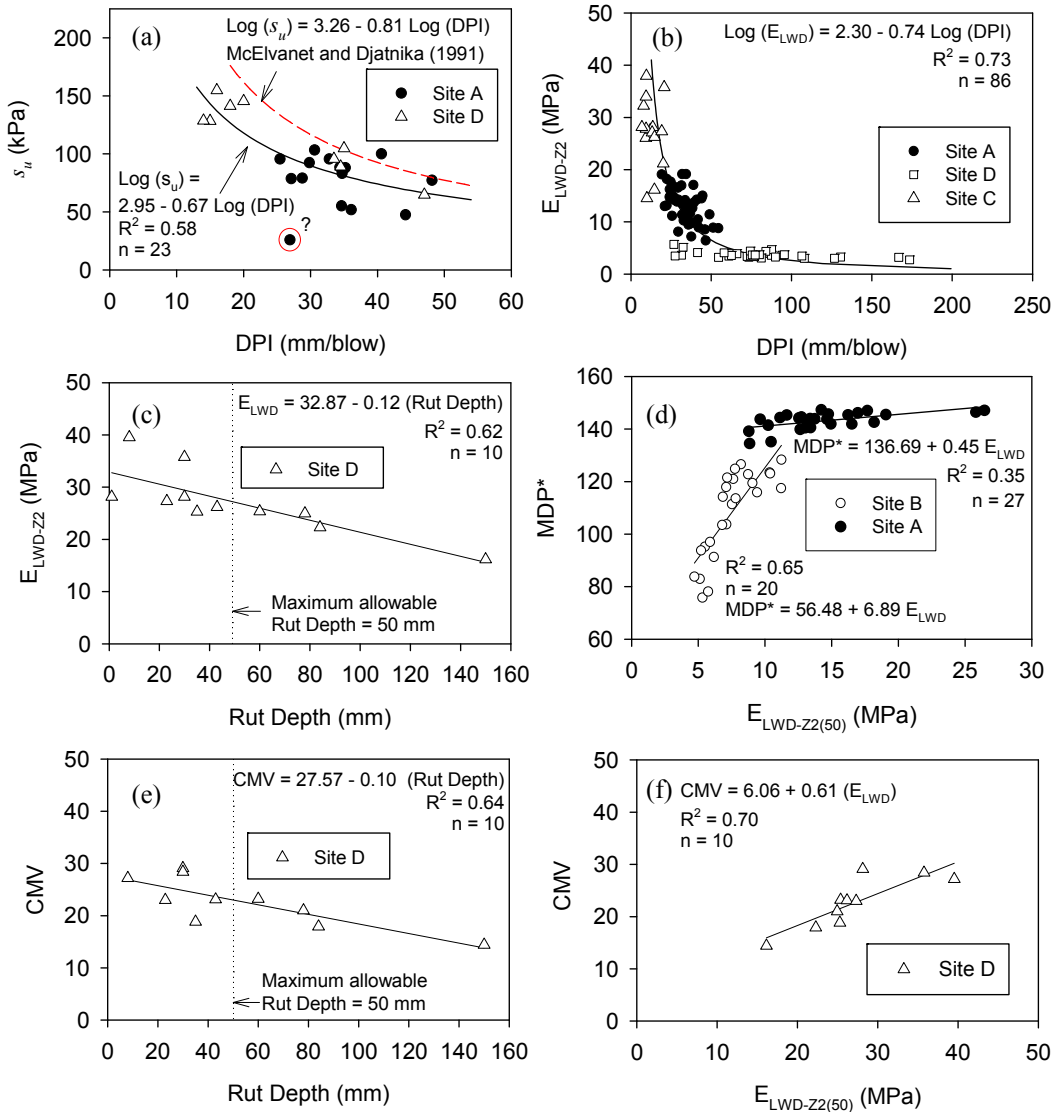


FIG. 4.3— Relationships between: (a) DPI and s_u , (b) DPI and E_{LWD} , (c) rut depth and E_{LWD} , (d) rut depth and CMV, (e) E_{LWD} and MDP^* , and (f) E_{LWD} and CMV.

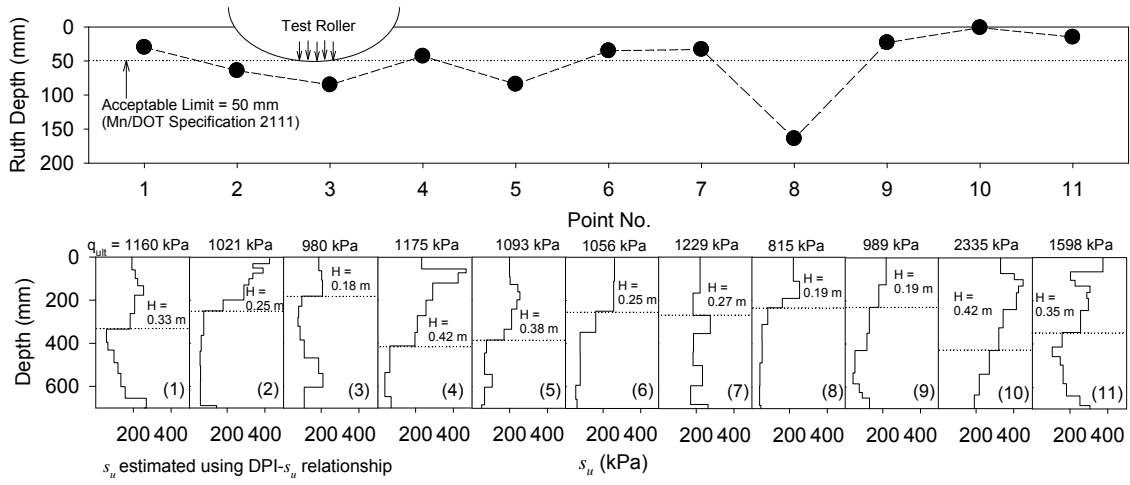


FIG. 4.4— Comparison of DCP- s_u profiles with rut depth measurements.

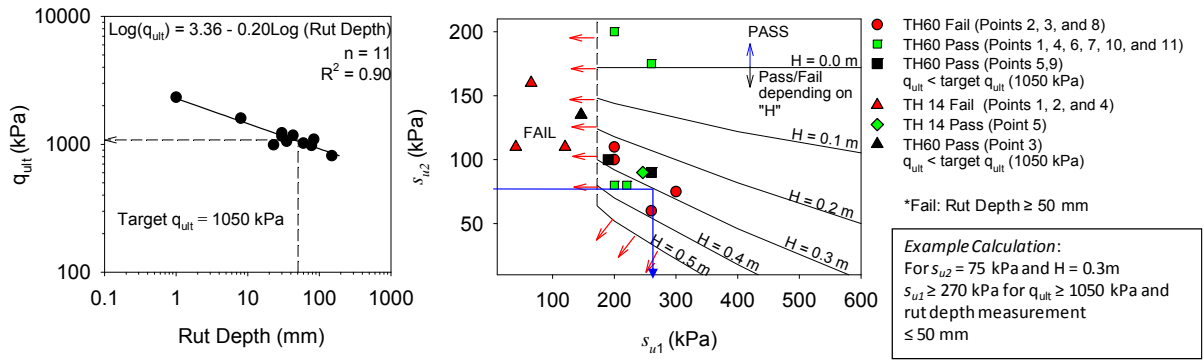


FIG. 4.5— (a) Relationship between calculated ultimate bearing capacity and measured rut depth, and (b) influence of undrained shear strength properties of top and bottom layers at different H (thickness of the top layer) to achieve a minimum $q_{ult} = 1050$ kPa.

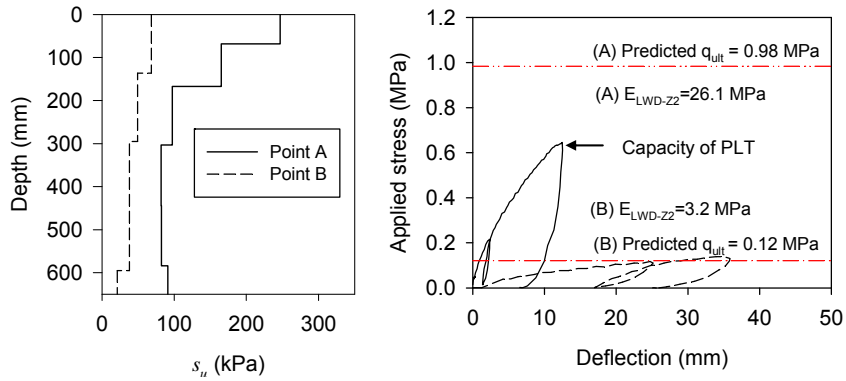


FIG. 4.6— Comparison of estimating ultimate bearing capacity from layered bearing capacity analysis and 300 mm plate load test measurements.

CHAPTER 5. IN-SITU MECHANISTIC CHARACTERIZATION OF GRANULAR PAVEMENT FOUNDATION LAYERS

Pavana KR. Vennapusa, David J. White, John Siekmeier, Rebecca Embacher

A paper to be submitted to the International Journal of Pavement Engineering, Taylor and Francis Journals.

5.1 Abstract

This paper presents experimental test results comparing falling weight deflectometer (FWD), light weight deflectometer (LWD), dynamic cone penetrometer (DCP), and piezocone (CPTU) mechanistic test measurements and roller-integrated compaction measurements on granular pavement foundation layers. To better understand and interpret the relationships between these different measurements, vertical and horizontal stresses induced by vibratory roller, FWD, and LWD dynamic loads are measured by instrumenting the granular base, subbase, and subgrade layers of a pavement section. In-ground stress measurements revealed differences in stress states in foundation materials under roller and LWD/FWD loading. Stress paths for roller induced vibratory loading during compaction, dynamic loads from FWD and LWD tests, and laboratory resilient modulus tests are compared. Insights into differences in measurement influence depths of different measurements are provided. Roller-integrated compaction measurements offer a significant advantage over other methods with 100% coverage and real-time data visualization. Some practical considerations in interpreting the relationships are discussed in this paper.

5.2 Introduction

Mechanistic-empirical procedures recently introduced into the AASHTO (2008) pavement design guide are considered a significant improvement over previous design procedures with more importance given to characterizing the mechanistic behavior of the pavement and underlying foundation layers. Different means suggested in the guide for characterization of the foundation layers include: (a) laboratory repeated load resilient

modulus tests, (b) non-destructive test measurements, (c) intrusive testing such as dynamic cone penetrometer (DCP), and (d) reliance on agency's experience. Many non-destructive test methods have been developed over the past five decades for characterizing the pavement foundation layer mechanical properties in-situ. A summary of these different methods is provided by Newcomb and Birgisson (1999).

While performing laboratory resilient modulus tests can provide a better assessment of the mechanistic behavior of the materials compared to in-situ tests, it is time consuming and also not always representative of field conditions. To that end, in-situ non-destructive testing methods are beneficial and also comparatively more measurements can be obtained within a short amount of time than laboratory testing. FWD and DCP tests have the advantage of characterizing the vertical non-uniformity of pavement foundation layers which is a common problem in compacted fill materials (see White et al. 2008b). Light weight deflectometer (LWD) which is a portable version of a FWD also provides an estimate of elastic modulus and is being widely evaluated by several state and federal agencies. Piezocone testing (CPTU) is a versatile sounding procedure that is used to characterize material behaviour type and provides an estimate of soil shear strength and stiffness properties as a near continuous record down to significant depths. Due to equipment and personnel cost limitations the test is unfortunately rarely used in pavement foundation layer characterization. Recently, there has been increasing demand in incorporating roller-integrated compaction monitoring technologies into earthwork construction and relating the measurements to pavement design parameters (see White et al. 2007a). These technologies are a significant improvement over traditional approaches as they can provide 100% coverage with real-time data visualization.

This paper presents experimental test results with comparison measurements between LWD, FWD, CPTU, and DCP point measurements and roller-integrated compaction measurements. The roller measurement values reported in this paper are Geodynamik Compaction Meter Value (CMV) and Resonant Meter Value (RMV). Further, results from an instrumented embankment test section of granular base, subbase, and subgrade layers measuring in-situ vertical and horizontal stresses induced under different measurements are provided. The objectives for instrumenting the foundation layers were to obtain insights into

differences in stress states in the foundation materials under roller-induced vibratory loading, LWD, and FWD loading and their measurement influence depths. Some key aspects relating to interpretation of roller measurement values and selection of appropriate test measurements when developing correlations are discussed in this paper.

5.3 Background

Significant efforts have been made by researchers over the past three decades to document and develop an understanding of relationships between different roller-integrated compaction monitoring technologies and soil physical and mechanical properties (e.g., Thurner and Sandström 1980, Forssblad 1980, Floss *et al.* 1983, Samaras *et al.* 1991, Brandl and Adam 1997, Kröber *et al.* 2001, Preisig *et al.* 2003, Thompson and White 2008, White and Thompson 2008, White *et al.* 2005, 2007a, 2007b, White *et al.* 2008a, 2008b). In general, vibratory based roller-integrated measurements are better correlated with stiffness based measurements (e.g., FWD, DCP) compared to dry unit weight measurements (see Thurner and Sandström 1980, Floss *et al.* 1991, Mooney *et al.* 2008). The correlations presented in the literature showed varying degree of uncertainty in the relationships, however. Some commonly identified reasons for poor correlations are: (a) differences in measurement influence depths between roller and in situ point measurements (see Figure 5.1), (b) difference in stress states during loading under roller and point measurements, and (c) heterogeneity in underlying layer stiffness. ISSMGE (2005) reports that a 12-ton dynamic roller has a measurement influence depth of up to 1.5 m. Conventional in-situ point measurements such as nuclear density gauge, soil stiffness gauge, LWD are believed to have influence depths of < 300 mm. FWDs, DCP, and static cone penetration tests (CPTU) have the ability to assess the properties of the underlying layers.

Roller-integrated CMV and RMV measurements and FWD, LWD, DCP, and CPTU point measurements are obtained from this study. A brief overview of these different measurements is presented below.

5.3.1 Roller-Integrated Compaction Measurements

5.3.1.1 Compaction Meter Value (CMV)

CMV is a dimensionless compaction parameter developed by Geodynamik that depends on roller dimensions, (i.e., drum diameter and weight), roller operation parameters (e.g., frequency, amplitude, speed), soil mechanical properties (e.g. strength and stiffness) and soil stratigraphy, and is determined using the dynamic roller response (Sandström 1994). It is calculated using Equation (5.1), where C is a constant (300), A_1 = the acceleration of the first harmonic component of the vibration, A_0 = the acceleration of the fundamental component of the vibration (Sandström and Pettersson 2004). CMV at a given point indicates an average value over an area whose width equals the width of the drum and length equal to the distance the roller travels in 0.5 seconds (see Figure 5.1) (Geodynamik ALFA-030).

$$CMV = C \cdot \frac{A_1}{A_0} \quad (5.1).$$

5.3.2 Resonant Meter Value (RMV)

RMV provides an indication of the drum behavior (e.g. continuous contact, partial uplift, double jump, rocking motion, and chaotic motion) and is calculated using Equation (5.2), where $A_{0.5}$ = sub-harmonic acceleration amplitude caused by jumping (the drum skips every other cycle). According to Adam and Kopf (2004), $RMV = 0$ theoretically indicates that the drum is in a continuous or partial uplift mode. When $RMV > 0$, drum enters into a double jump mode and transitions into rocking and chaotic modes. Based on numerical studies, Adam (1997) showed that as the soil stiffness increases CMV increases almost linearly for the roller drum in a continuous or partial uplift mode. With increasing soil stiffness, the drum transitions to double jump mode where RMV increases and CMV decreases rapidly. With further increase in ground stiffness, CMV decrease to a minimum value and then increases again. This relationship between drum operation mode, RMV, and ground stiffness is identified via numerical analyzed by Adam (1997) and Sandström (1994).

$$\text{RMV} = C \cdot \frac{A_{0.5}}{A_0} \quad (2)$$

5.3.2 In-Situ Point Measurements

Zorn and Dynatest LWDs setup with a 200-mm plate diameter, 10-kg drop weight, and 50 cm drop height were used to determine elastic modulus: (a) Zorn LWD and (b) Dynatest LWD. The elastic modulus was determined using Equation (5.3), where E = elastic modulus (MPa), d_0 = measured settlement (mm), ν = Poisson's ratio (assumed as 0.4), σ_0 = applied stress (MPa), a = radius of the plate (mm), and f = shape factor assumed as $\pi/2$. Tests were performed by preloading the test area with three seating drops and then followed by three test drops. The average modulus of the last three drops is reported as the E_{LWD} at that point. The calculated E_{LWD} values differ with the model due to differences in the mechanics and sensors used in the device (Vennapusa and White 2008a). To differentiate between the two devices used in this study the modulus values calculated from the Zorn device are reported as $E_{\text{LWD-Z2}}$ and from the Dynatest device are reported as $E_{\text{LWD-D2}}$ (subscript 2 in the symbol represents a 200-mm diameter plate).

$$E = \frac{(1-\nu^2)\sigma_0 a}{d_0} \times f \quad (5.3)$$

FWD test was performed by applying three seating drops using a nominal force of about 26.7 kN and followed by three test drops each at a nominal 26.7 kN and 53.4 kN force (F). The actual applied F was recorded using a load cell. The deflections were measured using geophones placed at the center of the plate and at 0.2 m, 0.3, 0.5, 0.6, 0.8, 0.9, 1.2, 1.52, and 1.8 m offsets from the center of the plate. A composite modulus value ($E_{\text{FWD-D3}}$) was calculated using measured deflection at the center of the plate from Equation (5.3). Modulus values of the underlying layers were back-calculated using Equation (5.4), where r_i is the radial distance from the center of the plate to the i^{th} sensor and $d_{0(r_i)}$ is the deflection measured at the i^{th} sensor.

$$E = \frac{(1-\nu^2)\sigma_0 a^2}{r_i d_{0(r_i)}} \times f \quad (4)$$

DCP tests were performed in accordance with ASTM D 6951. The tests were performed extending to a depth of about 2-m below surface using extension rods. Dynamic penetration index (DPI) with units of mm/blow was measured from the test. DPI is inversely related to soil strength/stiffness properties and is well discussed in the literature (see Livneh 1989, McElvanet and Djatnika 1991, Yoon and Salgado 2002). Chen *et al.* (2005) reported a correlation between DPI and back-calculated FWD modulus (E_{FWD}) as shown in Equation 5.5. A new correlation between DPI and E_{FWD} is developed as part of this study and is presented later in this paper. A major advantage of DCP is that it can create a near continuous vertical record of soil mechanical properties which are critical in earthwork QC/QA for detecting buried “weak” layers within compacted fill materials (see White *et al.* 2008b).

$$E_{FWD} (MPa) = 537.76(DPI)^{-0.665} \quad (5.5)$$

CPTU tests were performed using a cone with 60° taper angle and 10cm² area to measure tip resistance (q_c), sleeve friction (f_s), and pore pressure (u) during penetration. Tests were conducted at a nominal rate of penetration of 2 mm/s, and tip resistance was corrected to account for unequal areas above and below the porous element with respect to pore pressure measurements to calculate q_t . Schmertmann (1970) suggested an empirical relationship between q_t and Young’s modulus, E_s as shown in Equation (5.6). Konrad and Lachance (2001) presented a correlation between q_t and E_{FWD} for fine-grained subgrade soils as shown in Equation (5.7) for a 40kN FWD applied force on an asphalt pavement and for measured strains in the subgrade within 10⁻⁵ to 10⁻⁴. Similar to DCP, CPTU also has the advantage of creating a near continuous vertical record of soil mechanical properties but can reach significantly deeper depths than DCP.

$$E_s = 2q_t \quad (5.6)$$

$$\log(E_{FWD-D3}) = 0.473 \log(q_t) + 0.507 \quad (5.7)$$

5.3.3 Earth Pressure Cells

EPCs with a measurement range of 0-1000 kPa were used in this study to measure the total peak horizontal (σ_H) and vertical stresses (σ_V) induced by the roller, LWD, and FWD loading. The EPCs used were 100 mm diameter and 10 mm thick semiconductor type sensors made of two stainless steel plates welded together around their periphery and filled with deaired hydraulic fluid. EPCs were calibrated using a specially fabricated calibration chamber by placing the cells in compacted poorly graded ASTM silica sand.

5.4 Experimental Testing

Experimental testing was performed over a two-dimensional test strip with plan dimensions of about 3 m x 35 m. The test strip consisted of a granular base layer underlain by granular subbase and granular subgrade layers down to a depth of about 2.8 m below surface. Index properties of these materials are summarized in Table 5.1. Figure 5.2 shows CPTU results from the test strip showing interpreted soil profile and behavior type down to a depth of about 6 m below surface. Estimated drained peak friction angle (ϕ') values of the granular base, granular subbase and granular subgrade layers from CPTU results (Robertson and Campanella 1983) and Hough (1957) are summarized in Table 5.1. The subgrade was underlain by rubble/cobbles/old reclaimed pavement and natural sandy glacial deposits.

EPCs were installed in the granular base, subbase, and subgrade layers at depths of about 0.15 m, 0.30 m, 0.50 m, 0.65, 0.80 m, 1.04, and 1.20 m below surface (see Figure 5.3). The EPCs installed at depths 0.30 m, 0.65m, and 1.04 m depths were placed perpendicular to the alignment of the test strip to measure stresses in horizontal direction (σ_H). The rest of the EPCs were installed to measure stresses in vertical direction (σ_V). The EPCs were installed by carefully excavating the material and embedding the cells in a layer of calibration sand material. The calibration sand material was carefully hand compacted in thin layers to achieve good compaction around the sensors. The excavation was backfilled using the excavated material and was hand compacted in thin lifts. The test strip was compacted for ten roller passes to ensure good compaction was achieved in the backfilled area.

5.5 Stresses in Pavement Foundation Layers

Figure 5.3 shows vertical and horizontal stresses induced under roller vibratory loading with two different amplitude settings ($a = 0.85$ mm and 1.70 mm) (note that these stresses do not include geostatic stresses). Figure 5.4 shows peak vertical and horizontal stresses developed under the roller, 300-mm diameter FWD with applied $F = 26.7$ kN and $F = 53.4$ kN (showed as FWD(A) and FWD(B), respectively), and 200-mm LWD with $F = 6.3$ kN.

The horizontal and vertical loading regimes observed in Figure 5.3 are due to rotation of principal stresses in the layers due to the moving roller load. To explain this behavior, three positions are identified on Figure 5.3 at locations of peak horizontal and vertical stresses (Note that the sensors are all positioned vertically at position 2. When the roller drum is at position 1, the magnitude of horizontal stresses increase is more than the magnitude of vertical stresses ($\Delta\sigma_H > \Delta\sigma_V$). When the moving load is directly above the sensor (position 2), vertical stresses are significantly higher than the horizontal stresses ($\Delta\sigma_V > \Delta\sigma_H$). As the roller travels away from position 2, vertical stresses decrease and horizontal stresses increase ($\Delta\sigma_H > \Delta\sigma_V$) in the soil. When the load travels far away from the sensors, both vertical and horizontal stresses decrease. The horizontal stresses are not completely relieved in compacted fill materials due to residual “locked-in” stresses (σ_{hr}) developed during compaction process (Duncan and Seed 1986). Residual stresses were not measured in the current study but were estimated (see Figure 5.4) using K_0 hysteric model proposed by Duncan and Seed (1986) for free field conditions. The total unit weight (γ_t) and ϕ' values (average values determined from Table 5.1) assumed in calculating the residual and vertical overburden stresses (σ_{vo}) are shown in Figure 5.4.

The vertical stresses induced under the roller showed “spreading” of the stresses with depth, i.e, a vertical sensor at a deeper depth sensing greater vertical stresses than at shallow depths just before approaching position 2. Also shown in Figure 5.3 is a close-up view of the vertical stresses under $a = 0.85$ and 1.70 mm loading. During roller operation at $a = 1.70$ mm, the vibratory stress cycles were skipped every cycle which represents roller drum loss of contact with the ground. This is referred to as drum double jumping and is discussed later in

conjunction with roller-integrated measurements.

Figure 5.4 shows theoretical vertical and horizontal stress distributions under the roller and LWD/FWD plates based on Boussinesq elastic solutions (Poulos and Davis 1974). The stress distributions under the roller were determined assuming a uniformly loaded continuous strip footing with width B . The B and contact stress q_o values were adjusted to obtain a best fit through the measured peak stresses. A contact width of 0.2 m was found to fit the theoretical vertical and horizontal stress distributions well for both low and high amplitude vibratory loading. The vertical stress distributions under the FWD/LWD plate were well predicted by the theoretical solutions but not the horizontal stress distributions. The vertical stress distributions with depth can be used to characterize the measurement influence depth of the rollers by assuming the depth equals where the vertical stresses have decayed to 10% of their maximum stresses at the surface. Using this criteria, the measurement influence depth under the roller for both $a = 0.85$ mm and 1.70 mm loading conditions is estimated at about 0.9 m for the pavement structure tested in this study. The measurement influence depth under 300-mm FWD plate with $F = 53.4$ kN and $F = 26.7$ kN is about 0.6 m, and under 200-mm LWD plate is about 0.4 m.

Using the calculated residual stresses, the K_o values at different depths are calculated as the ratio of σ_{hr} and σ_{vo} from Figure 5.4. Considering the three positions described in Figure 5.3 (Positions 1, 2, and 3) as the main loading and unloading regimes under the roller load, and the estimated K_o values for the at-rest state, stress paths are developed for soil elements in granular base (depth = 0.08 m) and subbase layers (depth = 0.32 m). The stress paths are shown in Figure 5.5 for the two amplitude loading conditions. Stress path under the roller showed a hysteresis of extension and compression during loading and unloading phases due to rotation in principal stresses as described above. Stress paths for LWD and FWD dynamic loads, laboratory resilient modulus (M_r) test loads following AASHTO T-307 and NCHRP 1-28 A procedures for base and subbase materials is also provided in Figure 5.5 for comparison. Slope coefficients m are determined for the stress paths as shown in Figure 5.5. Comparison of these stress paths reveal following key observations which play an important role in interpreting these different measurements: (a) the mean stresses developed under a 300-mm FWD plate with $F = 53.4$ kN are quite similar to mean stresses developed under the

roller for $a = 1.7$ mm but the m coefficients for FWD loading is comparatively smaller than under roller loading, (b) m coefficients are quite similar for roller induced loads and resilient modulus test following the AASHTO T-307 procedure and final 5 sequences of NCHRP 1-28A procedure, (c) applied mean stresses and m coefficients for LWD loading are significantly smaller than roller and FWD induced stresses and m coefficients (d) the magnitude of mean stresses and m coefficients for LWD loading are somewhat similar to AASHTO T-307 M_r testing and initial sequences of NCHRP 1-28A testing for M_r , and (e) NCHRP 1-28A procedure captures a wide range of stress states with m values in the range of 0.2 to 0.8 and significantly higher normal and shear stresses than other measurements. These observations are of significance as it relates to a better interpretation of correlations between different measurements on stress dependent foundation materials.

5.6 Comparison of Roller-Integrated and In-Situ Point Measurements

Roller-integrated RMV and CMV measurements obtained from two different amplitude settings are presented in Figure 5.6 for pass 7 to 10. Figure 5.6a demonstrates the repeatability of CMV values under similar amplitude settings. Figure 5.6b shows the influence of RMV on CMV values at $a = 1.70$ mm setting. At $a = 0.85$ mm the RMV measurements were close to zero while at $a = 1.70$ mm the RMV values were significantly greater than zero indicating roller jumping. Roller jumping behavior is confirmed from stress cell measurements (see Figure 5.3). Results show a decrease in CMV with increasing RMV which is identified in the literature as a distinctive feature of this measurement system (see Adam 1997). This CMV-RMV behavior is related to ground stiffness. In-situ point measurements (E_{LWD-D2} , E_{LWD-Z2} , E_{FWD-D3} , and DPI) obtained from the test strip are presented in comparison with roller-integrated measurements in Figure 5.7. DCP, CPTU, and E_{FWD} profiles from two select locations are also shown in Figure 5.7. Point A is located in the area where the RMV was lower and Point B is located in the area where RMV was greater when operated at $a = 1.70$ mm. The profiles showed relatively stiff layered structure at Point A compared to Point B.

Correlations obtained between different measurements are summarized in Figure 5.8.

The relationships were aimed to predict E_{FWD-D3} or DPI which are primarily suggested in the design guide. Regression relationships are obtained for E_{FWD} obtained at two applied force levels. Comparatively, relationships for E_{FWD-D3} at $F = 26.7$ kN were slightly better with other in-situ point measurements and at $F = 53.4$ kN were slightly better with roller measurement values. All regression relationships are summarized in Table 5.2. Summary statistics (mean μ and coefficient of variation COV) of different measurements are summarized in Table 5.3.

Results showed relatively poor correlations between E_{FWD} and E_{LWD} with R^2 values between 0.2 and 0.6, but with limited data points. Also, as observed from in-ground stress data, the stress states in LWD and FWD testing were significantly different which can contribute to scatter in relationships. Correlation between E_{FWD} and DPI showed power relationship with R^2 values of about 0.7 and is close to the relationship proposed by Chen *et al.* (2005). E_{FWD-q_t} and $DPI-q_t$ relationships also showed power relationships with R^2 of about 0.7. A different trend in E_{FWD-q_t} is observed than equations proposed by Konrad and Lachanche (2001) and Schmertman (1970). The relationship presented by Konrad and Lachanche (2001) was based on three data points and Schmertman's equation was based on correlations to static plate load modulus, however. To the authors' knowledge, this is the first study to document E_{FWD-q_t} and $DPI-q_t$ relationships.

Simple linear regression relationships between roller-integrated CMV and in-situ point measurements are presented in Figure 5.9, separately for low and high amplitude settings. The relationships are developed by pairing in-situ test measurement with spatially nearest roller measurement point with aid of GPS measurements. Despite limited data points, CMV relationships with E_{FWD-D3} and DPI showed good correlations with R^2 in the range of 0.6 to 0.7. Relationships with E_{LWD-Z2} and E_{LWD-D2} showed no correlation. Again, the reason is likely because of significant differences in the stress states under these devices. A relationship documented by White *et al.* (2007b) for a granular base material (classified as A-1-b) between CMV and Keros 200-mm plate diameter LWD device (E_{LWD-K2}) is presented in the figure as a reference. The E_{LWD-K2} and E_{LWD-D2} measurements are strongly correlated and are close to $R^2 = 1$ line (*see* Vennapusa and White 2008b). Another regression line is plotted on Figure 5.9 for E_{LWD-Z2} based on a relationship documented by Vennapusa and White

(2008b) between E_{LWD-K2} and E_{LWD-Z2} measurements ($E_{LWD-K2} = 1.75 E_{LWD-Z2}$). Although there is scatter, the E_{LWD-D2} and E_{LWD-Z2} measurements matched the trend of existing relationships. Regression relationships between CMV and in-situ point measurements are in Table 5.2 and summary statistics (mean μ and coefficient of variation COV) are summarized in Table 5.3.

Relationships between different point measurements and CMV at high amplitude setting are also shown in Figure 5.9. Due to the effect of RMV at high amplitude operation as described above, no trend was seen in the relationships. To statistically assess the influence of RMV on CMV, multiple regression analysis was performed as presented in Figure 5.10. The analysis was performed by incorporating amplitude, RMV, and E_{FWD-D3} measurements as independent variables into a multiple linear regression model to predict CMV. Statistical significance of each variable was assessed based on p - and t - statistics. The selected criteria for identifying the significance of a parameter included: p -value < 0.05 = significant, < 0.10 = possibly significant, > 0.10 = not significant, and t -value < -2 or $> +2$ = significant. The p -value indicates the significance of a parameter and the t -ratio value indicates the relative importance (i.e., higher the absolute value greater the significance). Based on this criterion, analysis results presented in Figure 5.10 indicated a strong significance of RMV in predicting CMV, while E_{FWD-D3} was somewhat significant. Amplitude was not found statistically significant; therefore, it was removed from the model. Statistically significant relationships were not found with other in-situ point measurements.

The effect of RMV on CMV has been discussed in the literature but it lacked attention in an implementation standpoint. A statistically significant correlation was possible in this current study by incorporating RMV into a multiple regression model; however, it is preferable to perform calibration testing in low amplitude setting (about less than 1 mm) to avoid complex interpretation and analysis of results with roller jumping. The interpretation of CMV data thus must not be absent of evaluating RMV. An example approach to evaluate CMV with RMV results in a specification/quality assurance standpoint is described in Vennapusa and White (2008b).

5.7 Summary and Conclusions

Relationships between LWD, FWD, CPTU, and DCP mechanistic measurements from experimental tests conducted over granular pavement foundation layers are presented in this paper. Further, results from an instrumented embankment test section of granular base, subbase, and subgrade layers with in-situ vertical and horizontal stresses induced under different measurements are presented. Stress paths were developed based on in-ground stresses induced by roller, and FWD/LWD loading to obtain insights into differences in stress states in foundation materials for different loading conditions. Some key conclusions from this paper are as follows:

- Stress path under the roller showed a hysteresis of extension and compression during loading and unloading phases due to rotation in principal stresses under moving roller load.
- For the pavement structure tested in this study, mean stresses developed under a 300-mm FWD plate with $F = 53.4$ kN are quite similar to mean stresses developed under the roller for $a = 1.7$ mm but the stress path slope coefficient m for FWD loading is comparatively smaller than for roller loading.
- Applied mean stresses and m coefficients for LWD loading are significantly smaller than roller and FWD induced stresses and m coefficients – a likely contributor to scatter in relationships between roller and E_{LWD} measurements.
- Using criteria for characterizing measurement influence depth as the depth to decay stresses to 10% of maximum stresses at surface, the measurement influence depths under roller, 300-mm FWD plate, and 200-mm LWD plate is estimated as 0.9 m, 0.6 m, and 0.4 m. No difference was observed in the influence depth with change in amplitude or increasing dynamic load under FWD plate.
- Comparison between CPTU, FWD, and DCP measurements showed good correlations with R^2 values greater than 0.6. Comparison between FWD and LWD measurements showed poor correlations. The reasons are attributed partly due to limited data and partly due to significant difference in stress states in the material under FWD and LWD loading.

- Comparison between FWD, DCP, and roller-integrated CMV showed good correlations with R^2 values around 0.6.
- Roller jumping (as measured by RMV) affected the CMV values and consequently the correlations. A statistically significant correlation was possible in this current study by incorporating RMV into a multiple regression model to predict CMV. However, for practical purposes, it is preferable to perform calibration testing in low amplitude setting (about less than 1 mm) to avoid complex interpretation and analysis of results with roller jumping. .

5.8 Acknowledgements

The Minnesota Department of Transportation (Mn/DOT) and the Federal Highway Administration (FHWA) sponsored this study under Mn/DOT Contract No. 89256, Work Order No. 2. Numerous Mn/DOT personnel, district staff and Peterson Contractors personnel assisted the authors in identifying and providing access to grading projects for testing. The authors would also like to thank Assistant Scientist Heath Gieselman, graduate research assistant Brad Fleming, and undergraduate research assistants Andrew Weber, Alexandra Buchanan, and Kevin McLaughlin who provided assistance with the ISU Geotechnical Mobile Lab in field and lab testing.

5.9 References

- AASHTO T-307. *Standard Method for Determining the Resilient Modulus of Soils and Aggregate Materials*. American Association of State Highway and Transportation Officials, Transportation Research Board.
- AASHTO (1998). *Mechanistic-Empirical Pavement Design Guide – A Manual for Practice*, Interim Edition, American Society of State Highway and Transportation Officials (AASHTO), July.
- Adam, D. (1997). “Continuous compaction control (CCC) with vibratory rollers.” *Proc., 1st Australia-Newzealand Conf. on Environmental Geotechnics – GeoEnvironment 97*,

Melbourne, Australia, 26-28 November.

- Adam, D., and Kopf, F. (2004). "Operational devices for compaction optimization and quality control (Continuous Compaction Control & Light Falling Weight Device)." *Proc., of the Intl. Seminar on Geotechnics in Pavement and Railway Design and Construction*, December, Athens, Greece (Invited paper), 97-106.
- Brandl, H., and Adam, D. (1997). "Sophisticated continuous compaction control of soils and granular materials." *Proc. 14th Intl. Conf. Soil Mech. and Found. Engrg.*, Hamburg, Germany, 1-6.
- Chen, D.H., Lin, D.F., Liau, P.H., Bilyeu, J. (2005). "A correlation between dynamic cone penetrometer values and pavement layer moduli," *Geotechnical Testing Journal*, Vol. 28, No. 1, 42-49.
- Duncan, J.M., and Seed, R.B. (1986). "Compaction-induced earth pressures under K_0 – conditions." *Journal of Geotechnical Engineering*, ASCE, 112(1), 1-22.
- Forssblad, L. (1980). "Compaction meter on vibrating rollers for improved compaction control", *Proc., Intl. Conf. on Compaction*, Vol. II, 541-546, Paris.
- Floss, R., Gruber, N., Obermayer, J. (1983). "A dynamical test method for continuous compaction control." *Proc. 8th European Conf. on Soil Mech. and Found. Engrg.*, H.G. Rathmayer and K. Saari, eds., May, Helsinki, 25-30.
- Florida DOT (2003). *Test Report – FHWA GeoGauge Study SPR-2(212) Validation of Depth of Influence*, Florida Department of Transportation, January.
- Geodynamik ALFA-030. *Compactometer, Compaction Meter for Vibratory Rollers*, ALFA-030-051E/0203, Geodynamik AB, Stockholm (Sweden).
- Hough, B.K. (1957). *Basic Soil Engineering*, The Ronald Press Company, NY.
- ISSMGE. (2005). *Roller-Integrated continuous compaction control (CCC): Technical Contractual Provisions, Recommendations, TC3: Geotechnics for Pavements in Transportation Infrastructure*. International Society for Soil Mechanics and Geotechnical Engineering.

- Konrad, J. and Lachance, D. 2001. Use of in-situ penetration tests in pavement evaluation. *Canadian Geo-technical Journal*, 38 (5), 924–935.
- Kröber, W., Floss, E., Wallrath, W. (2001). “Dynamic soil stiffness as quality criterion for soil compaction,” *Geotechnics for Roads, Rail Tracks and Earth Structures*, A.A.Balkema Publishers, Lisse /Abingdon/ Exton (Pa) /Tokyo, 189-199.
- Livneh, M. (1989). Validation of correlations between a number of penetration tests and insitu California bearing ratio tests, *Transportation Research Record*, No. 1219, Journal of the Transportation Research Board.
- McElvaney, J. and Djatnika, I. 1991. Strength evaluation of lime-stabilized pavement foundations using the dynamic cone penetrometer. *Australian Road Research*, 21(1): 40–52.
- Mooney, M., Rinehart, B., White D.J., Vennapusa, P. Thompson, M. Facas, N., Musimbi, O, Gieselman, H. (2008). *Intelligent Soil Compaction Systems*, NCHRP 21-09 Report, Transportation Research Board (in review).
- NCHRP 1-28A (2003). *Harmonized Test Methods for Laboratory Determination of Resilient Modulus for Flexible Pavement Design*. National Cooperative Highway Research Program, Transportation Research Board, Washington, D.C.
- Newcomb, D.E., Birgisson, B. (1999). *Measuring In Situ Mechanical Properties of Pavement Subgrade Soils*. Synthesis of Highway Practice 278, National Cooperative Highway Research Program, National Academy Press, Washington, D.C.
- Preisig, M., Caprez, M., and Ammann, P. (2003). “Validation of continuous compaction control (CCC) methods.” *Workshop on Soil Compaction*, September, Hamburg.
- Poulos, H.G., Davis, E.H. (1974). *Elastic Solutions for Soil and Rock Mechanics*. John Wiley and Sons, Inc. New York.
- Robertson, P.K., Campanella, R.G (1983), “Interpretation of cone penetration tests – Part I (sand)”, *Canadian Geotechnical Journal*, Vol. 20, No. 4, 718-733.
- Samaras, A., Lamm, R., and Treiterer, J. (1991). “Application of continuous dynamic

- compaction control for earthworks in railroad construction.” *Transportation Research Record*, No. 1309, Journal of the Transportation Research Board, 42-46.
- Sandström, Å. (1994). *Numerical simulation of a vibratory roller on cohesionless soil*, Internal Report, Geodynamik, Stockholm, Sweden.
- Sandström A.J. and Pettersson, C.B. 2004. Intelligent systems for QA/QC in soil compaction. *Proc., 83rd Annual Transportation Research Board Meeting*, January 11-14, Washington, D.C.
- Schmertmann, J. H. (1970). “Static cone to compute static settlement over sand”, *Journal of Soil Mechanics and Foundation Division*, ASCE, 96, No. SM3, 1011-1043.
- Thompson, M., and White, D. (2008). “Estimating compaction of cohesive soils from machine drive power.” *J.of Geotech. and Geoenviron. Engg*, ASCE (in press).
- Thurner, H. and Sandström, Å. 1980. A new device for instant compaction control. *Proceedings of the International Conference on Compaction*, Vol II: 611-614, Paris.
- Vennapusa, P. and White, D. J. (2008a). “Comparison of light weight deflectometer measurements for pavement foundation materials,” *Geotechnical Testing Journal*, ASTM (in review).
- Vennapusa, P. and White, D. J. (2008b). “Geostatistical analysis of spatially referenced roller-integrated compaction measurements,” *Journal of Geotechnical and Geoenvironmental Engineering*, ASCE (in review).
- White, D.J, Jaselskis, E., Schaefer, V., and Cackler, E. (2005). “Real-time compaction monitoring in cohesive soils from machine response.” *Transportation Research Record*, No. 1936, National Academy Press, 173-180.
- White, D.J., Thompson, M. and Vennapusa, P. (2007a). *Field validation of intelligent compaction monitoring technology for unbound materials*. Final Report MN/RC-2007-10, Minnesota Department of Transportation, St. Paul, MN.
- White, D.J, Thompson, M., Vennapusa, P. (2007b). *Field study of compaction monitoring systems: self-propelled non-vibratory 825G and vibratory smooth drum CS-533 E*

- rollers*, Final Report, Center of Transportation Research and Education, Iowa State University, Ames, Ia.
- White, D., and Thompson, M. (2008). "Relationships between in-situ and roller-integrated compaction measurements for granular soils." *J. of Geotech. and Geoenviron. Engg* (in press).
- White, D., Thopmson, M., Vennapusa, P., and Siekmeier, J. (2008a). "Implementing intelligent compaction specifications on Minnesota TH 64: Synopsis of measurement values, data management, and geostatistical analysis." *Transportation Research Record* , No. 2045, Journal of the Transportation Research Board, 1-9.
- White, D. J., Vennapusa, P., Gieselmann, H., Johanson, L., Siekmeier, J. (2008b), "Alternatives to heavy test rolling for cohesive subgrade assessment," *Eighth Intl. Conf. on Bearing Capacity of Roads, Railways, and Airfields*, University of Illinois at Urbana-Champaign (in review).
- Yoon, S., Salgado, R. (2002). *Dynamic Cone Penetration Test (DCPT) for Subgrade Assesment*, FHWA/IN/JTRP – 2002/30, Joint Transportation Research Program, Purdue University, West Lafayette, IN.

TABLE 5.1—Summary of soil index properties

Parameter	Granular Base	Granular Subbase	Granular Subgrade
USCS classification	SW	SP	SC
AASHTO classification	A-1-b	A-1-b	A-2-4
Standard Proctor			
w_{opt} (%)	8.2	8.9	11.5
γ_{dmax} (kN/m ³)	20.0	18.7	18.5
Drained friction angle, ϕ'			
CPTU ^a	–	44 to 46	44 to 48
Hough (1957) ^b	38 to 46	32 to 36	38 to 46

^aBased on empirical relationships between vertical effective overburden stress σ_{vo} , cone corrected tip resistance q_t , and drained peak friction angle (ϕ') proposed by Robertson and Campanella (1983).

^bBased on classification of dense sands.

TABLE 5.2—Summary of regression relationships

Relationship	n	R ²
<i>FWD Applied Force, F ~ 26.7 kN</i>		
E_{FWD-D3} (MPa) = 76.31 + 1.04 E_{LWD-Z2} (MPa)	11	0.55
E_{FWD-D3} (MPa) = 99.88 + 0.50 E_{LWD-D2} (MPa)	11	0.24
E_{FWD-D3} (MPa) = 43.53 (q_t) ^{0.45} (MPa)	100	0.70
E_{FWD-D3} (MPa) = 422.84 (DPI) ^{-0.60} (mm/blow)	157	0.65
E_{FWD-D3} (MPa) = 75.42 + 2.65 CMV	11	0.50
<i>FWD Applied Force, F ~ 53.4 kN</i>		
E_{FWD-D3} (MPa) = 68.26 + 1.31 E_{LWD-Z2} (MPa)	11	0.52
E_{FWD-D3} (MPa) = 106.73 + 0.55 E_{LWD-D2} (MPa)	11	0.20
E_{FWD-D3} (MPa) = 37.11 (q_t) ^{0.49} (MPa)	100	0.62
E_{FWD-D3} (MPa) = 341.99 (DPI) ^{-0.51} (mm/blow)	157	0.52
E_{FWD-D3} (MPa) = 59.87 + 3.56 CMV	11	0.59
DPI (mm/blow) = 22.42 - 0.39 CMV	10	0.69
DPI (mm/blow) = 78.35 (q_t) ^{-0.97} (mm/blow)	371	0.69

TABLE 5.3—Summary statistics of roller and in-situ point measurements at surface

Measurement	μ	COV
Roller $a = 0.85$ mm	32.1	15
Roller $a = 1.70$ mm	16.7	49
E_{FWD-D3} (MPa) ($F \sim 26.7$ kN)	160.4	13
E_{FWD-D3} (MPa) ($F \sim 53.4$ kN)	173.8	15
E_{LWD-D2} (MPa)	122.4	17
E_{LWD-Z2} (MPa)	80.6	18
DPI (mm/blow)	9.7	16

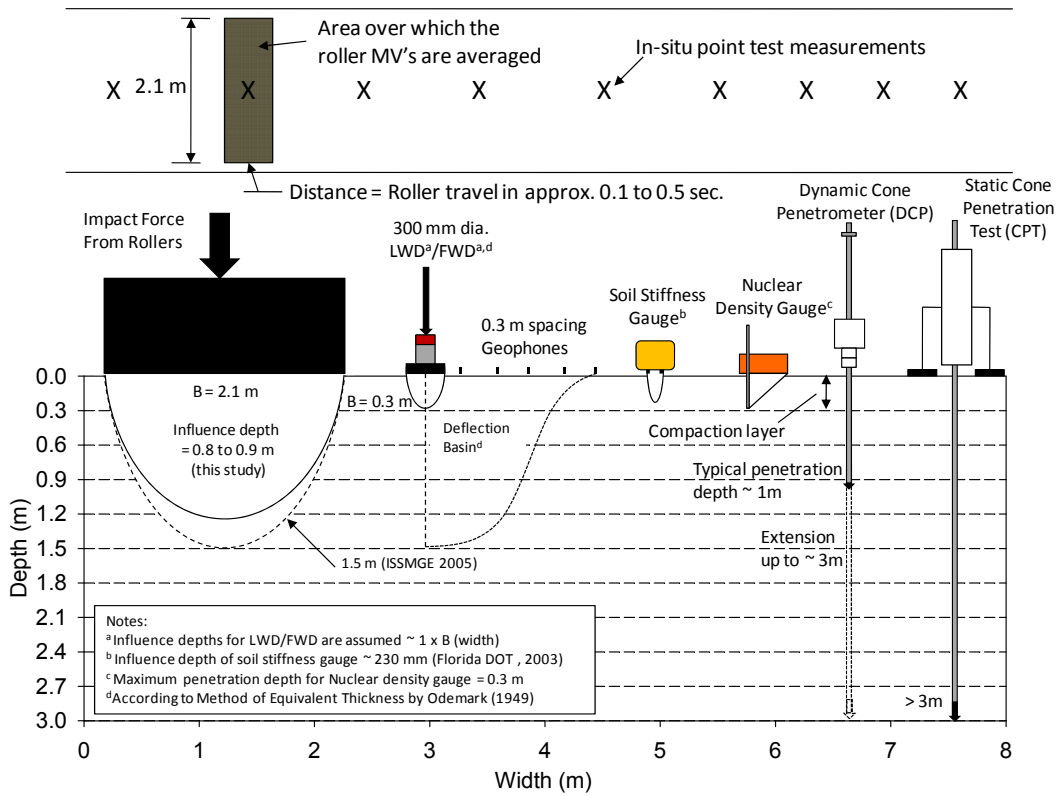


FIG. 5.1— Illustration of differences in measurement influence depths of different testing devices

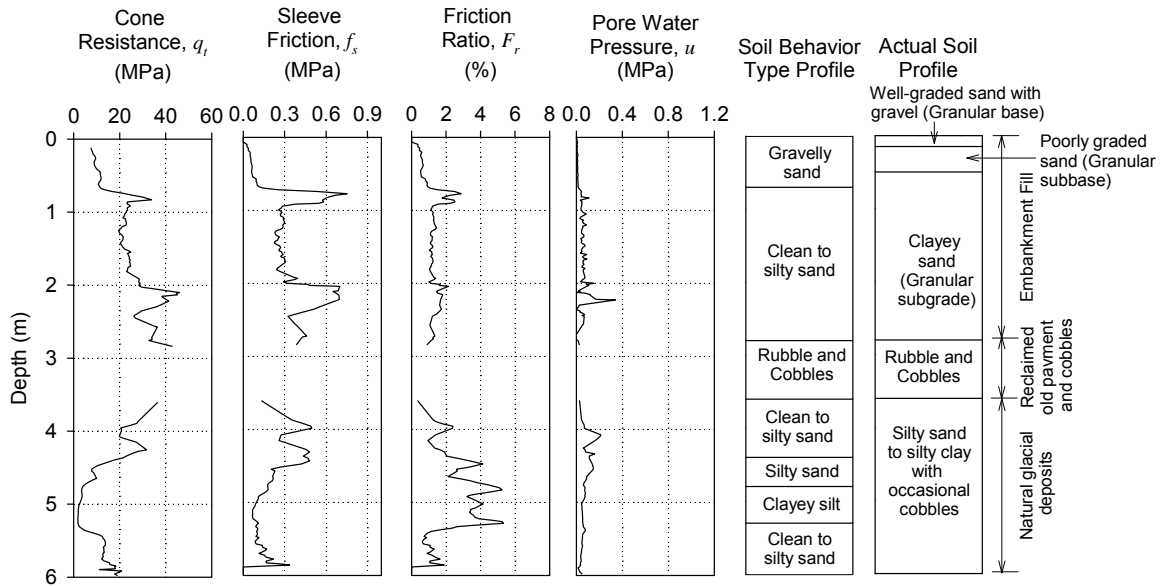


FIG. 5.2— Example CPT profile from a test location in the test strip area describing general foundation soil information

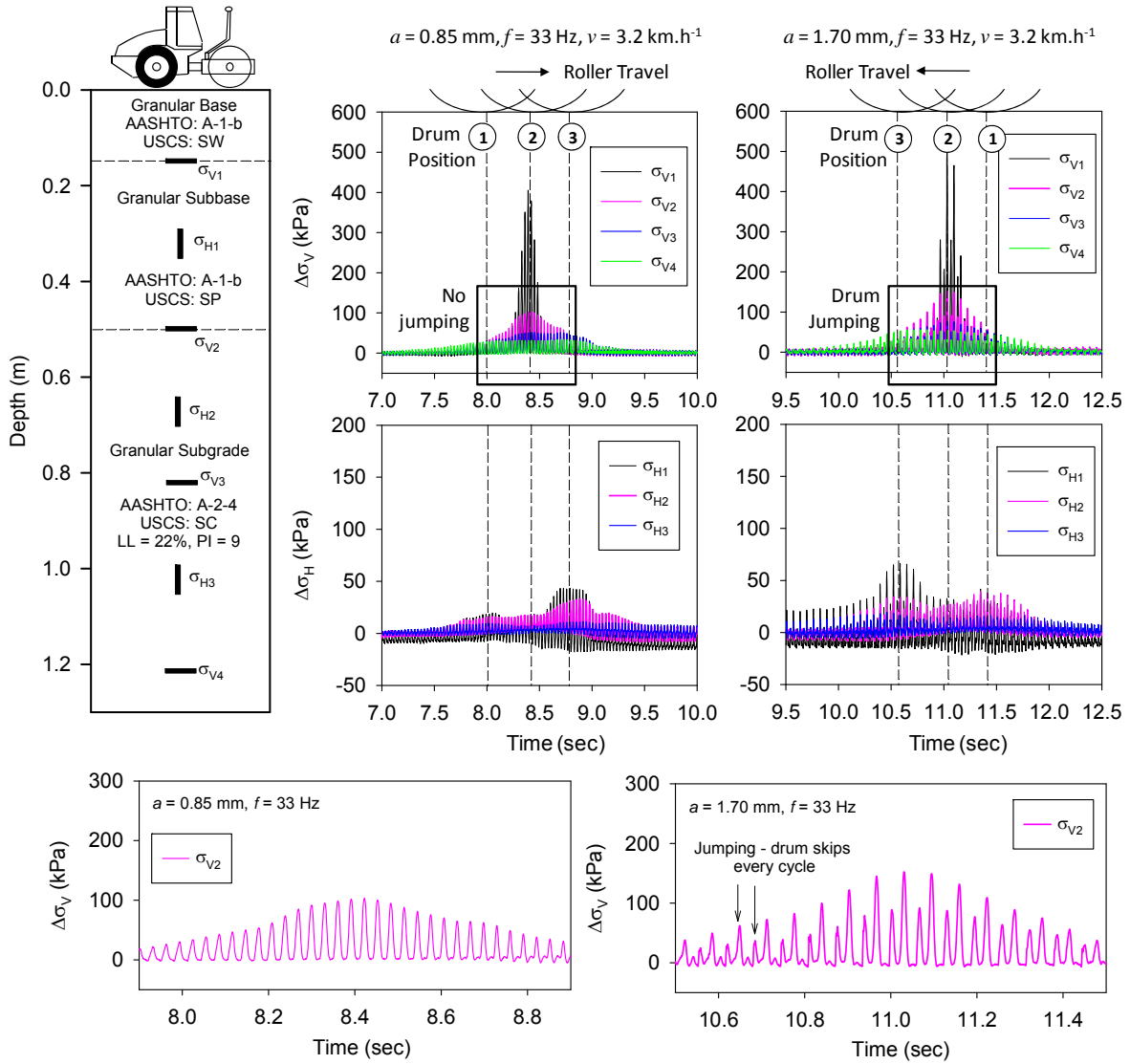


FIG. 5.3— Total vertical and lateral stresses induced by roller during vibratory loading at a = 0.85 and 1.70 mm nominal settings and drum jumping at a = 1.70 mm.

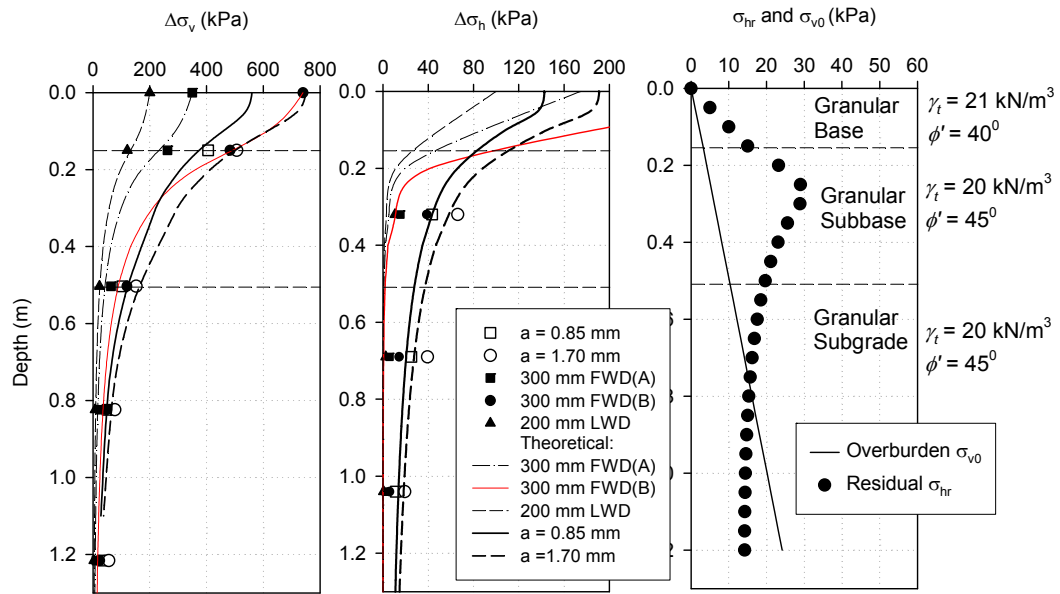


FIG. 5.4— Peak vertical and lateral stress increase profiles (measured and theoretical Boussinesq) for roller induced vibratory loads, and FWD and LWD dynamic loads, and estimated residual stresses to calculate K_o from Duncan and Seed (1986).

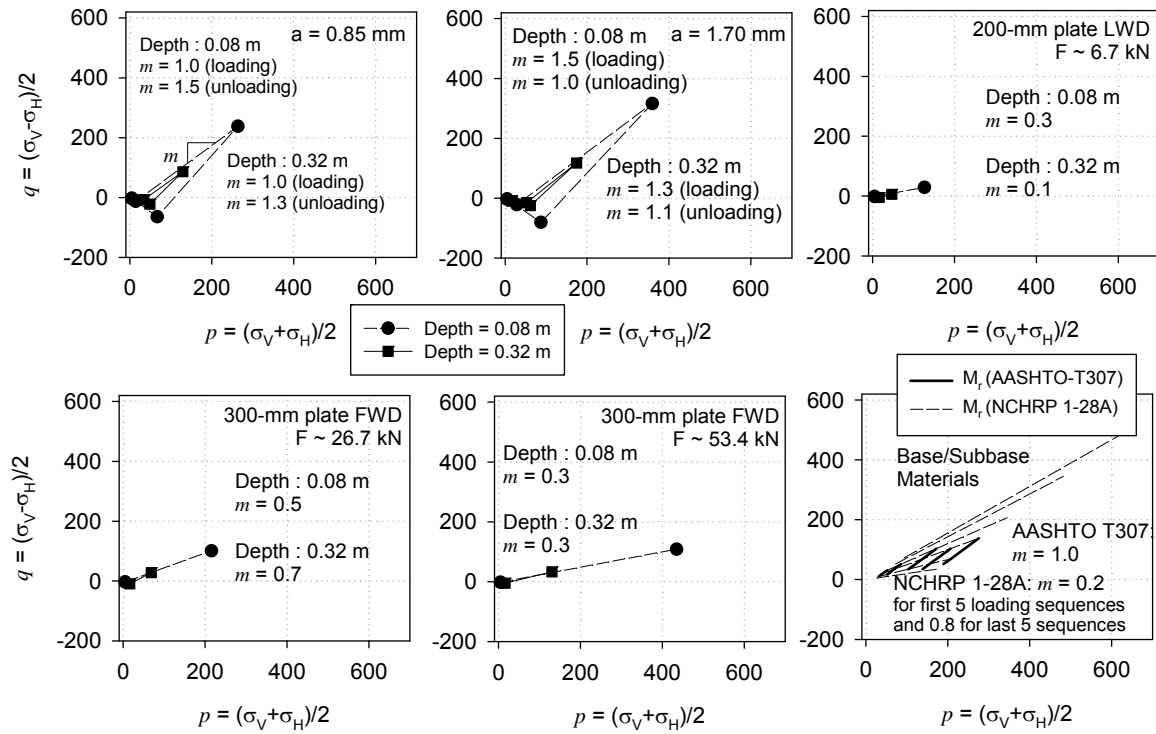


FIG. 5.5— Comparison of total stress paths under roller vibratory load (Positions 1 to 2 loading and Positions 2 to 3 unloading), FWD and LWD dynamic loads, and stresses applied during laboratory M_r tests on base/subbase materials.

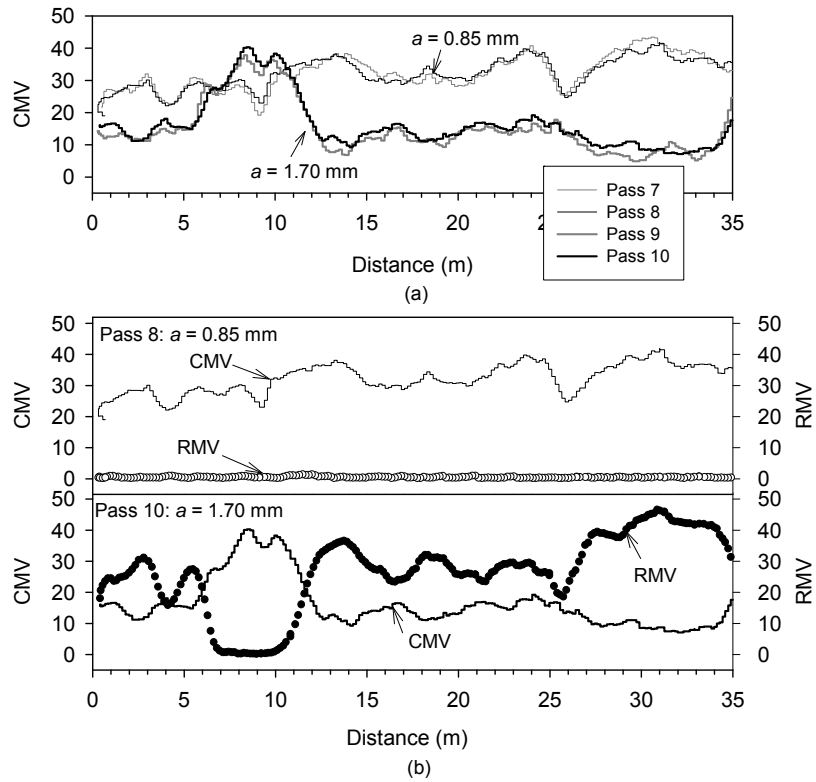


FIG. 5.6— Roller-integrated measurements from test strip with nominal $v = 3.2$ km/h and $f = 30$ Hz settings: (a) repeatability of CMV at two amplitude settings, (b) influence of RMV on CMV measurements.

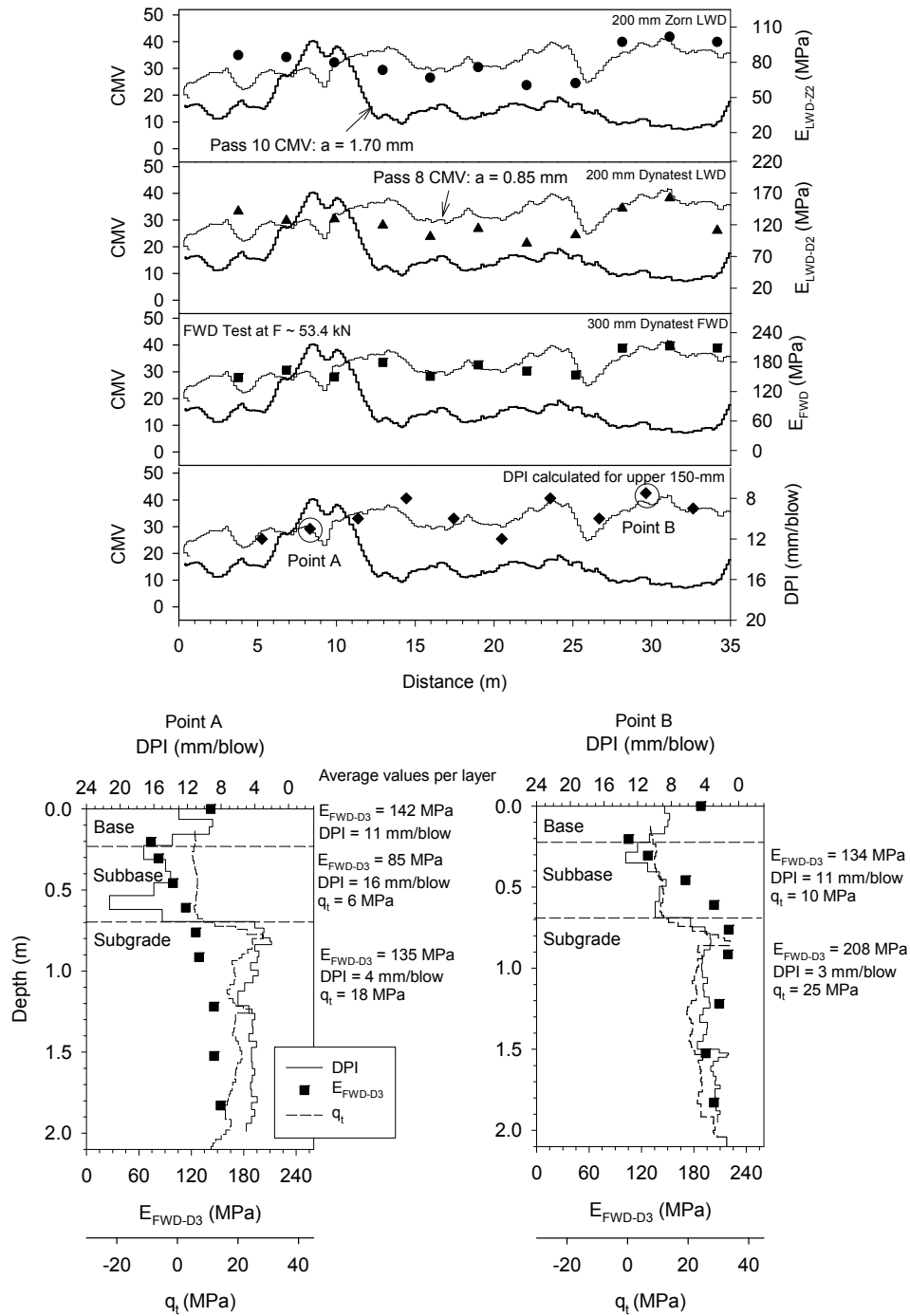


FIG. 5.7— Comparison of roller-integrated compaction measurements with in-situ mechanistic point measurements – DCP index, CPT q_t , and E_{FWD} profiles at two select points.

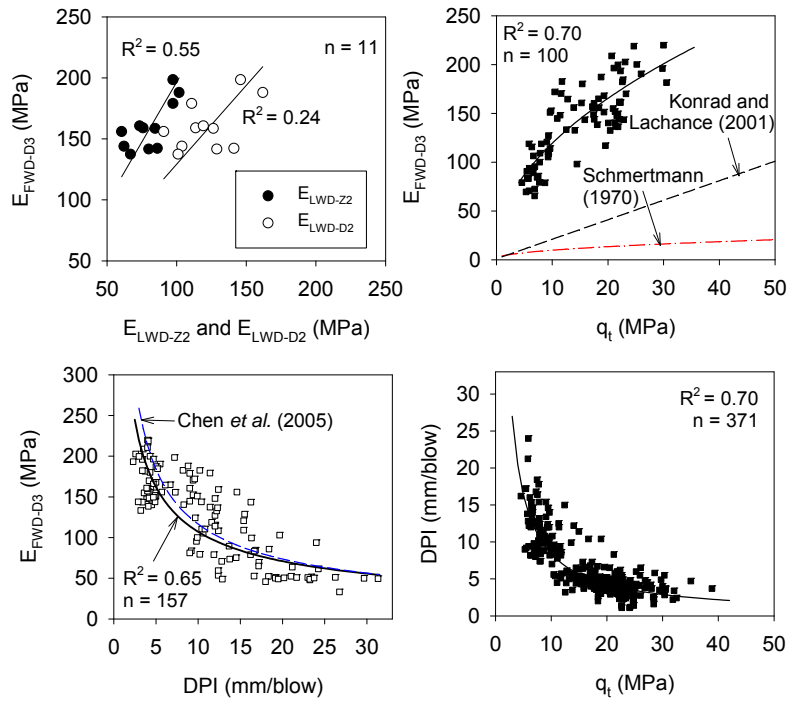


FIG. 5.8—Relationships between different measurements (E_{FWD-D3} at $F \sim 26.7$ kN).

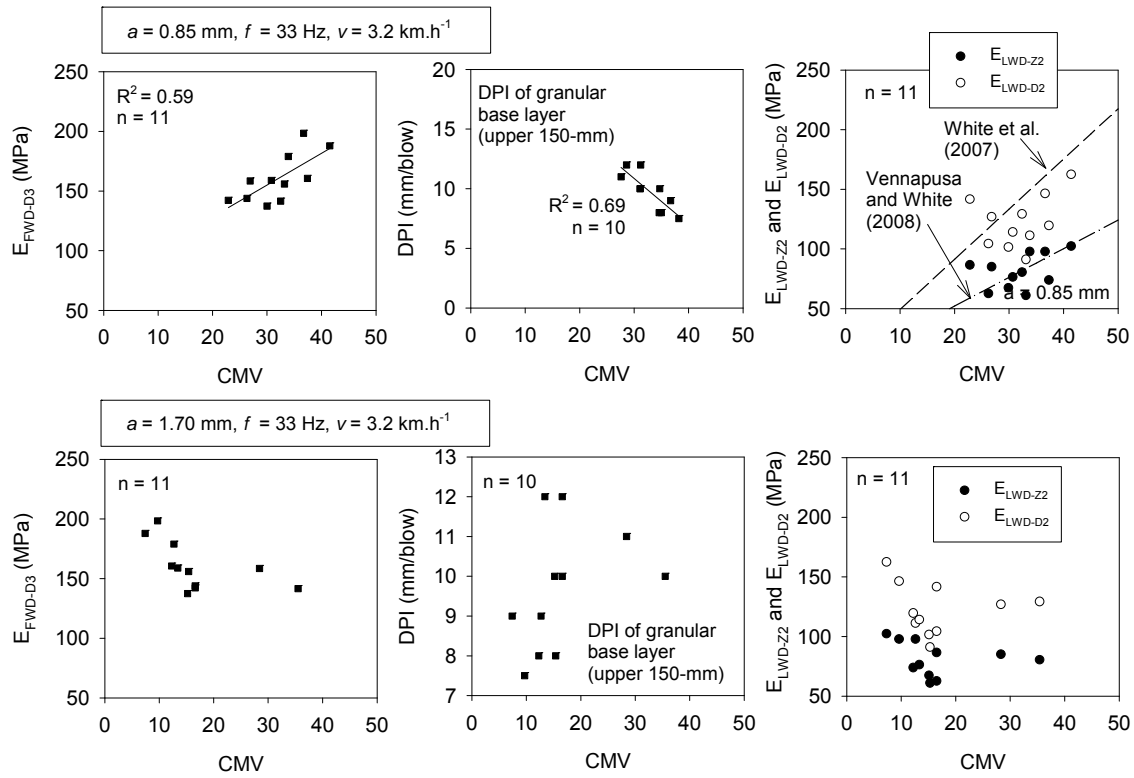


FIG. 5.9— Relationships between roller-integrated CMV and point measurements (E_{FWD-D3} at F ~ 53.4 kN).

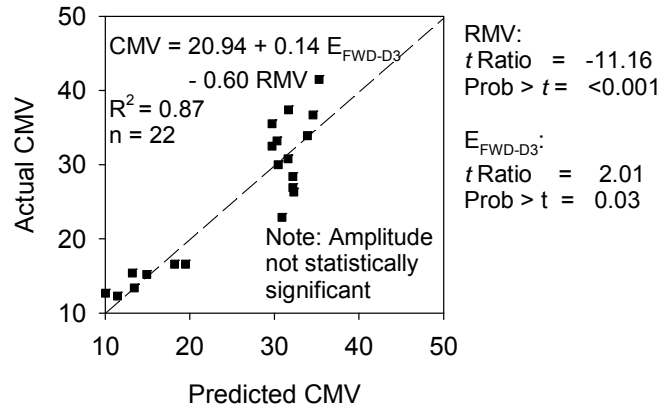


FIG. 5.10— Results of multiple regression analysis illustrating the effect of RMV.

CHAPTER 6. CONCLUSIONS AND RECOMMENDATIONS FOR FUTURE WORK

6.1 Summary

This dissertation provides results of experimental investigation and analysis on three different RICM measurements and six different in-situ strength/stiffness test methods for characterizing pavement foundation layers. The RICM measurements include: compaction meter value (CMV), resonant meter value (RMV), and machine drive power (MDP). The in-situ test methods include: falling weight deflectometer (FWD), light weight deflectometer (LWD), static plate load test device (PLT), dynamic cone penetrometer (DCP), and heavy test roller. The results and analysis from this investigation are presented as four dissertation chapters above and are categorized into three major topics: (a) review and investigation of different LWD devices for use in earthwork QC/QA (chapter 2), (b) geostatistical analysis of spatially referenced RICM measurements to characterize spatial non-uniformity of constructed pavement foundation layers and to improve QC methods during construction (chapter 3), (c) in-situ mechanistic characterization of pavement foundation layers using different in-situ test methods and RICM (chapters 4 and 5). Specific conclusions related to each topic are provided in the chapters above. General conclusions and anticipated benefits from this research, and recommendations for future research are provided below.

6.2 Conclusions

6.2.1 Review and investigation of LWD devices

An extensive review of literature and experimental test results on LWDs presented in chapter 2 demonstrate the issues need to be considered when interpreting LWD modulus (E_{LWD}) values. The findings are expected to aid ASTM in developing a standard test method for LWD testing and in successful implementation of these devices in earthwork QC/QA practice. Some key conclusions are as follows:

- Based on the review and experimental test results, major factors that influence E_{LWD} are identified as the size of loading plate, plate contact stress, type and location of

deflection transducer, plate rigidity, and to some extent loading rate, buffer stiffness, and the measurement of load versus assumption of a constant load based on laboratory calibration.

- LWD devices that use accelerometers that measure deflection of the plate (e.g. Zorn) are expected to measure larger deflections compared to devices that measure deflections on the ground with a geophone (e.g. Keros/Dynatest and Prima). This difference in deflection measurements is identified as the primary contributor to differences in E_{LWD} between different devices.
- E_{LWD} increases with decreasing plate diameter and the trend is sensitive to material stiffness. This finding is consistent with results presented in the literature with static PLT measurements.
- The Zorn E_{LWD} increases with increasing plate contact stresses with stiffer material presenting a greater increase in E_{LWD} . The Keros and Dynatest devices showed practically no influence of applied contact stresses above 100 kPa.
- Variations observed in Dynatest and Keros E_{LWD} by modifying the buffer stiffnesses are insignificant when the results are compared at similar applied contact stresses.
- E_{LWD} is strongly correlated to conventionally used PLT initial modulus and is poorly correlated with PLT reload modulus.
- The variability observed with Zorn E_{LWD} is generally lower compared to Keros and Dynatest E_{LWD} values. This is of consequence as it relates to determining appropriate number of QA tests depending on the variability to achieve good reliability.

6.2.2 Geostatistical Analysis on RICM measurements

Geostatistical analysis using semivariogram modeling for RICM measurements to characterize and quantify non-uniformity of compacted fill materials, and help improve process control methods are presented in Chapter 3. Geostatistical analysis and spatially referenced RICM represent a paradigm shift in how compaction analysis and specifications could be implemented in the future. Some key conclusions from the analysis results are as follows:

- Semivariogram modeling requires attention to some critical aspects which include:

- (a) performing exploratory data analysis to examine the distribution and assess the need for transformation, (b) determining non-stationarity in the data that may require polynomial trend surface analysis, (c) modeling anisotropy (directional semivariograms herein showed that this is generally not an issue because of limited data points in the transverse direction), and (d) understanding and exercising the semivariogram model fitting process.
- Geostatistics could aid the contractor in identifying localized poorly compacted areas or areas with highly non-uniform conditions that need additional compaction or other modification and would contribute to improved uniformity. This information could also be used to target QA testing by the field engineers.
 - Geostatistical parameters derived from RICM data can provide better characterization of the spatial variability of soil engineering properties. If the parameters can be linked to suitable analytical/numerical models, new insights into spatial load-deformation analysis can be developed.

6.2.3 Mechanistic Characterizations of Pavement Foundation Layers

Use of different mechanistic measurements along with interrelationships between these different measurements to characterize cohesive subgrades and granular subgrade and base/subbase layers is presented in Chapters 4 and 5. Heavy test roller, DCP, LWD, and RICM (CMV and MDP) were used for cohesive subgrades (Chapter 4), and LWD, FWD, CPTU, DCP, and RICM (CMV and RMV) were used for granular pavement foundation layers (Chapter 5). The findings are expected to aid in successful implementation of these different measurement methods into QC/QA practice and lay a foundation to establish a link with pavement design parameters in a mechanistic standpoint. Some key conclusions from the experimental test results and analysis are as follows:

- Correlations developed between RICM and in-situ test measurements showed positive trends but with varying degrees of uncertainty in relationships. Considering the significant advantage of RICM technologies with 100% coverage and positive trends in the relationships, it is concluded that the measurements can serve as a reliable indicator of compaction quality of cohesive and granular pavement

foundation layers.

- Roller jumping (as measured by RMV) affects the CMV values and consequently the correlations with in-situ test measurements. The effect of RMV on CMV has been discussed in the literature but it lacked attention in an implementation standpoint. To avoid complex interpretation and analysis of results with roller jumping, it is suggested that comparison tests with in-situ test measurements be performed with low amplitude setting (about less than 1 mm) operation.
- Heavy test rolling identified deep soft layers on cohesive subgrades with excessive rutting at the surface under the roller wheel. Layered bearing capacity analysis using DCP-undrained shear strength profiles showed that rut depths at the surface are empirically related to the ultimate bearing capacities under the roller wheel. A simple chart solution was developed using the layered bearing capacity analytic solutions to determine target shear strength properties of a layered soil to avoid rut failures under the test roller.
- Using criteria for characterizing measurement influence depth as the depth to decay stresses to 10% of maximum stresses at surface, the measurement influence depths under roller, 300-mm FWD plate, and 200-mm LWD plate are estimated as 0.9 m, 0.6 m, and 0.4 m. No difference was observed in the influence depth with change in amplitude or increasing dynamic load under FWD plate.
- In-ground stress measurements showed that the stress path under the roller indicates a hysteresis of extension and compression in pavement foundation layers due to rotation in principal stresses under moving roller load.
- Normal stresses developed under a 300-mm FWD plate with 53.4 kN applied force are quite similar to the normal stresses developed under the roller for $a = 1.7$ mm but the stress path slope coefficient m for FWD loading is smaller than for roller loading.
- Applied mean stresses and m coefficients for LWD loading are significantly smaller than roller and FWD induced stresses and m coefficients – a likely significant contributor to scatter in relationships between roller and E_{LWD} measurements.
- CPTU tip resistance, FWD, and DCP measurements showed correlations with R^2 values greater than 0.6.

6.3 Recommendations for Future Research

The following future work is recommended to build upon the findings from this research:

- Independently verify deflections of the plate and of the soil under the plate for different LWD devices using high resolution laser-based measurements. This will provide insights into the differences observed in deflection measurements depending on the type and location of the deflection sensors used in different LWDs.
- Analyze the differences in stress distributions under different geometry LWD plates (solid plate and a plate with a hole at the center) to better explain the materials' response to applied stresses and their relationships to resulting modulus values.
- Continue developing a database of spatial statistical parameters of constructed pavement foundation layers to help relate these parameters with pavement performance monitoring data (e.g., crack survey inspections, etc.).
- Link spatial statistics with pavement surface layer distresses from spatial load-deformation analysis using analytical/numerical models.
- Continue documenting relationships between RICM and conventionally used strength/stiffness based in-situ test measurements for different material types and field conditions.
- Develop understanding on the influence of stress path on the mechanistic properties of granular and cohesive materials to better explain the scatter in relationships between RICM and different in-situ test measurements.
- Analyze layered soil profiles obtained from in-situ point measurements (e.g., FWD, DCP, and CPTU) by accounting for the stress-dependency nature the materials using laboratory tests and in-ground instrumentation. This will potentially provide a lead way to incorporating RICM measurements into pavement design.

ACKNOWLEDGMENTS

I would like to express my deepest appreciation to my mentor and my committee chair Professor David White who has the attitude and the substance of a genius with continuous spirit of adventure in regard to research. Without his exceptional support, guidance and persistent help, this dissertation would not have been possible. I would like to thank my committee members Professors Max Morris, Vern Schaefer, Charles Jahren, and Halil Ceylan for serving on my committee and providing constructive comments on my work.

The Minnesota Department of Transportation (Mn/DOT), Federal Highway Administration (FHWA), and Caterpillar, Inc., Iowa State University's Center of Transportation Research and Education (CTRE) and Earthworks Engineering Research Center (EERC) sponsored the work published in this thesis. I would like to thank John Siekmeier and Rebecca Embacher with Mn/DOT for providing helpful insights and comments on LWD testing. Numerous Mn/DOT personnel, district staff, Peterson Contractors personnel, and Mathiowetz Construction Co. personnel assisted in identifying and provided access to field projects. I would like to acknowledge the help of Paul Corcoran, Tom Congdon, Donald Hutchen, Allen Declerk, and Glen Feather at CAT for their assistance with the field and lab testing.

I would like to thank my dear friend and colleague Heath Gieselman for his incredible support and helpful insights into my work throughout my stay at Iowa State University. I would like to acknowledge the help of Dr. Mark Thompson (formerly graduate student), Thang Phan, John Puls, Dan Enz, Brad Fleming, Luke Johansen, Rachel Goldsmith, Jiake Zhang, Andrew Weber, Alexandra Buchanan, Kevin McLaughlin, Owen Berg, Michael Kruse, Amy Heurung, and Michael Blahut of Iowa State University who provided assistance with the ISU Geotechnical Mobile Lab in field and lab testing.

Last but not the least; I would like to thank my mom, dad, sister, brother-in-law, my best friend and fiancé, many dear friends, and colleagues for their amenable support throughout my studies which cannot be expressed in words.